Photocatalysis of aqueous perfluorooctanoic acid by TiO_2 and Ga_2O_3 assisted with peroxymonosulfate under UV and visible light

By

Bentuo Xu

A Dissertation Submitted in Fulfilment for the Degree of

Doctor of Philosophy

School of Civil and Environment Engineering

Faculty of Engineering and Information Technology

University of Technology Sydney

New South Wales, Australia

April 2020

Certificate of original authorship

I, Bentuo Xu, declare that this thesis, is submitted in fulfilment of the requirements for the award of PhD, in the FEIT at the University of Technology Sydney.

This thesis is wholly my own work unless otherwise reference or acknowledged. In addition, I certify that all information sources and literature used are indicated in the thesis.

This document has not been submitted for qualifications at any other academic institution.

This research is supported by the Australian Government Research Training Program.

Signature of Student

Production Note:
Signature removed prior to publication.

Bentuo Xu

Date: 13th April 2020

Acknowledgements

First and foremost, I would like to express my sincere gratitude to my principal supervisor, Prof. John L. Zhou for his invaluable guidance and supports during my PhD study. He always inspired me when I had difficulties and gave me many significant suggestions to help me solving the problems. In addition, he taught me how to write technical papers in a logical and systematic manner, which significantly improved my English level and published papers in the journals. Meanwhile, I am very grateful to my co-supervisor Ali Altaee for his contribution and comments to my papers. I also would like to thank Dr. Abu Hasan Johir, the manager of environmental engineering laboratories, for the technical supports and guidance. Whenever I met difficulties in the lab, he always gave me the help timely.

I gratefully acknowledge the dual doctoral degree program of University of Technology Sydney (UTS) – Shanghai University that provided the opportunity for me to have two doctoral degrees from these two prestigious universities. Especially, many thanks to China Scholarship Council (CSC) and UTS for providing the financial support during my stay in Australia.

I would like to express my appreciation to Boshir for his hearty welcome when I was a freshman and technical assistance with revising my papers. I am also thankful to my lovely colleges Yuhan Huang, Romina, Kireesan, Jiawei Ren, Mingwei Yao, Dongle Chen, Qiang Hao, and Xiaoqing Liu for their supports and contributions. Thanks to my friends Jinsong Cao, Haodong Chan, Xiaoling Zhang, Yingdong Feng, Shichao Chen, Pu Lin, Yili Jiang and Tengyi Jiang for their care and love.

Finally, I am indebted to all my family and friends their unconditional support and encouragement.

Dedication

This thesis is deeply dedicated to the following people:

To my lovely parents

Xiuru Xu

&

Xiaowei Chen

For their unconditional support, enthusiastic encouragement

and endless love

Table of Contents

List of Figures

scavengers) on the PFOA degradation in Vis/TiO_2/PMS system within 8 h (300 W visible light, [PFOA] = 50 mg L^{-1}, [PMS] = 0.15 g L^{-1}, [TiO_2] = 0.05 g L^{-1}). Insert showing the fitting of degradation curves within 6 h and degradation rate constant (*k*) derived.

Fig. 6-10. The main photocatalysis by TiO_2/PMS for PFOA degradation (Xu et al., 2020).

Fig. 7-1. (A) Degradation of PFOA in wastewater samples including influent and effluent from a wastewater treatment plant under UV 254 nm and 185 nm. (B) The rate of TOC removal by Ga_2O_3/PMS under 254 nm and 185 nm UV light. ([PFOA] = 50 mg L^{-1}, [PMS] = 0.45 g L^{-1}, [Ga_2O_3] = 0.25 g L^{-1}).

Fig. 7-2. (A) Degradation of wastewater samples including influent and effluent from a wastewater treatment plant and (B) the rate of TOC removal by TiO_2/PMS under 300 W visible light, 254 nm and 185 nm UV light.

Fig. 7-3. (A) Comparison between Ga_2O_3/PMS and TiO_2/PMS for PFOA removal in pure water under 185 nm, 254 nm UV light and (B) 300 W visible light.

Fig. 8-1. Different types of photocatalytic reactors for practical applications: (A) suspension photocatalytic reactor; (B) photocatalytic pool with g-C_3N_4 on structured Al_2O_3 ceramic foam; (C) catalyst coated optical fibre reactor. The figures are referred from the ref. (Dong et al., 2014; Hatat-Fraile et al., 2017; Xu et al., 2017b).

List of Tables

Table 3-5

The target compounds of PFAS analysed, and their MS/MS parameters.

Table 3-6

Analytical data for PFAS standards using UHPLC-MS/MS method.

Table 4-1

Comparison of Photocatalytic conditions for PFOA removal by TiO_2/PMS in this study and other catalysts in previous literatures.

Table 4-2

The band gap energy of commercial In_2O_3, Ga_2O_3, TiO_2, CeO_2 and CdS.

Table 4-3

The key experimental parameters and their values in this study.

Table 5-1

The key experimental parameters and their values in this study.

Table 6-1

Comparison of Photocatalytic conditions for PFOA removal by TiO_2/PMS in this study and other catalysts in previous literatures.

Table 7-1

Characteristics of the effluent taken from a municipal wastewater plant in Sydney, Australia.

Abbreviations

Bismuth oxychloride = BiOCl

Benzoquinone = BQ

Bismuth sulfide = Bi_2S_3

Carbon-fluorine = C-F

Carbon nitride = C_3N_4

Cerium dioxide = CeO_2

Cadmium sulfide = CdS

Disodium ethylenediaminetetraacetate = EDTA-Na_2

Dissolved organic matter = DOM

Dissolved oxygen = DO

Dry weight = dw

Gallium oxide = Ga_2O_3

Perchloric acid = $HClO_4$

Porous nanoplates = PNPs

Indium trioxide = In_2O_3

Membrane bioreactor = MBR

Multiple reaction monitoring = MRM

Nanoporous nanospheres = NPNs

Nanoplates = NPs

Hydroxyl radicals = •OH

Perfluoroalkyl substances = PFAS

Perfluorobutanoic acid = PFBA

Perfluorocarboxylic acids = PFCA

Perfluoroheptanoic acid = PFHpA

Perfluorohexanoic acid = PFHxA

Perfluorooctanoic acid = PFOA

Perfluorooctane sulfonic acid = PFOS

Perfluoropentanoic acid = PFPeA

Peroxymonosulfate = PMS

Relative standard deviation = RSD

Scanning electron microscope = SEM

tert-butyl alcohol = TBA

tert-butanol = *t*-BuOH

Trifluoroacetic acid = TFA

Titanium dioxide = TiO_2

Titanate nanotubes (TNTs)

Total organic carbon = TOC

Multiwall carbon nanotube = MWCNT

Wet weight = ww

Wastewater treatment plant = WWTP

X-ray diffraction = XRD

Zinc oxide = ZnO

Nomenclatures

E_g = optical band edge

Φ = quantum yield

pH_{PZC} = zero charge

C_0 = initial concentration

C_t = concentration at min *t*

k = rate constant

k_f = the fluence-based first-order rate constant

$\tau_{1/2}$ = half-life

O_3 = ozonation

hv = photon

C-F = carbon-fluorine

$SO_4^{\bullet-}$ = sulfate radicals

h^+ = hole

e^- = electron

F^- = fluorine ion

List of publications

1st author journal articles:

(1). ***Bentuo Xu**, Mohammad B. Ahmed, John L. Zhou, Ali Altaee. Visible and UV photocatalysis of aqueous perfluorooctanoic acid by TiO_2 and peroxymonosulfate: Process kinetics and mechanistic insights. ***Chemosphere*** 243 (2020) 125366.

(2). ***Bentuo Xu**, John L. Zhou, Ali Altaee, Mohammad B. Ahmed, Md Abu Hasan Johir, Jiawei Ren, Xiaowei Li. Improved photocatalysis of perfluorooctanoic acid in water by Ga_2O_3/UV system assisted by peroxymonosulfate. ***Chemosphere*** 239 (2020) 124722.

(3). ***Bentuo Xu**, Mohammad Boshir Ahmed, John L. Zhou, Ali Altaee, Minghong Wu, Gang Xu. Graphitic carbon nitride based nanocomposites for the photocatalysis of organic contaminants under visible irradiation: progress, limitations and future directions. ***Science of the Total Environment*** 633 (2018) 546-599.

(4). **Bentuo Xu**, Minghong Wu, Mingnan Wang, Chenyuan Pan, Wenhui Qiu, Liang Tang, Gang Xu. Polybrominated diphenyl ethers (PBDEs) and hydroxylated PBDEs in human serum from Shanghai, China: a study on their presence and correlations. ***Environmental Science and Pollution Research*** 25 (2018) 3518-3526.

(5). ***Bentuo Xu**, Mohammad Boshir Ahmed, John L. Zhou, Ali Altaee, Minghong Wu, Gang Xu. Photocatalytic removal of perfluoroalkyl substances from water and wastewater: Mechanism, kinetics and controlling factors. ***Chemosphere*** 189 (2017) 717-729.

(6). **Bentuo Xu**, Minghong Wu, Chenyuan Pan, Yan Sun, Debao Yuan, Liang Tang, Gang Xu. Aquatic photolysis of hydroxylated polybromodiphenylethers under direct UV irradiation: a case study of 2'-HO-BDE-68. ***Environmental Science and Pollution Research*** 24 (2017) 14409-14416.

(7). **Bentuo Xu**, Gang Xu, Minghong Wu. Distribution and toxic effects of polybrominated diphenyl ethers (PBDEs) in organism. ***Journal of Shanghai University (Natural Science Edition)*** 23 (2017) 235-243.

Participation work:

(1). Minghong Wu, **Bentuo Xu**, Gang Xu*, Mingnan Wang, Jing Ma, Chenyuan Pan, Rui Sun, Tao Han, Liang Tang. Occurrence and profiles of polybrominated diphenyl ethers (PBDEs) in riverine sediments of Shanghai: a combinative study with human serum from the locals. ***Environmental Geochemical Health.*** 30 (2017) 729-738.

(2). Jianguo Sheng, Wenhui Qiu, **Bentuo Xu**, Hui Xu, Chong Tang. Monitoring of heavy metal levels in the major rivers and in residents' blood in Zhenjiang City, China, and assessment of heavy metal elimination via urine and sweat in humans. ***Environmental Science and Pollution Research.*** 11 (2016) 11034-11045.

(3). Chenyuan Pan, Ming Yang, Hai Xu, **Bentuo Xu**, Lihui Jiang, Minghong Wu, Tissue bioconcentration and effects of fluoxetine in zebrafish (*Daniorerio*) and red crucian cap (*Carassius auratus*) after short-term andlong-term exposure. ***Chemosphere.*** 205 (2018) 8-14.

(4). Minghong Wu, Chenyuan Pan, Ming Yang, **Bentuo Xu**, Xiangjie Lei, Jing Ma, Ling Cai, Jingsi Chen. Chemical analysis of fish bile extracts for monitoring endocrine disrupting chemical exposure in water: Bisphenol A, alkylphenols, and norethindrone. ***Environmental toxicology and chemistry.*** 35 (2016) 182-190.

(5). Gang Xu, Sihan Ma, Liang Tang, Rui Sun, Jiajia Xiang, **Bentuo Xu**, Yangyang Bao, Minghong Wu. Occurrence, fate, and risk assessment of selected endocrine disrupting chemicals in wastewater treatment plants and receiving river of Shanghai, China Chemosphere. ***Environmental Science and Pollution Research.*** 23 (2017) 25442-25450.

(6). Minghong Wu, Tao Han, Gang Xu, Chao Zang, Yijie Li, Rui Sun, **Bentuo Xu**, Yan Sun, Fenfen Chen, Liang Tang. Occurrence of Hexabromocyclododecane in soil and road dust from mixed-land-use areas of Shanghai, China, and its implications for human exposure. ***Science of the Total Environment.*** 559 (2016) 282-290.

(7). Minghong Wu, Jingcheng Pei, Ming Zheng, Liang Tang, Yangyang Bao, **Bentuo Xu**, Rui Sun, Yanfeng Sun, Gang Xu, Jianqiu Lei. Polybrominated diphenyl ethers (PBDEs) in soil and outdoor dust from a multi-functional area of Shanghai: Levels, compositional profiles and interrelationships. ***Chemosphere.*** 118 (2015) 87-95.

(8). Minghong Wu, Wenyan Shi, Peng Yuan, Xinhao Sheng, **Bentuo Xu**, Xiangxin He, Gang Xu, Jing Ma, Xiaoyong Deng, Ming Yang. Method of removing estrogen biological toxicity in water and device of electron beam radiation disposing water. ***Inventive patent.*** 2014100015401. (2016, authorized)

Publications made during the PhD candidature including articles not entirely related to the Thesis. Articles with asterisk marked were related to the thesis.

Awards

1. 2017 HDR Students Publication Award from Faculty of Engineering and Information Technology (FEIT), University of Technology Sydney (UTS) for publishing in high quality journals.

PhD Dissertation Abstract

Author: Bentuo Xu

Date: 13th April 2020

Thesis title: Photocatalysis of aqueous perfluorooctanoic acid by TiO_2 and Ga_2O_3 assisted with peroxymonosulfate under UV and visible light

Faculty: Faculty of Environmental and Information Technology

School: Civil and Environmental Engineering

Supervisors: Prof. Dr. John Zhou (Principal supervisor)

Dr. Ali Altaee (Co-supervisor)

Abstract

Perfluorooctanoic acid (PFOA) has attracted considerable attention worldwide due to its widespread occurrence and environmental impacts. However, a suitable technology for PFOA controlling is worthwhile to be investigated nowadays. This thesis studied the photocatalysis by different catalysts and found that Ga_2O_3 and TiO_2 had better performance for PFOA removal than CeO_2, In_2O_3 and CdS. In addition, Ga_2O_3 mixed with peroxymonosulfate (PMS) was investigated for the PFOA degradation under UV light. It showed excellent performance and that 100% of PFOA was degraded within 90 min and 60 min under 254 nm and 185 nm UV irradiation, respectively. PFOA in real wastewater exhibited similar degradation efficiency and 75-85% TOC was removed by Ga_2O_3/PMS under 254 nm UV irradiation. Thus, a good method with well degradation efficacy was established in this thesis for aqueous PFAS removal. Moreover, this thesis investigated the PFOA photodegradation by using powerful visible light (300 W, 829.6 mW cm^{-2}) in the presence of catalyst TiO_2 with PMS activation, which achieved 100% PFOA removal within 8 h. The presence of organic compounds in real wastewater

reduced the degradation efficacy of PFOA by 18-35% in Vis/TiO_2/PMS system. Therefore, PFOA could be controlled under no matter UV light or visible light by TiO_2/PMS system.

Gallium oxide (Ga_2O_3), titanium dioxide (TiO_2), cerium dioxide (CeO_2), indium oxide (In_2O_3), and cadmium sulfide (CdS) are commonly used under UV light as photocatalyst for the pollutants degradation. In this study, these five catalysts were applied for the photodegradation of PFOA and the performance decreases as: Ga_2O_3 > TiO_2 > CeO_2 > In_2O_3 > CdS. Notably, CdS had almost no capability for PFOA removal. The initial pH, quantum yield and band gap energy were used to explain the various catalytic ability among these catalysts. Significantly, the band gap energy decreases as: Ga_2O_3 > TiO_2 > CeO_2 > In_2O_3 > CdS, which exactly matched their degradation performance. Thus, band gap energy was significantly related to the photocatalytic ability for PFOA removal. Further, according to the scavenger experiments, photogenerated holes rather than electrons played the main roles in degrading PFOA by TiO_2, CeO_2 and In_2O_3. In comparison, photogenerated conduction band electrons were more important when photocatalysis was carried out with Ga_2O_3.

This research focused on the photocatalytic process for the treatment of PFOA in water by Ga_2O_3 and peroxymonosulfate (PMS) mixed directly in the PFOA solution under different light sources. The results showed excellent performance that 100% of PFOA was degraded within 90 min and 60 min under 254 nm and 185 nm UV irradiation, respectively. Moreover, the degradation efficacy was unaffected by initial PFOA concentration from 50 ng L^{-1} to 50 mg L^{-1}. Acidic solution (pH 3) improved the degradation process as high amount of PFOA was adsorbed on the surface of Ga_2O_3 via Coulombic attraction, leading to the promoted photocatalytic efficacy. The quantum yield in the PMS/Ga_2O_3 system under UV light (254 nm) was estimated to be 0.009 mol

Einstein^{-1}. Scavengers such as *tert*-butanol (*t*-BuOH), disodium ethylenediaminetetraacetate (EDTA-Na_2) and benzoquinone (BQ) were added into PFOA solution to assess the roles of sulfate radicals ($SO_4^{\bullet-}$), superoxide radical ($O_2^{\bullet-}$) and photogenerated electrons (e^-) as the active species with strong redox potentials for PFOA degradation in PMS/Ga_2O_3/UV system. Through the analysis of the intermediates, PFOA was degraded stepwise from long chain compound to shorter chain intermediates. In addition, PFOA in the real wastewater exhibited similar degradation efficiency and 75-85% TOC was removed by Ga_2O_3/PMS under 254 nm UV irradiation. Therefore, Ga_2O_3/PMS system was highly effective for PFOA photodegradation under UV irradiation, which has potential to be applied for the perfluoroalkyl substances (PFAS) treatment in water and wastewater.

This research also studied the PFOA photodegradation by using powerful visible light (300 W, 829.6 mW cm^{-2}) in the presence of catalyst TiO_2 with PMS activation. The addition of PMS induced a significant degradation of PFOA on TiO_2 under visible light compared with sole TiO_2 or PMS treatment. Under powerful visible light, 0.25 g L^{-1} TiO_2 and 0.75 g L^{-1} PMS in the solution at initial pH 3 was advantageous for the PFOA degradation, and achieved 100% PFOA removal within 8 h. Under UV light irradiation at 254 and 185 nm wavelength, TiO_2/PMS resulted in an excellent performance of almost 100% PFOA removal within 1.5 h, attributed to the high absorbance ability of UV light by the catalyst. The intermediates analysis showed that PFOA was degraded from long carbon chains to shorter chains in a stepwise manner. Furthermore, scavenger experiments indicate that $SO_4^{\bullet-}$ radicals from PMS and photogenerated holes from TiO_2 played an essential role in degrading PFOA. The presence of organic compounds in real wastewater reduced the degradation efficacy of PFOA by 18-35% in visible-TiO_2-PMS

system. In general, TiO_2-PMS could be an ideal and effective catalyst for the degradation of PFOA from wastewater using either visible or UV light source.

Keywords: Chemical bonds; Gallium oxide; Peroxymonosulfate; Photocatalysis; Perfluorooctanoic acid; Photogenerated electrons; Sulfate radicals; Visible light

Chapter 1. Introduction

1.1. Background

Perfluoroalkyl substances (PFAS) are anthropogenic compounds that have been used in industrial, military, and commercial applications since the 1950s (Houtz et al., 2013). These chemicals are very stable as the carbon-fluorine (C-F) bond is very strong with a bond energy of 544 kJ mol^{-1}, clearly indicating their persistent in the environment (Wang et al., 2008). PFAS have drawn the increasing attention in recent years mainly because they are potential reproductive and developmental toxins, endocrine disrupters, and carcinogens (Ding and Peijnenburg, 2013; Gorrochategui et al., 2014), although the relationship between PFAS and particular human disease is not established yet. It is a fact that PFAS exist not only in different environmental media but also in human body (**Table 1-1**). Well-known PFAS such as perfluorooctanoic acid (PFOA) and perfluorooctane sulfonic acid (PFOS) (molecular structure as shown in **Fig. 1-1**) both commonly constitute high proposition of PFAS that have been detected in the aquatic environment (Estrellan et al., 2010). The source of PFAS in the environment can be divided into direct and indirect pathways (Wang et al., 2008). The direct route represents the emission from the manufacture and use of PFAS, or wastewater treatment plants (WWTPs) (Gallen et al., 2014). The indirect route refers to the long-range transport and degradation products from precursor compounds such as fluorotelomer alcohols and perfluorooctane sulfonyl fluoride (Armitage et al., 2006; Armitage et al., 2009). Furthermore, it was reported that the direct route accounts for more than 80% of the total source for PFAS in the environment (Pistocchi and Loos, 2009). The transport of such compounds could also be separated into atmospheric and aqueous transport pathways (Prevedouros et al., 2006). The atmospheric transport involves that PFAS diffusing into the atmosphere before deposition onto land or in water. The aqueous transport involves the dissolution in water and transport by the currents to the other water matrices. The contamination of PFAS in

the aquatic environment has been widely reported. In Spanish rivers, PFAS were found to be 43 ng/L (Flores et al., 2013). A suit of 16 PFAS were detected in one WWTP in China, with concentrations ranging from 0.04 to 91 ng/L in the influent. In addition, high PFOA concentration was detected in both the influent (2–91 ng L^{-1}) and effluent (3–107 ng L^{-1}) from WWTP's (Zhang et al., 2013). Moreover, serious PFAS water contamination was reported for the industrialized cities such as Dalian, China (Chen et al., 2017b) and Tokyo, Japan (Murakami et al., 2011). Furthermore, as high as 68.6 ng/L of PFOA was detected in the Korean coastal water (Naile et al., 2010). Overall, water contamination by PFAS is widespread demonstrating a variety of sources and potential persistence.

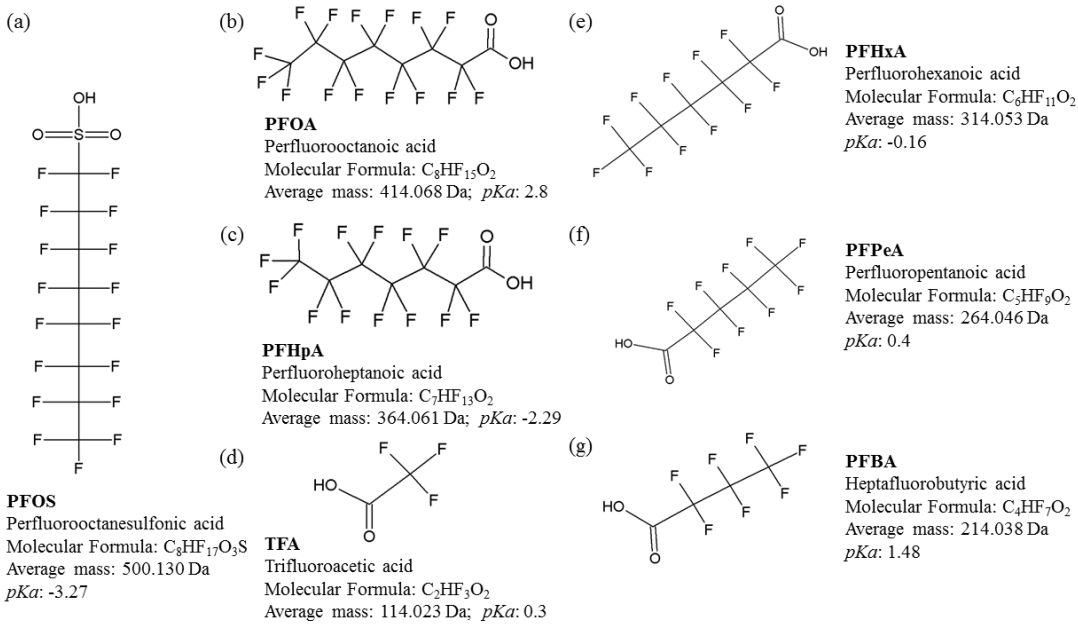

Fig. 1-1. Molecular structure and chemical properties of (a) PFOS, (b) PFOA, (c) PFHpA, (d) TFA, (e) PFHxA, (f) PFPeA, and (g) PFBA.

Over the years, the technologies for PFAS removal from water have been developed with various decomposition efficacies due to the physical and chemical stability of C-F bonds (Cao et al., 2010; Chen, et al., 2015b). Treatment by sorption, filtration, biodegradation, and membrane bioreactor (MBR) were evaluated at bench scale

(Appleman et al., 2014; Kwon et al., 2017; Yates et al., 2014). Nevertheless, sorption and filtration are non-destruction methods that just transfer the contaminants from one medium to another and the waste still needs to be further managed (Urtiaga et al., 2015). As for MBR and biodegradation, these methods have been proven to be inefficient for PFAS removal in many WWTPs (Kwon et al., 2017; Yu et al., 2014). For example, when investigating MBR performance for the removal of PFOA and PFOS, it was reported that the removal efficiencies of these two compounds were less than 7% (Yu et al., 2014). This is probably because most microorganisms do not have the ability to decompose PFAS in water. Thus, technologies that cleavage C-F bonds are more suitable for PFAS removal. As an alternative, photolysis is recognized as an appealing option, which could degrade a variety of toxic substances e.g. agrochemicals in the presence of artificial or solar light, and is environmentally friendly and cost effective (Kitsiou et al., 2009). However, the strong bonding energy of the direct photolysis for the removal of PFAS from water is still of low efficacy. UV light (254 nm wavelength) was used for the photodegradation of PFOA in dilute aqueous solution, and observed no removal of PFOA within the reaction period of 300 min (Giri et al., 2011). In comparison, by utilizing the photon (*hv*) absorption capacity of some catalysts, heterogeneous photocatalysis has been developed to decompose PFAS, which can be conducted under a wider range of light wavelength as shown in **Fig. 1-2**. During heterogeneous photocatalysis, the contaminant and catalyst exist in different phases and the process could be described as absorbing *hv* and then generating negatively charged electron (e^-) and positively charged hole (h^+) pairs. They will migrate to the surface of the photocatalyst particles and react with the adsorbed contaminant, resulting in its decomposition. It has been proven that heterogeneous photocatalysis catalysts such as titanium dioxide (TiO_2), gallium oxide (Ga_2O_3), and indium trioxide (In_2O_3) are far more effective for PFAS removal than direct photolysis

(Chen et al., 2011; Li et al., 2013b). There are about seven review articles on PFAS degradation and removal (Arvaniti and Stasinakis, 2015), but to the authors' knowledge there is no review article on the heterogeneous photocatalysis of PFAS.

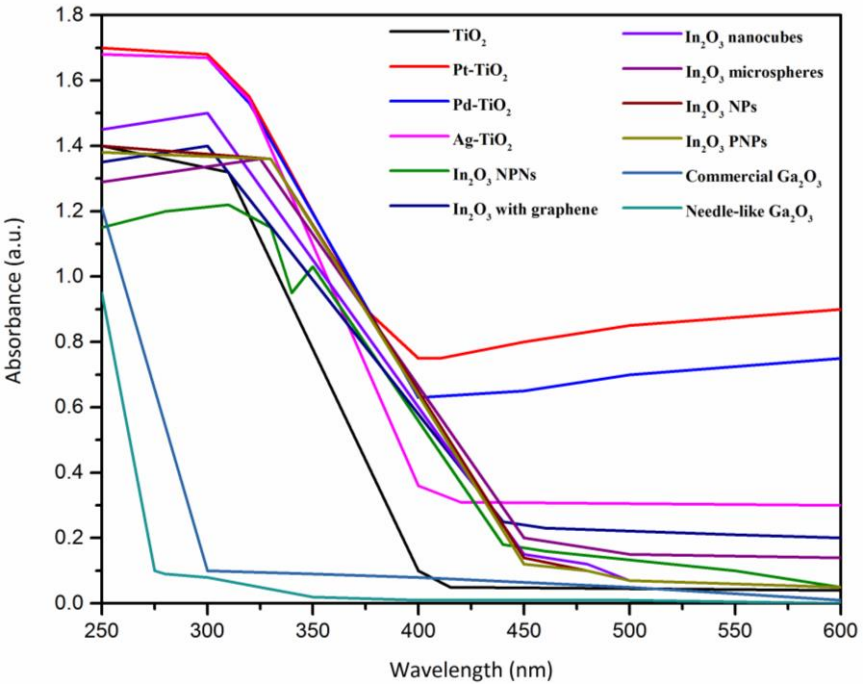

Fig. 1-2. UV-vis absorption spectra of different catalysts.

Table 1-1

Concentrations of PFOA and PFOS in different matrices showing min–max (mean).

Sample type	Unit	Area/Country	PFOA	PFOS	Reference
River water	ng L^{-1}	Red river, Vietnam	0.13–0.40 (0.32)	<0.03–0.04 (0.01)	(Lam et al., 2017)
River water	ng L^{-1}	Bormida river, Italy	253–6480 (1613)	<LOD–109 (8)	(Valsecchi et al., 2015)
River water	ng L^{-1}	Bohai sea, China	4.06–61900 (844)	0–131 (11.2)	(Chen et al., 2017a)
River Water	ng L^{-1}	Yellow river, China	2.01–41.8 (11.5)	2.65–41.0 (10.8)	(Zhao et al., 2016)
Lake sediment	ng g^{-1} dw[a]	48 lakes all over China	0.006–1.10 (0.296)	0.001–0.76 (0.319)	(Qi et al., 2016)
Indoor dust	ng g^{-1} dw	Birmingham, UK	<0.98–6000 (550)	20–1000 (370)	(Goosey and Harrad, 2011)
Outdoor jackets	μg m^{-2}	Idstein, Germany	0.02–171 (9.803)	0.01–0.54 (0.033)	(Gremmel et al., 2017)
Fish	ng g^{-1} ww[b]	Vltava river, Czech Republic	0.007–0.375 (0.039)	0.572–61.3 (14.5)	(Svihlikova et al., 2015)
Human blood	ng mL^{-1}	Norilsk, Russia	0.33–1.40 (0.89)	3.61–8.38 (6.11)	(Hanssen et al., 2013)
Human blood	ng mL^{-1}	Athens, Greece	1.68–10.21 (3.88)	6.97–30.36 (14.93)	(Vassiliadou et al., 2010)
Human blood	ng mL^{-1}	Queensland, Australia	3.1–3.4 (3.02)	1.9–5.6 (3.68)	(Eriksson et al., 2017)
Human liver	ng g^{-1}dw	Melbourne, Australia	0.16–2.25 (0.518)	0.375–12.5 (5.03)	(Yeung et al., 2013)
Human breast milk	μg L^{-1}	Nantes, France	<LOD–0.224 (0.082)	<LOD–0.330 (0.092)	(Wohlfahrt-Veje et al., 2014)

[a] dw = dry weight， [b] ww = wet weight

1.2. Research motivation and scopes

As a well-known contaminant, PFOA has been studied for its photodegradation in some previous literature. However, different catalysts have ability for aqueous PFOA removal and insufficient evidence was provided for the mechanism during the reaction. The previous studies only drawn attention on the modified catalysts under UV light irradiation and never tried to work with sulfate radicals for PFOA removal. Herein, the focus of this PhD research is to investigate the effectiveness of common commercial catalysts for PFOA photocatalysis. Moreover, PMS was firstly added to assist photocatalysis of TiO_2 or Ga_2O_3. The enhancement of PFOA degradation performance by the integrated system (TiO_2/PMS or Ga_2O_3/PMS) is explored and the photocatalytic mechanism and kinetic are also discussed.

The objectives of this study are to

i) review currently representative studies on PFOA photodegradation by different catalysts and the experimental conditions;

ii) critically evaluate the efficiently heterogeneous photocatalysis for PFAS degradation by five commercial catalysts of TiO_2, Ga_2O_3, In_2O_3, CeO_2 and CdS;

iii) explore the photocatalytic performance of Ga_2O_3 with PMS under 185 and 254 nm UV light irradiation and explain the promoted reasons;

iv) assess photodegradation efficacy by TiO_2/PMS under UV light and visible light, and provide the explanation for the photocatalytic capability under different light resources;

v) demonstrate the main roles of active species (i.e. photogenerated holes, electrons, hydroxyls and superoxide radical anions) in the system of TiO_2/PMS and Ga_2O_3/PMS under UV light irradiation.

vi) discuss the impact of external conditions, such as initial pH, the dose of catalysts, and PFOA concentration, on the photodegradation efficiency.

1.3. Research significance

This research provides a promising and effective way to promote the efficacy of PFOA photodegradation. The catalysts were easily prepared by mixing commercial Ga_2O_3 or TiO_2 with PMS in water. In addition, TiO_2/PMS firstly achieve 100% PFOA degraded under visible light (300 W, 829.6 mW cm^{-2}), providing the possibility for PFOA treatment under visible light irradiation. Hence, the information given in the study will be of great significance to further investigation regarding the PFOA control and practical application of water and wastewater treatment. The specific points of innovations were listed as follows:

- Commercial catalysts were used in the study without modification, indicating the low cost of energy and financial of the new technology;
- By experiments, Ga_2O_3 and TiO_2 outperformed In_2O_3, CeO_2 and CdS for PFOA removal;
- Commercial Ga_2O_3 could degrade almost 100% PFOA within 10 h under UV light;
- The band gap energy of the selected materials was sequenced from large to low as Ga_2O_3 > TiO_2 > CeO_2 > In_2O_3 > CdS, which exactly matched the photodegradation performance from good to poor in this study;
- 100% PFOA was degraded within 60 min in Ga_2O_3/PMS/UV system under 185 nm UV light, which was comparatively higher efficacy compared with previous studies;

- $SO_4^{\bullet-}$, $O_2^{\bullet-}$ and photogenerated electrons were the key active species in Ga_2O_3/PMS/UV system during photocatalysis;
- The excited e^- could activate MPS to produce SO_4^- radicals as $S_2O_8^{2-} + 2e^- \rightarrow 4SO_4^{\bullet-}$, which explains that photodegradation efficiency was much better in PMS/Ga_2O_3/UV system than by sole Ga_2O_3 or PMS;
- 100% PFOA was degraded within 9 h by TiO_2/PMS under powerful visible light (300 W, 829.6 mW cm^{-2}), which was creatively achieved in the this study;
- $SO_4^{\bullet-}$ and photoinduced holes were the main active species by TiO_2/PMS;
- The holes and electrons could be generated on the surface of TiO_2 irradiated by powerful visible light and HSO_5^- could react with photogenerated electrons to form sulfate radicals ($SO_4^{\bullet-}$) as $HSO_5^- + e^- \rightarrow SO_4^{\bullet-} + OH^-$, thus leading to the outperformance of TiO_2/PMS than sole TiO_2 or PMS in degrading PFOA;
- In the application of this technology, Ga_2O_3/PMS and TiO_2/PMS could remove 75% and 65% TOC in wastewater under 254 nm UV light irradiation, respectively.

1.4. Thesis outline

The thesis consists of eight chapters, of which the main contributors are displayed in **Fig. 1-3**.

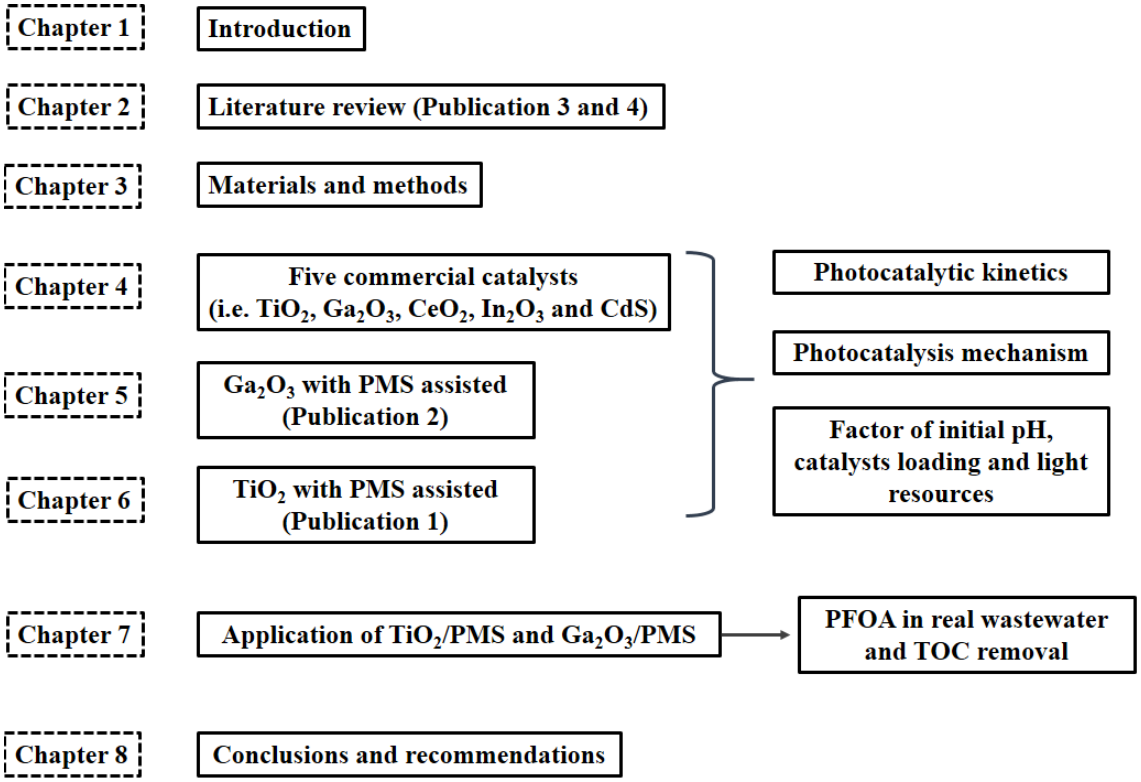

Fig. 1-3. Main structure of this thesis.

Chapter 1 entitled as "Introduction" presents the background of this study and identifies the currently development related to PFAS treatment, together with the research motivation, research scopes and their significance. The framework of the thesis is also presented in the chapter.

Chapter 2 entitled as "Literature review" offers a review of previous studies including the photocatalytic mechanism and photodegradation kinetics during the reaction process. Furthermore, different kinds of catalysts and the factors affecting the degradation efficacy were also discussed in the chapter.

Chapter 3 entitled as "Materials and methods" provides the detailed materials and methods. It includes the chemicals information, experimental set-up, operation conditions, detecting method for target compounds and characterization methods of catalysts.

Chapter 4 entitled as "Photolysis of PFOA by five commercial catalysts under UV irradiation" evaluates the five commercials catalysts of TiO_2, Ga_2O_3, In_2O_3, CeO_2 and

CdS. The photocatalytic mechanism was explored by discussing the initial pH effect, photon energy absorbed, band gap of different catalysts and interaction between chemical bonds.

Chapter 5 entitled as "Improved photocatalysis of perfluorooctanoic acid in water and wastewater by Ga_2O_3/UV system assisted by peroxymonosulfate." The effect of catalysts loading, solution pH, initial PFOA concentration and light resources were also discussed.

Chapter 6 entitled as "Visible and UV photocatalysis of aqueous perfluorooctanoic acid by TiO_2 and peroxymonosulfate: Process kinetics and mechanistic insights" introduces the notable achievement of 100% PFOA removal by TiO_2/PMS under visible light. In addition, the photodegradation performance under 185 nm and 254 nm UV light were also described. The advantages and proposed degradation mechanism were investigated in this chapter.

Chapter 7 entitled as "Comparison of Ga_2O_3 and TiO_2 with PMS and potential application" compares the photocatalytic performance between Ga_2O_3/PMS and TiO_2/PMS for PFOA in water and wastewater. Besides, TOC removal by Ga_2O_3/PMS and TiO_2/PMS were also assessed in this chapter.

Chapter 8 entitled as "Conclusions and recommendations" summarizes the work and major conclusions from this study and address further research needs and trends, which was significant for the topic of PFOA treatment.

Chapter 2. Literature review

2.1. Introduction

As the world is facing increasing challenges in the field of energy crisis and environmental pollution, the use of renewable energy to control environmental pollution is of high priority. As an inexhaustible and environmental friendly resource, solar energy is considered as the most ideal power, which enables photodegradation to be a favourable technology for controlling environmental contamination (Bahnemann, 2004; Malato et al., 2002). By comparison, other treatment methods such as electrochemistry (Stilwell and Park 1988), filtration (Simon et al., 2009), biodegradation (Pagga and Brown, 1986), and membrane bioreactor (Quintana et al., 2005) all have the drawback of energy consumption. However, for the practical applications of photolysis, low efficacy of solar energy utilization is the main obstacle. Thus, photocatalysis, especially semiconductor photocatalysis, becomes popular due to the advantages of using renewable resources, cost-effectiveness, safety, and comparatively high efficacy of pollutant removal (Xu et al., 2017a). For example, TiO_2, zinc oxide (ZnO), bismuth sulfide (Bi_2S_3), and carbon nitride (C_3N_4) all have been reported to perform well in photocatalysis (He, 2017; Konyar et al., 2017; Zhou et al., 2017a). These semiconductors possess the ability to adsorb the light and produce photogenerated electron and hole pairs, which have redox ability to degrade environmental contaminants. In addition, the doping of catalyst such as TiO_2 by gold (Au) has enabled the catalyst to perform significantly better under visible light (Sornalingam et al., 2018).

2.2. Photocatalytic mechanism

The mechanism of heterogeneous photocatalysis is summarized in **Fig. 2-1**. When the catalyst absorbs an *hv* (UV light with wavelength from 10 nm to 400 nm) with energy equal to or greater than its band gap, a pair of e^--h^+ is generated. The band gap energy is

critical for this process; too wide or too narrow band gap will be ineffective for photocatalysis. When the band gap of the catalyst is too wide, the light irradiation can only induce a few or even no e^- transition from valence band to conduction band. Although the generated e^--h^+ pair has strong oxidizing-reduction capability, its efficacy for contaminant removal is limited due to the small quantity (**Fig. 2-2(1)**). With the band gap narrowing, the quantity of e^--h^+ pairs are raised. However, when the band gap is too narrow, the efficacy is reduced because the oxidizing-reduction capability of e^--h^+ pair is too weak even though its quantity is increased (**Fig. 2-2(5)**). Thus, a suitable band gap of the catalyst is essential for its photocatalysis efficiency (Chen, et al., 2015b).

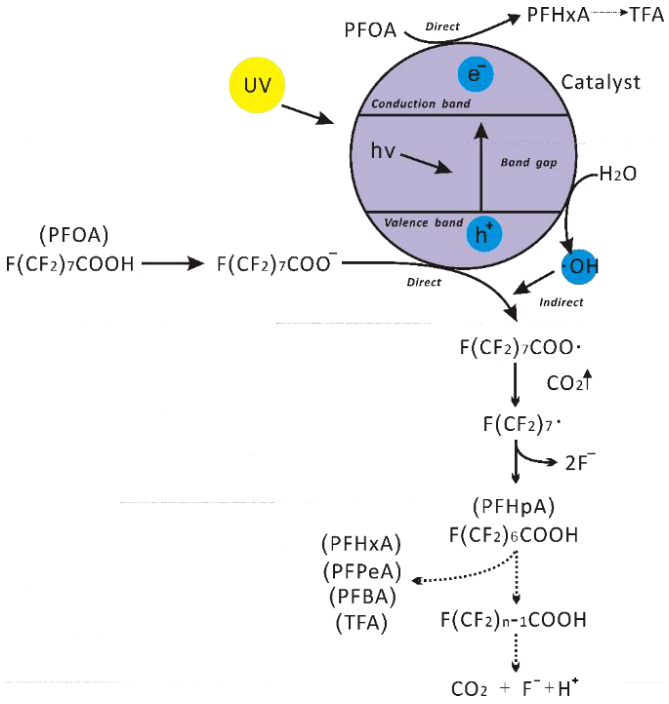

Fig. 2-1. Mechanism of heterogeneous photocatalysis process, from Xu et al. (2017).

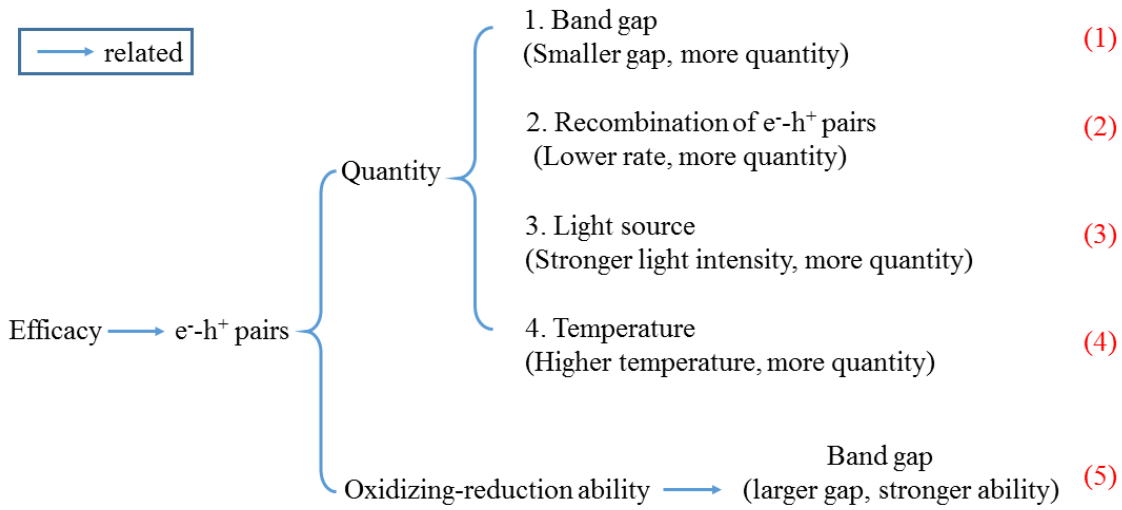

Fig. 2-2. The relationship between efficacy and e^--h^+ pairs, from Xu et al. (2017).

Once generated, the e^--h^+ pair will separate into a free e^- and a free h^+. The h^+ in the valence band has high oxidation capacity which can degrade PFAS directly (Hoffmann et al., 1995). In addition, hydroxyl radicals (•OH) were produced by h^+ reacted with H_2O and electron capture, which have a well-known degradation ability for a wide range of organic compounds through H-atom abstraction to form water. However, in the case of PFAS especially PFOA, all H-atoms have been replaced by F-atoms in the carbon chain, thus PFOA is inert to •OH attack ($k_{\bullet OH + PFOA} \leqslant 10^5\ M^{-1}\ s^{-1}$) (Kutsuna et al., 2006). Therefore, the less transformation from h^+ to •OH occurs in the photocatalytic system, the better efficacy will be achieved for PFOA degradation. Besides h^+, e^- moves to the surface of the catalyst and reacts with adsorbed water to form hydrated electrons (e^-_{aq}). PFAS molecules adsorbed on the catalyst surface can be attacked by the e^-_{aq} and degraded into shorter-chain compounds. The specific reaction mechanism is presented in **Fig. 2-2.** The heterogeneous photocatalysis process (using TiO_2 as an example) can be described in Eqs. (2.1)–(2.12) (Qu et al., 2010):

$$TiO_2 + h\nu \rightarrow TiO_2\ (h^+ + e^-) \quad (2.1)$$

$$TiO_2\ (h^+) + H_2O \rightarrow TiO_2 + \bullet OH + H^+ \quad (2.2)$$

PFOA decomposed by h^+

$$F(CF_2)_nCOOH + H_2O \rightarrow F(CF_2)_nCOO^- + H_3O^+ \quad (2.3)$$

$$F(CF_2)_nCOO^- + h^+ \rightarrow F(CF_2)_nCOO\bullet \quad (2.4)$$

$$F(CF_2)_nCOO\bullet \rightarrow F(CF_2)_n\bullet + CO_2\uparrow \quad (2.5)$$

$$F(CF_2)_n\bullet + O_2 + H_2O \rightarrow F(CF_2)_{n-1}COOH + 2F^- \quad (2.6)$$

PFOA decomposed by e^-

$$F(CF_2)_nCOOH + e^- \rightarrow (CF_2)_nCOOH\bullet + F^- \quad (2.7)$$

$$(CF_2)_nCOOH\bullet + H_2O \rightarrow (CF_2)_nHCOOH + \bullet OH \quad (2.8)$$

$$(CF_2)_nHCOOH + e^- \rightarrow C_nF_{2n-1}COOH\bullet + F^- \quad (2.9)$$

$$C_nF_{2n-1}COOH\bullet + H_2O \rightarrow C_nF_{2n-1}H_2COOH + \bullet OH \quad (2.10)$$

$$C_nF_{2n-1}H_2COOH \rightarrow C_{n-1}F_{2n-1}\bullet + \bullet CH_2 + COOH\bullet \quad (2.11)$$

$$C_{n-1}F_{2n-1}\bullet + COOH\bullet \rightarrow F(CF_2)_{n-1}COOH \quad (2.12)$$

where $F(CF_2)_nCOOH = F(CF_2)_7COOH$, $F(CF_2)_6COOH$, …, or $F(CF_2)_2COOH$.

Overall, the photo-generated e^--h^+ pairs are the main contributors to contaminant degradation so their quantity and redox capability decide the degradation efficacy of photocatalysis (Wang and Zhang, 2011). The specific efficacy influenced by e^--h^+ pairs is exhibited in **Fig. 2-2** and discussed based on the particular catalyst and ambient controlling factors.

2.3. Intermediates during photocatalysis process

During the heterogeneous photocatalysis process, the long chain PFAS will be degraded into various shorter chain compounds e.g. perfluoroheptanoic acid (PFHpA), perfluorohexanoic acid (PFHxA), perfluoropentanoic acid (PFPeA), perfluorobutanoic acid (PFBA), and trifluoroacetic acid (TFA), as the main intermediates with In_2O_3 catalysts (Li et al., 2012b). The molecular structures of the intermediates are shown in

Fig. 1-1. The degradation kinetics during the reaction period are presented in **Fig. 2-3A**, where the intermediates show a concentration increase followed by a reduction. The concentrations of all intermediates except PFHpA are under 5 mg L^{-1} at 180 min. As shown in **Fig. 2-3B**, the concentrations of PFHpA all increase initially and reach a plateau within 30-60 min followed by a decreasing trend. Of the four different catalysts tested, In_2O_3 NPNS and needle-like Ga_2O_3 show the best performance. During the photodegradation process, C-F bonds are destroyed so that the concentration of F^- as a product is increasing with the reaction time.

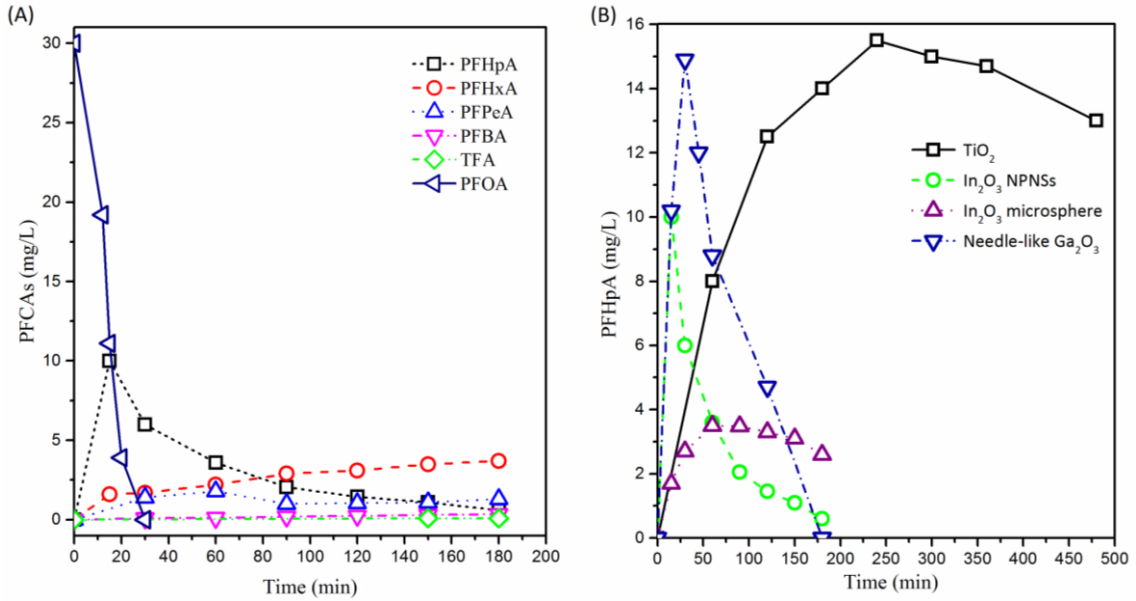

Fig. 2-3. (A) Time-dependent change of intermediates during PFOA decomposition by using In_2O_3 NPNSs. PFOA was 100% degraded within 30 min during this process. (B) PFHpA concentrations (mg L^{-1}) during the photodecomposition process by different catalysts.

2.4. Photodegradation kinetics

Based on the conclusions drawn from the literature, the photodegradation of PFAS follows the pseudo first order kinetics and the Langmuir-Hinshelwood approach can be

introduced to simulate the reaction kinetics during the photocatalysis process (Okitsu et al., 2005):

$$r = k\frac{KC}{1+KC} \quad (2.13)$$

where r is the reaction rate, k is a reaction rate constant, C is the concentration of PFAS, and K is the equilibrium absorption constant. When the chemical concentration C is of micromolar level, namely $KC \ll 1$, Eq. 2.13 can be simplified as follows:

$$r = k\,C = k_{app}\,C \quad (2.14)$$

The pseudo-first order kinetics are calculated below:

$$\ln\left(\frac{C}{C_0}\right) = -k_t\,t \quad (2.15)$$

where k_t is the pseudo time-based first-order rate constant of PFOA degradation.

The fluence-based first-order rate constant k_f ($cm^2\ mJ^{-1}$) is calculated as follows (Zhang et al., 2017):

$$k_f = \frac{k_t}{I_E} \quad (2.16)$$

where I_E is the average light intensity ($mW\ cm^{-2}$).

The half-life ($\tau_{1/2}$) of the reactants is described below:

$$\tau_{1/2} = \frac{\ln 2}{k_t} \quad (2.17)$$

The defluorination ratio of PFOA (D_f) is calculated as follows:

$$D_f = \frac{C_{F^-}}{C_0 \times 15} \times 100\% \quad (2.18)$$

where C_{F^-} is the molar concentration of fluoride ion, C_0 is the initial concentration of PFOA, and the factor of 15 corresponds to the number of fluorine ions (F^-) in one PFOA molecule.

As only very limited literature provided the I_E values in their research, k_t is the most common value for comparing among different catalyst systems in this review, therefore the data should be read in conjunction with the source and strength of light.

2.5. Efficacy of heterogeneous photocatalysis for PFAS decomposition

2.5.1. *Performance of TiO_2 and modified TiO_2 photocatalysts*

As a common semiconductor material, TiO_2 remains a favorable photocatalyst choice due to its chemical and physical stability, availability, low cost, nontoxicity and the ability to degrade a diverse range of chemicals from water (Sornalingam et al., 2016). It was reported that perfluorocarboxylic acids (PFCA) with perfluorinated carbon chain (n = 7–9) could be decomposed by more than 85% within 420 min treatment by TiO_2 photocatalysis irradiated with a 16 W (254 nm) low-pressure mercury UV-lamp (Panchangam et al., 2009). Nevertheless, due to the high recombination rate of e^--h^+ pairs and comparatively large band gap (3.2 eV) of TiO_2, the results show that k_t is very low (0.0001 min^{-1}) and $\tau_{1/2}$ is as long as 6931 min in pure TiO_2-UV system (Behafarid and Cuenya, 2012). Targeting on these drawbacks, TiO_2 modified with other elements or compounds were investigated to improve the degradation efficiency as listed in **Table 2-1**. Firstly, when using TiO_2 as the catalyst for PFOA degradation, it was observed the k_t value was enhanced 46 times at pH < 3.0 due to the presence of 0.15 M perchloric acid ($HClO_4$), compared with no acid addition (Panchangam et al., 2009). This suggests that TiO_2 at low pH has better photocatalytic ability, which is mainly due to positive surface charges of TiO_2 (pH_{PZC} = 6.2), thus TiO_2 could act as the acceptor of negatively charged e^-, which reduces the recombination of e^--h^+ pairs. On the other hand, perchloric acid is a miscible strong Bronsted-Lowry acid, which can readily dissociate in water to produce perchlorate ions with active species (E = 1.42 V), leading to the improved performance.

Secondly, a composite TiO_2 with multiwall carbon nanotube (MWCNT) and the molecularly imprinted polymer-modified TiO_2 nanotubes (MIP–TiO_2 NTs) were separately investigated and both exhibited better efficacy of PFOA photodegradation (90%

removal within 480 min; 85% removal within 480 min) compared with pure TiO_2 (Song et al., 2012). This is mainly because that the MWCNT and the nanostructure of MIP–TiO_2 NTs can improve the contact of PFOA with TiO_2 and transport e^- efficiently to reduce recombination rate of e^--h^+ pairs (**Fig. 2-2(2))**.

Thirdly, transition-metal modified TiO_2 is another significant technology to assist with decomposing PFAS in aqueous solutions. Comparing with pure TiO_2, heavy metals (e.g. Cu, Fe, Pb) and transition metals (e.g. Pt, Pd, Ag) modified TiO_2 display significant catalytic activity as shown in **Table 2-1**. Among them, the best performing photocatalysis for PFOA removal is obtained by Pt-TiO_2 (100% removal within 300 min) and the worst is by Fe-TiO_2 (60% removal within 480 min). The enhancement can be attributed to the two reasons. Firstly, the addition of metal elements on TiO_2 could reduce the band gap energy hence enhancing the quantity of e^--h^+ pairs to degrade PFOA (**Fig. 2-2(1)**) (Chen et al., 2016). Secondly, the addition of metal nanoparticles acts as electron sinks to store the excess e^- in conduction band and reduces the recombination rate of e^--h^+ pairs, so e^--h^+ pairs can be utilized fully in PFOA decomposition process (Chai et al., 2011). However, different metals have varying degrees of these capabilities, among which TiO_2 combining with Pt is the most significant method for improving the efficacy with k_t being 99% higher than that of pure TiO_2.

Table 2-1

Photocatalytic removal of PFOA by TiO_2 and its modification with other compounds or elements.

Catalyst characteristics				Energy of light		Degradation efficacy					Reference
Catalyst	Catalyst dosage ($g\ L^{-1}$)	Band gap (eV)	Specific surface areas ($m^2\ g^{-1}$)	Light source	Light intensity ($mW\ cm^{-2}$)	C_0 ($mg\ L^{-1}$)	Removal (reaction period)	k_t (min^{-1})	k_f ($cm^2\ mJ^{-1}$)	$\tau_{1/2}$ (min)	
TiO_2	0.5	3.14	22.9	400 W, λ=254 nm		50	15% (720 min)	0.0001		6931.0	(Chen, et al., 2015b)
TiO_2 with $HClO_4$	0.7	3.14	10.3	16 W, λ=254 nm	0.45	50	86% (420 min)	0.0047	1.74×10^{-4}	149.0	(Panchangam et al., 2009)
TiO_2–MWCNTs	1.6			300 W, λ=365 nm		30	90% (480 min)	0.0019		364.8	(Song et al., 2012)
MIP– TiO_2 NTs	800 $cm^2\ La^{-1}$			23 W, λ=254 nm		30	85% (480 min)	0.0036		193.0	(Wu et al., 2016)
TiO_2 with Cu	0.5			400 W, λ=254 nm		50	80% (480 min)	0.0031		224.0	(Chen et al., 2015b)
TiO_2 with Fe	0.5			400 W, λ=254 nm		50	60% (480 min)	0.0015		462.0	(Chen et al., 2015b)
TiO_2 with Pb	0.5	3.2		400 W, λ=254 nm		50	98% (480 min)	0.0086		81.0	(Chen et al., 2016)
TiO_2 with Pt	0.5	2.92	47.5	125 W, λ=365 nm	5.3	60	100% (300 min)	0.0121	0.38×10^{-4}	57.2	(Li et al., 2016)
TiO_2 with Pd	0.5	2.92	50.1	125 W, λ=365 nm	5.3	60	98% (420 min)	0.0073	0.23×10^{-4}	95.2	(Li et al., 2016)
TiO_2 with Ag	0.5	2.92	48.2	125 W, λ=365 nm	5.3	60	45% (420 min)	0.0021	0.07×10^{-4}	331.0	(Li et al., 2016)

[a] Four pieces of the prepared material (active area of 800 $cm^2\ L^{-1}$) were used.

2.5.2. *Performance of Ga_2O_3 and modified Ga_2O_3 photocatalysts*

Nanostructured gallium oxide (β-Ga_2O_3) with a wide band gap (E_g = 4.8 eV) was found to possess more powerful photocatalytic ability due to its higher oxidation-reduction potential compared with TiO_2 (E_g = 3.2 eV) (Shao et al., 2013a). It was reported that PFOA could be destroyed completely by β-Ga_2O_3 powder and demonstrated that this catalyst was superior to TiO_2 (19 times improvement in k_t value) (Zhao and Zhang, 2009). As TiO_2 possessed low activity to decompose PFOA due to the large conversion from h^+ to •OH, the occurrence of e^--h^+ pairs were investigated in the Ga_2O_3/UV system (Zhao et al., 2015a). The photocatalysis experiment was conducted containing *tert*-butyl alcohol (TBA) which is a good scavenger for the photo-induced h^+. The results show that TBA had a positive effect on the degradation of PFOA, indicating that e^- played a more important role in degrading the contaminant than h^+ in PFOA photocatalysis by Ga_2O_3.

However, for the same reason as for TiO_2, the fast recombination of e^--h^+ pairs and adsorption capacity for the pollutant also limit the photocatalytic performance of Ga_2O_3. Improvement for the catalyst should be explored to increase the degradation efficacy. Three other types of Ga_2O_3 were synthesized to enhance the photodecomposition efficiency for PFAS and the results are presented in **Table 2-2**. Specifically, sheaf-like β-Ga_2O_3 has better photocatalytic performance (100% removal of PFOA within 45 min) than commercial β-Ga_2O_3 (15% removal of PFOA within 180 min) because interface between nanoplates in the sheaf structure provides more adsorption and reaction sites with the enlarged surface area (Shao et al., 2013a). A needle-like nanostructured β-Ga_2O_3 was synthesized (Shao, et al., 2013b) which had a specific surface area of 25.95 m^2/g and a large number of pores (4–25 nm). The needle-like Ga_2O_3 exhibits wonderful photocatalytic activity for PFOA decomposition as its first-order rate constant (k_t) is 0.038 min^{-1}, 18 times higher than that of commercial Ga_2O_3 (**Table 2-2**). Besides, β-Ga_2O_3

nanorod was used as the catalyst for PFAS photodecomposition in an anaerobic atmosphere (bubbling rate of N_2 is 40 mL min^{-1}) (Zhao et al., 2015a). The results of the high rate constant (k_t = 0.043 min^{-1}) suggest that anaerobic atmosphere was better than the aerobic atmosphere for PFOA decomposition by β-Ga_2O_3 due to the high catalytic capacity of e^- in Ga_2O_3/UV system (Zhao et al., 2015a). Therefore, it is hypothesized that needle-like β-Ga_2O_3 will have better efficacy in photodegrading PFOA from water with N_2 addition.

2.5.3. *Performance of In_2O_3 and modified In_2O_3 photocatalysts*

It was reported that In_2O_3 possessed significant photocatalytic activity for PFOA decomposition, with k_t about 59 times higher than that of TiO_2 (Li et al., 2012a). Such significant photocatalytic activity of In_2O_3 catalyst comes from physicochemical properties of In_2O_3. For example, In_2O_3 has higher absorption capacity for PFOA than TiO_2. It can terminate carboxylic group of PFOA molecules tightly by forming bidentate or bridge configurations, and has stronger destroyer of e^--h^+ pairs produced during the photocatalysis process, thereby increasing the photocatalytic oxidation of PFOA (Li et al., 2012a). In addition, according to periodic table, indium metal is more electropositive (situated in period 5 and group 13) than gallium (situated in period 4 and group 13) and has a larger ionic radius (0.92 Å) than gallium (0.62 Å). These physical properties of indium could make it a better catalyst. Furthermore, •OH formation was monitored in the TiO_2/UV and In_2O_3/UV systems, separately (Li et al., 2012a; Li et al., 2012b). Similar results are achieved that the intensities of •OH generated in TiO_2 suspension are much greater than those in In_2O_3 suspension, which suggests that h^+ produced in the valence band of TiO_2 largely transformed into •OH, while less changes occur in the In_2O_3/UV

system. Thus, In_2O_3 may have better degradation efficacy for PFOA removal than TiO_2 under UV irradiation.

However, due to the similar disadvantages on the single catalyst, considerable attempts were made to improve the photocatalytic performance for PFOA decomposition, e.g. changing In_2O_3 nanostructure or modifying it with other compounds (**Table 2-2**). By changing the morphology of In_2O_3, the decomposition efficacy is improved due to the rearagment on the surface, coordination and specific surface area of the catalyst. The following five different nanostructured In_2O_3 i.e. In_2O_3 nanoporous nanospheres (NPNs), In_2O_3 microspheres, In_2O_3 nanocubes, In_2O_3 non porous nanoplates (NPs) and In_2O_3 porous nanoplates (PNPs) were synthesized as photocatalysts in previous studies (Li et al., 2013b; Li et al., 2012b). As shown in **Table 2-2**, they are all found to have better performance degrading PFOA compared with original In_2O_3. In addition, based on the reaction time for 100% PFOA removal, the degradation ability for PFOA follows the order: In_2O_3 microspheres (within 17 min) > In_2O_3 PNPs (within 30 min) = In_2O_3 NPNs > In_2O_3 NPs (within 42 min) > In_2O_3 nanocubes (within 120 min). According to the k_t and $\tau_{1/2}$ values from PFOA decomposition experiments, In_2O_3 PNPs (k_t = 0.158 min^{-1}, $\tau_{1/2}$ = 4.4 min) are better than In_2O_3 microspheres (k_t = 0.130 min^{-1}, $\tau_{1/2}$ = 5.3 min). Moreover, it is worth mentioning that the In_2O_3 PNPs, microspheres, NPNs, NPs and nanocubes have a Brunauer–Emmett–Teller surface area of 156.9, 42.3, 39, 18.9 and 13.6 m^2/g, respectively, which are directly related to their decomposition abilities. Such a relationship is explained by the fact that a high surface area could offer more adsorption and photocatalytic reaction centres, further it reduces the distance of the exaction needs to diffuse to the surface, which are beneficial for the subsequent decomposition (Li et al., 2013b).

Besides, graphene and cerium oxide (CeO_2) are also used to decorate In_2O_3 for better photocatalytic ability. As a monolayer of two-dimensional carbon atomic sheet, graphene has an excellent mobility of charge carriers, large surface, optical transparency, and chemical stability (Wang et al., 2012). Graphene could play an important role in carrying excited e^- from the semiconductor to the e^- acceptor. Thus, it has an efficient separation of photo-generated e^--h^+ pairs as reported (Li et al., 2011; Zhang et al., 2009). However, the photocatalytic activity is also dependent on the exposed surface of In_2O_3 and suitable enwrapping of graphene sheet (Li, et al., 2013a). In addition, CeO_2 has been used widely as a common co-catalyst such as CeO_2/TiO_2, ZrO_2/CeO_2 and CeO_2/Ag_3PO_4 with a positive effect on the photocatalytic activity (Dai et al., 2003). When investigating the photocatalytic decomposition of PFOA on CeO_2/In_2O_3 composite, it was previously observed that the catalyst possessed higher photocatalytic activities than pure CeO_2 or In_2O_3 (90% improvement in k_t compared with pure In_2O_3), which was probably due to the synergistic effect between CeO_2 and In_2O_3 in CeO_2/In_2O_3 composite (Jiang et al., 2016). Nevertheless, the modification of In_2O_3 to change its morphology usually needs an advanced technology, which means increasing production costs and relatively low production yield (Li et al., 2013a). On the contrary, graphene and CeO_2 have mature preparation methods and it's easier to make their combination with In_2O_3 (Jiang et al., 2016). Thus, during the evaluation of treatment technology for practical applications, both treatment efficiency and cost for the preparation of catalysts should be fully considered (Merino et al., 2016).

Table 2-2

Photocatalytic removal of PFOA by In_2O_3 and Ga_2O_3 catalysts.

Catalyst characteristics				Energy of light		Degradation efficacy					
Catalyst	Catalyst dosage (g L^{-1})	Band gap (eV)	Specific surface areas (m^2 g^{-1})	Light source	Light intensity (mW cm^{-2})	C_0 (mg L^{-1})	Removal (reaction period)	k_t (min^{-1})	k_f (cm^2 mJ^{-1})	$\tau_{1/2}$ (min)	Reference
Ga_2O_3	0.5	4.68	11.5	14 W, λ=254 nm		0.5	15% (180 min)	0.002		395.4	(Zhao and Zhang, 2009)
Sheaf-like Ga_2O_3	0.5		36.1	14 W, λ=254 nm		0.5	100% (45 min)	0.024		29.0	(Shao et al., 2013a)
Needle-like Ga_2O_3	0.5	4.57	25.95	14 W, λ=254 nm		0.5	100% (40 min)	0.038		18.2	(Shao et al., 2013b)
Ga_2O_3 with N_2	0.5			50 W, λ=254 nm	35	10	100% (90 min)	0.043	0.20×10^{-4}	16.3	(Zhao et al., 2015a)
In_2O_3	3.4	3.14	12.6	23 W, λ=254 nm		40	75% (240 min)	0.006		110.0	(Li et al., 2012b)
In_2O_3 NPNs	0.5		39.0	23 W, λ=254 nm		30	100% (30 min)	0.100		7.1	(Li al., 2012a)
In_2O_3 microspheres	0.5		42.3	15 W, λ=254 nm		30	100% (17 min)	0.130		5.3	(Li et al., 2013b)
In_2O_3 nanocubes	0.5		13.6	15 W, λ=254 nm		30	100% (120 min)	0.030		23.1	(Li et al., 2013b)
In_2O_3 NPs	0.5			15 W, λ=254 nm		30	100% (42 min)	0.073		9.5	(Li et al., 2013b)
In_2O_3 PNPs	0.5		156.9	15 W, λ=254 nm	3.2	30	100% (30 min)	0.158	8.23×10^{-4}	4.4	(Li et al., 2014)
In_2O_3 with graphene	0.5			15 W, λ=254 nm		30	100% (180 min)	0.008		86.6	(Li et al., 2013a)
β-Ga_2O_3 with N_2	0.5			50 W, λ=254 nm		10	100% (90 min)	0.043		16.3	(Zhao et al., 2015a)
In_2O_3 with 0.86% CeO_2	0.4			500 W, λ=254 nm		100	100% (60 min)	0.063		11.0	(Jiang et al., 2016)

Table 2-3

Photocatalytic removal of PFAS by different catalysts.

Catalyst	Catalyst dosage	Light source	C_0 (mg L^{-1})	Removal (reaction period)	k_t (min^{-1})	Reference
TNTs	0.2 g L^{-1}	400 W, λ=254 nm	50	59% (1440 min)	2.02	(Chen et al., 2011)
BiOCl nanosheets	0.5 g L^{-1}	10 W, λ=254 nm	0.02	100% (720 min)	0.0014	(Song et al., 2017)
Ozonation/TiO_2	25 mg h^{-1}, 0.2g L^{-1}	28 W, λ=254 nm	10	100% (240 min)	0.0042	(Huang et al., 2016)

2.5.4. *Performance of other catalysts*

In addition to the popular materials such as TiO_2, In_2O_3 or Ga_2O_3 for heterogeneous photocatalysis, other catalysts and their photocatalytic abilities are summarized in **Table 2-3**. Titanate nanotubes (TNTs) were used for the photodegradation of PFAS, which possessed high specific surface area (150 m^2 g^{-1}), photocatalytic properties, and ion-exchange capabilities (Ou and Lo, 2007). PFOA exists as an anionic compound in solutions and can be adsorbed easily via the positive charges on the TNT surfaces with the help of UV irradiation. However, although TNTs are better adsorbents than TiO_2 for PFOA removal, their photodegradation efficacy is still lower than the other catalysts as shown in **Table 2-2**. Bismuth oxychloride (BiOCl), as a family of layered ternary oxide semiconductors, possesses the valence band position around 3.6 eV, which is more positive than that of TiO_2 (3.2 eV) and In_2O_3 (2.8 eV) (Xiao et al., 2012; Xu and Schoonen, 2000). In addition, the layered structure affords BiOCl a high availability of h^+ during the photocatalysis process because it enhances the separation of photo-generated charges and decreases the surface trapping of photo-generated carriers (Li et al., 2013b). Moreover, BiOCl has a high density of surface oxygen atoms and small formation energy for its abundant oxygen vacancies that can both act as e^- scavengers delaying e^--h^+ pairs recombination and bind contaminants more strongly than normal oxide sites (Guan et al., 2013; Meng and Kaxiras, 2010). These features enable BiOCl to

perform better in PFAS photodegradation under UV irradiation (Song et al., 2017). In addition, PFOA degradation by photocatalytic ozonation (O_3) has been researched and the efficacy (100% removal of PFOA within 360 min) is better than BiOCl and TNTs (Huang et al., 2016). As O_3 has strong redox potential (2.07 eV), its reaction reduces the recombination of photo-generated e^--h^+ pairs and increases the degradation rate of PFOA by O_3 (Wang and Zhang, 2011). Furthermore, other elements such as cadmium, tin, rhodium or palladium may also function well or even become better catalyst for the photodegradation of PFOA, although they need to be examined carefully.

2.5.5. *Comparative removal performance by different catalysts*

The efficacy of heterogeneous catalysis is presented in **Fig. 2-4** based on the removal percentage and rate constant (k_t) of contaminant decomposition, respectively. **Fig. 2-4A** shows the photodecomposition efficiencies by different catalysts such as TiO_2, In_2O_3 and Ga_2O_3, and their best performing modified forms, and it can be observed that In_2O_3 has better efficacy than that of the others. With some modification in the morphology of catalyst, In_2O_3 microspheres decompose 100% of PFOA within 30 min and its k_t value is 26 times as high as the value of pure In_2O_3. In addition, Ga_2O_3 nanorod with N_2 degrades 100% PFOA within 90 min, with increased k_t value being more than 22 times higher than that of commercial Ga_2O_3. Pt-TiO_2 also has better performance as the k_t is 120 times higher than pure TiO_2. Therefore, it can be concluded that once a particular catalyst is chosen, both modifying the molecular structure and combining with other metal are effective approaches to enhance the efficacy of PFAS photodegradation. By comparing the different catalysts' performance in heterogeneous photocatalysis, the k_t values are summarized as boxplots (**Fig. 2-4B**) which show that In_2O_3 performs best

followed by Ga_2O_3. However, as a classic catalyst, TiO_2 shows the lowest ability to decompose PFAS under photo irradiation.

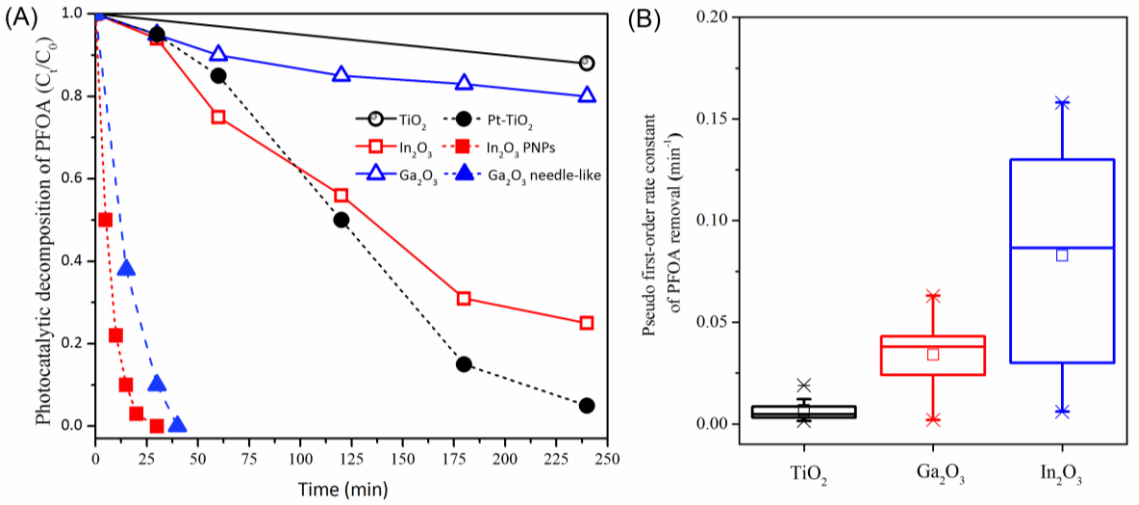

Fig. 2-4. (A) Photocatalytic decomposition of PFOA by TiO_2, Ga_2O_3, In_2O_3 and their modified forms. (B) Boxplot of pseudo first-order rate constants (k_t) of PFOA removal by three different catalysts.

Based on the k_f value provided in several systems as shown in **Tables 2-1** and **2-2**, the results show that In_2O_3 PNPs have the highest k_f value (8.23×10^{-4} cm^2 mJ^{-1}), followed by TiO_2 with $HClO_4$ (1.74×10^{-4} cm^2 mJ^{-1}). On the performance of TiO_2 with $HClO_4$, 86% removal of PFOA is achieved in 420 min but the realistic contact time for an advanced oxidation process in a WWTP is about 10 min which seemly indicates that this catalyst are not practically useful. However, it may be due to the low wattage of the lamp (16 W) and light intensity (0.45 mW cm^{-2}) used in the experiment because the k_f of TiO_2 with $HClO_4$ could be as high as 1.74×10^{-4} cm^2 mJ^{-1}, which is better than the value of TiO_2 with metal and Ga_2O_3 with N_2. Thus, these catalysts, which need long contact

time for the pollutant removal, are still worth to be researched and applied in wastewater treatment when the light intensity is promoted to some extent.

2.6. Factors affecting PFAS photocatalysis

2.6.1. *Light source*

The efficacy of heterogeneous photocatalysis is largely dependent on the photo-induced e^--h^+ pairs. So the light source absorbed by the contaminant and catalysts plays an important role in the decomposition process (**Fig. 2-2(3))** (Li et al., 2012b). The UV-vis absorption spectra of different catalysts (**Fig. 1-2**) shows that all the catalysts have obvious absorption in the UV zone ranging from 200 to 380 nm. The optical band edge of metal-TiO_2 is approximately 425.4 nm, which shows a slight red shift compared with TiO_2 (395.2 nm). This shift might be due to the quantum confinement effect defined as in the atomic realm, when the size of a particle decreases to nano scale, the decrease in confining dimension makes the energy levels discrete and widens up the band gap and ultimately the band gap energy also increases. So the catalyst needs to absorb relatively shorter wavelength light to make electronic transition happen. Thus, the optical band edge of the catalyst will shift. Similarly, among different nanostructure of In_2O_3, or between commercial Ga_2O_3 and needle-like Ga_2O_3, the optical band edge is changeable. Calculating from the optical band edge ($E_g = 1239.95/\lambda$), the band gap energies of metal-TiO_2 and TiO_2 are 2.92 and 3.14 eV, respectively. In the same way, the band gap is estimated to be 2.8, 2.72, 2.76, 2.68, 2.72, and 2.8 eV for In_2O_3 NPNs, In_2O_3 with graphene, In_2O_3 nanocubes, In_2O_3 microspheres, In_2O_3 NPs, and In_2O_3 PNPs, respectively. Significantly, the band gap energies for the commercial Ga_2O_3 and needle-like Ga_2O_3 are as high as 4.68 and 4.57 eV, respectively because their optical band edge is below 300 nm, suggesting that they need to absorb relatively light of short wavelength.

2.6.2. *Solution temperature*

So far, little research has been conducted to investigate the influence of reaction temperature on the efficacy of heterogeneous photocatalysis for PFAS removal (**Fig. 2-2(4)**). However, this influence could be learned from other treatment technologies when dealing with PFOA. For example, in the advanced oxidation technology, the reaction temperature has a high impact on the decomposition efficiency of PFAS (Lee et al., 2010). Specifically, when the reaction temperature was under 20 °C, 81% of PFOA was degraded in persulfate oxidation systems (Lee et al., 2012). However, the reaction duration was reduced to 240 min when the temperature was raised to 80 °C in the same system (Hori et al., 2008a). The results are mostly attributed to the enhancement of quantum yield (Φ) as the temperature increases so that abundant sulfate radicals are formed more quickly to degrade PFOA (Zhang et al., 2006). Moreover, in the process of photolysis, the investigation concerning the temperature effect on the PFAS degradation has been conducted (Zhang et al., 2006). The results (**Table 2-4**) indicate that higher temperature enables better performance in dealing with contaminant degradation under UV irradiation, because of the increased Φ with the rising temperature so the proportion of PFOA molecules at excited state involved in degradation process is rising. Thus, it can be reasonably speculated that when the temperature is increased during the heterogeneous photocatalysis process, the promoted Φ will support more PFOA photodegradation. On the other hand, too high temperature may cause the inactivation of catalyst as its molecular morphology could be destroyed (Williams and Brindle, 2002). However, catalysts are usually synthesized under high temperature calcination (TiO_2–MWCNT composites via 550 ℃ ; In_2O_3 porous microspheres via 500 °C; and Ga_2O_3 powder via 700 °C) and their structures are stable under 100 °C (Li et al., 2013b). Thus, it is likely that increasing solution temperature e.g. (20–30 ℃) will improve the photodegradation

efficacy and increase photocatalysis rates. Further study should be conducted to test and verify this conclusion.

Table 2-4

Photolytic decomposition, kinetic parameters and quantum yield (Φ) for PFOA degradation at different temperatures. The light source was provided by the mercury lamp (500 W) and the initial concentration of PFOA solution was 30 mg L^{-1}. The specific data are from reference (Zhang et al., 2016).

T (°C)	Decomposition condition ($C\ C_0^{-1}$)					$\tau_{1/2}$ (min)	k_t (min^{-1})	Φ (sec^{-1})
	30 min	60 min	90 min	120 min	180 min			
25	0.78	0.68	0.55	0.4	0.35	99.9	0.007	1.55×10^{-4}
45	0.67	0.48	0.3	0.25	0.17	51.8	0.013	2.99×10^{-4}
65	0.35	0.05	0.03	0.01	0	17.3	0.040	8.93×10^{-4}
85	0.1	0.02	0	0	0	9.0	0.077	1.72×10^{-3}

2.6.3. *Solution pH*

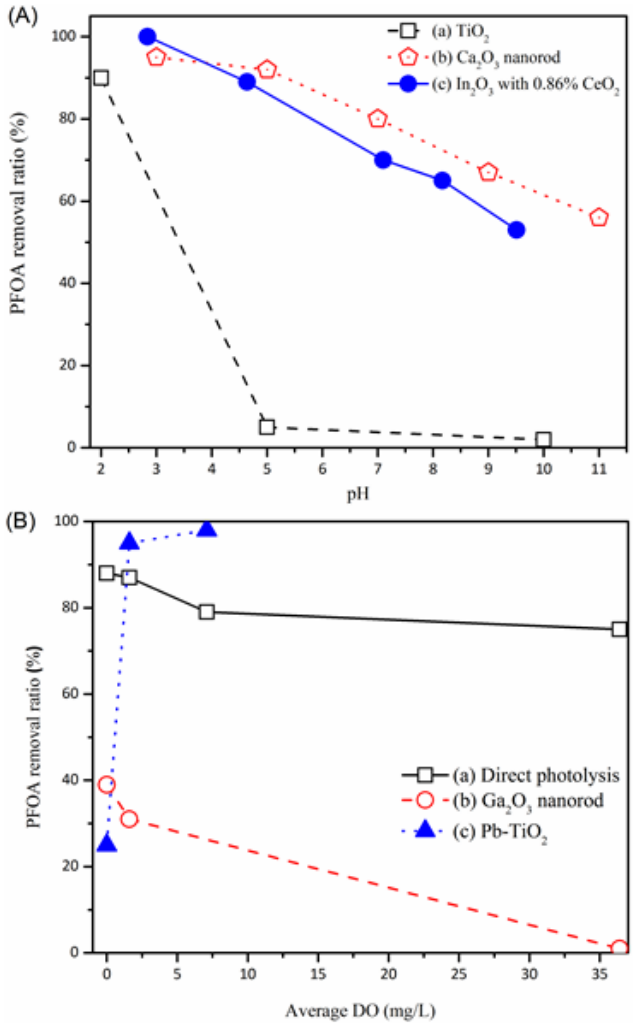

Fig. 2-5. (A) Influence of the initial pH on PFOA degradation by various photodecomposition methods. (B) Influence of DO on PFOA degradation by various photodecomposition methods. Specific experimental parameters were shown in **Table 2-5**.

The pH affects the dissociation of ionizable chemicals such as PFOA in solution and consequently, influences their photocatalytic performance. Thus, the photodecomposition of PFOA is evaluated at various initial pH conditions by the three main catalysts as shown in **Fig. 2-5A**. Under TiO_2-UV photodegradation, PFOA exhibits 90% removal at pH 2, which drops significantly to 5% when pH is increased to 5. It

further decreases to 2% under alkaline condition at pH 10. Such a trend is related to the fact that the pH point of zero charge (pH_{PZC}) of pure TiO_2 is 6.2 (Chou and Liao, 2005). Therefore, the surface of TiO_2 catalyst is positively charged at pH < pH_{PZC}, and negatively charged at pH > pH_{PZC}. On the other hand, the pK_a of PFOA is around 2.8 (Burns et al., 2008; Goss, 2007), so PFOA will ionize and occur primarily as perfluorocarboxylic anions even at acidic pH values, e.g. approximately 50%, 91% and 99% ionization at pH 1, 2 and 3 respectively. As a result, the acidic condition of pH 2 creates the optimum environment for the interactions between the positively charged TiO_2 and the substantial amount of ionized PFOA, while at the same time there are significant interactions between TiO_2 and the negatively charged e^- hence inhibiting e^--h^+ pair recombination. Furthermore, a significant impact of initial pH on the catalytic decomposition for PFOA on both β-Ga_2O_3 nanorod and In_2O_3 with 0.86% CeO_2 has been investigated (Jiang et al., 2016). As shown in **Fig. 2-5A**, with the initial pH increasing, the photocatalytic degradation ratio of PFOA gradually decreases. For these two different catalysts, there are similar reasons accounting for this trend. In the β-Ga_2O_3 nanorod photodegradation process, it can be explained that the pH_{PZC} of pure Ga_2O_3 is pH 9 (Kosmulski, 2001) and the lower the pH value is, the more positively charged the β-Ga_2O_3 surface will become. Due to the function of Coulombic attraction, the concentration of PFOA anions adsorbed on the surface of the catalyst is high at low pH condition, which promotes photocatalytic decomposition efficacy. For In_2O_3, as the pH_{PZC} of pure In_2O_3 is 8.7 (Kosmulski, 2001), the surface of In_2O_3 is positively charged when the pH is lower than 8.7, so perfluorocarboxylic anions will interact strongly with In_2O_3 with 0.86% CeO_2 by electrostatic interaction, leading to a high PFOA removal ratio. In summary, for the three major catalysts used in the photocataylsis process, acidic pH is favourable and positively improves the efficacy of PFAS decomposition.

Table 2-5

Specific parameters of the pH and DO influence experiments.

Fig. 2-5A	Light intense (W)	C_0 (mg L^{-1})	Reaction period (min)
(a) TiO_2[a]	16/6 (pH=2/4, 10)	50	360
(b) Ca_2O_3 nanorod	35	10	180
(c) In_2O_3 with CeO_2	500	100	60
Fig. 2-5B			
(a) Direct photolysis	20	1	180
(b) Ca_2O_3 nanorod	15	40	180
(c) Pb-TiO_2	400	50	60

[a] $HClO_4$ was added at acid condition.

2.6.4. *Dissolved oxygen*

DO is another interesting factor for the photodecomposition of PFAS which have been investigated (Chen et al., 2016). The effect of DO on photodecomposition of PFOA were studied by using N_2, no gas, air and O_2 supply to create DO values of 0, 1.6, 7.1 and 36.4 mg L^{-1}, respectively (Giri et al., 2012). In the direct photolysis process, PFOA removal by these four different DO conditions is presented in **Fig. 2-5B** with the highest removal being observed at 0 mg L^{-1} of DO. With the DO value increasing, the photodegradation efficacy is decreasing. When the DO reaches 36.4 mg L^{-1}, the removal is 14% lower than the value under 0 mg L^{-1} of DO. It can be explained that in the direct photolysis process, reactive oxygen species such as •OH are not essential to decompose PFAS, which means that direct rather than indirect UV photolysis is the main degradation pathway (Schröder and Meesters, 2005). Therefore, abundant O_2 in solution may lead to reactive oxygen species formation and result in the indirect reaction occurring. A similar tendency is also found in the photocatalysis process with the catalyst Ga_2O_3 nanorod (**Fig. 2-5B(b)**) where 39% PFOA removal is observed with no DO but almost no decomposition happens when DO is 36.4 mg L^{-1} in the solution. The results are due to the fact that in the Ga_2O_3 nanorod system, e^- is the main destroyer in the anaerobic atmosphere; with increasing DO, h^+ gradually becomes more abundant with less e^-. However, as already

proved, e^- has much better degradation ability for PFOA than h^+ in the Ga_2O_3-UV system (Shao et al., 2013a). Therefore, in aerobic solution, as the main participant of h^+ in PFOA degradation, the photodegradation efficacy is expected to decline.

Interestingly, an opposite trend of PFOA removal with DO in photocatalysis by the catalyst Pb-TiO_2 has been also reported (Chen et al., 2016). PFOA removal ratio is 0.25 when the solution is sparged with N_2 (DO = 0 mg L^{-1}), which substantially increases to 0.95 without any gas sparging (DO = 1.6 mg L^{-1}) and further increases to 0.98 when the solution is purged with air (DO = 7.1 mg L^{-1}). This distinct difference may be explained by h^+ performing better in TiO_2-UV system than in Ca_2O_3 system. In addition, the presence of O_2 could inhibit recombination rate of e^--h^+ pairs. Furthermore, as Pb serves as a trap to catch up e^-, the recombination of e^--h^+ pairs are inhibited. Thus, increasing DO value enhances the decomposition efficacy for PFAS removal in the Pb-TiO_2/UV system. In summary, DO effect on PFOA photocatalysis is highly varied and complex depending on performance of e^--h^+ pairs. DO has a negative effect of PFOA degradation when e^- is in large quantity with strong reduction ability or the direct photolysis under UV light is the main process. Otherwise, if h^+ performs well and the recommendation is inhibited, DO has a positive effect. Besides, it is significant to mention that the DO influence on the In_2O_3/UV system is never to be investigated. Based on the previous study (Li et al., 2012b), h^+ was playing an important role in degrading PFOA so it is reasonable to predict that DO has a positive effect on the efficacy. However, further extensive research is needed to explore the mechanism.

2.6.5. *Dissolved organic matter*

DOM is normally considered to be a significant factor that affects photodegradation process due to the generation of DOM-derived oxidative intermediates

or their physicochemical quenching effects (Lyu et al., 2015). Therefore, to assess the feasibility of three main catalysts (TiO_2, In_2O_3, Ga_2O_3) to degrade PFAS in wastewater, the photocatalysis efficacies for PFOA removal in WWTP effluent are summarized in **Fig. 2-6A** (Li et al., 2013b; Li et al., 2012b). It can be observed that PFOA decomposition in wastewater under UV irradiation is obviously retarded compared with the degradation efficacy in pure water and the photocatalytic ability under UV light followed the order as needle-like Ga_2O_3 > In_2O_3 > TiO_2. Specifically, the needle-like Ga_2O_3 degraded 100% PFOA in wastewater which was spiked with 500 μg L^{-1} of PFOA within 180 min however this reaction period could be shortened to 40 min when the contaminant was from pure water. The same phenomenon is also observed in the In_2O_3 photocatalysis process. In pure water, 69% PFOA could be degraded by In_2O_3 within 180 min when the experimental solution was spiked with 100 μmol L^{-1} of PFOA; however, this value was decreased to only 10% when the contaminant was from wastewater. Such difference in PFOA degradation is likely due to the presence of DOM in high concentrations in real wastewater. These results are attributed to the fact that DOM most likely occupies the surface of the catalysts instead of PFOA, leading to less adsorption capacity of this pollutant. As a result, the PFOA photodecomposition is largely inhibited and the efficacy is reduced.

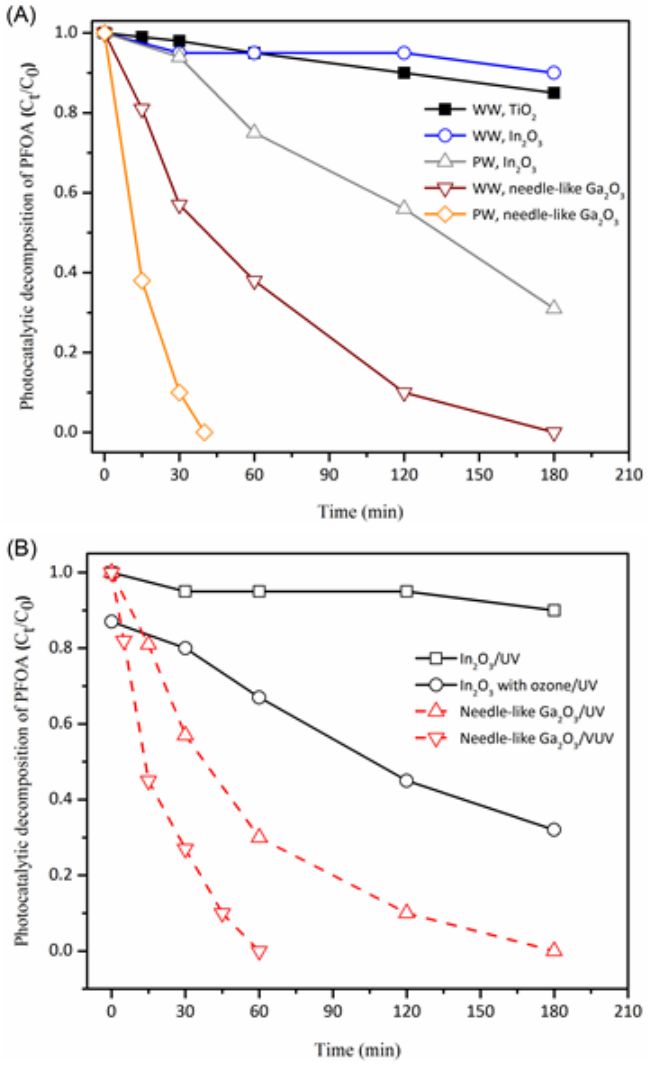

Fig. 2-6. (A) Kinetics of PFOA photocatalysis in wastewater (WW) and pure water (PW) by catalysts of TiO_2, In_2O_3, and needle-like Ga_2O_3 under UV irradiation. The data were from references (Li et al., 2012a; Shao et al., 2013a; Shao et al., 2013b). (B) PFOA degradation in WW by In_2O_3 and Needle-Ga_2O_3 with some modifications for efficacy improvement.

Two significant methods were examined to solve this problem (Li et al., 2012a; Shao, et al., 2013b). Firstly, ozone gas (~8 mg L^{-1} h^{-1}) was added in the wastewater photodegradation by In_2O_3/UV compared with no ozone gas addition and the results are shown in **Fig. 2-6B**. The ozone addition largely promotes the efficacy of PFOA removal

in wastewater, due to the fact that the addition of ozone could promote abundant photo-produced h^+ to react with PFOA rather than recombining with photo-produced e^- (Zsilák et al., 2014). Thus, the recombination of e^--h^+ pairs is inhibited so the photocatalytic removal of PFOA is accelerated. Secondly, needle-like Ga_2O_3 in combination with vacuum UV (VUV) irradiation (λ = 185 nm) was conducted and the efficacy is exhibited in **Fig. 2-6B** with its k_t value of 0.059 which is much higher than the value in the needle-like Ga_2O_3/UV system. This is because that VUV light has a shorter wavelength of 185 nm and higher energy which could eliminate the adverse influence of DOM. Some novel catalysts such as In_2O_3 microspheres, In_2O_3 PNPs, and Pt-TiO_2 which have high PFOA degradation performance in water have not been examined in treating real wastewater, hence the potential negative influence of DOM should be further investigated.

2.7. Practical applications of PFOA degradation

WWTP is considered to be the most significant source of PFAS in the aquatic environment because traditional treatment technologies in WWTP cannot sufficiently remove PFAS from wastewater influent (Sinclair and Kannan, 2006). For example, Monte Carlo simulation was used to calculate the likely range of PFAS emissions from WWTP in South Korea, and the model showed that the emission of 13 PFAS to the environment (wastewater + sludge) was 4.03 ton y^{-1}. Among them, the major compounds were 1.19 ton y^{-1} of PFOA and 1.01 ton/y of PFOS (Kwon et al., 2017). They also reported that wastewater from WWTP was identified as a major emission source, accounting for 65% of the total PFAS emission. Thus, there is an urgent need to improve wastewater treatment technology for effective PFAS removal in order to prevent serious water pollution in the environment.

Wastewater is highly complex in chemical composition due to the presence of many organic and inorganic substances e.g. DOM and bicarbonate. DOM is also a significant scavenger of oxidants and reductants as discussed above. Under realistic conditions, the impact of DOM for PFAS removal will be much worse. For bicarbonate in wastewater, as it has the same carboxyl group as PFOA, the competition between them will reduce the amount of PFOA adsorbed on catalyst surface hence its photodegradation. Thus, factors need to be considered for the practical application of PFOA degradation. Firstly, the photocatalytic degradation of PFOA can be conducted in a tubular quartz vessel reactor under UV irradiation. A low-pressure mercury lamp (15 W) emitting 254 nm UV light is set up which can be not only provide adequate light intensity (3–6 mW cm^{-2}) but also energy-saving when dealing with wastewater (Li et al. 2014). Secondly, needle-like Ga_2O_3, In_2O_3 PNPs, or In_2O_3 microspheres can be used as the catalyst because needle-like Ga_2O_3 has been proven to be efficient (100% PFOA removal within 180 min) dealing with wastewater. In_2O_3 PNPs or In_2O_3 microspheres is able to degrade FPOA in pure water efficiently (100% PFOA removal within 30 min and 17 min, respectively), so it is worth to test their performance in wastewater. Thirdly, during the degradation process, controlling factors should be set up as follows for the best efficacy: room temperature to save energy; acidic solution (pH = 4) to promote high adsorption of PFAS and performance of e^--h^+ pairs; ozone addition to eliminate the adverse influence of DOM; contact period of 60-180 min for the complete degradation of PFAS. Furthermore, as the boiling point of PFOA is 189 °C, heat treatment (e.g. 200 °C) can be applied for the regeneration of the catalyst to be efficiently reused.

2.8. Conclusions

A variety of heterogeneous photocatalysis technologies to effectively decompose PFAS have been reported, thanks to the function of photo-induced e^--h^+ paris and different intermediates are produced during the reaction process. TiO_2, Ga_2O_3, and In_2O_3 are the main catalysts that have been studied. In addition, modification to the morphology or structure of the catalysts with certain materials can effectively improve the degradation efficacy of PFAS under UV irradiation. Environmental factors such as light source, reaction temperature, solution pH, DO and DOM are found to affect the photodecomposition process. Specifically, the catalysts could absorb the light source in the wavelength of 200–380 nm abundantly. Acidic solution is favorable for the majority of catalysts when degrading PFAS due to the function of Coulombic attraction. Increasing reaction temperature (< 100 °C) promotes the removal efficacy because of the higher proportion of PFOA molecules at excited state. In addition, DO shows both positive and negative effects depending on the performance of e^- and h^+ in degrading PFOA. DOM mostly plays a negative role during PFAS decomposition. During wastewater application, PFOA photodegradation is reduced in comparison with pure water, and needle-like Ga_2O_3 photocatalyst has better performance than In_2O_3 and TiO_2. Therefore, it is worthwhile to further investigate these catalysts under different conditions and explore the photocatalytic mechanism deeply. For example, which catalyst has the better performance on PFAS removal under similar external condition? In addition, peroxymonosulfate (PMS) is now drawing great attentions by scientists as its strong oxidizing activated by UV light. While the effect of metal oxide coupled with PMS on PFAF photodegradation need to be evaluated in the lab. And the interaction between sulfate radicals ($SO_4^{\bullet-}$) and photogenerated hole and electrons during photocatalysis are worthwhile to be discussed.

Chapter 3. Materials and methods

3.1. Introduction

This chapter describes the chemicals and materials used for conducting experiments, the equipment used for measuring compounds quantitatively and the experimental setups.

3.2. Chemicals

The chemicals used in this research with their supplier and purity are listed in **Table 3-1**. All solutions were prepared using Milli-Q water (18.2 MΩ cm, Milli-pore Corp., Billerica, MA). All chemicals were used as received.

Table 3-1

List of chemicals and materials.

Compound	Supplier	Purity
Methanol	Fisher Scientific	Optima LC/MS grade
Ultrapure water (Milli-Q)	Merck Millipore	18.2 MΩ, 3 ppb TOC
PFOA	Sigma-Aldrich	95%
PFHpA	Sigma-Aldrich	99%
PFHxA	Sigma-Aldrich	⩾ 97%
PFPeA	Sigma-Aldrich	97%
PFBA	Sigma-Aldrich	98%
PFPrA	Sigma-Aldrich	97%
TFA	Sigma-Aldrich	⩾ 99%
TiO_2 (P25)	Degussa	≥ 99.5%
Ga_2O_3	Sigma-Aldrich	≥ 99.99%
In_2O_3	Sigma-Aldrich	99.99%
CeO_2	Sigma-Aldrich	99.99%
CdS	Sigma-Aldrich	99.99%
Oxone	Sigma-Aldrich	97%
tert-butanol (*t*-BuOH)	Sigma-Aldrich	≥ 99.5%
Disodium ethylenediaminetetraacetate (EDTA-Na_2)	Sigma-Aldrich	≥ 97%
Benzoquinone (BQ)	Sigma-Aldrich	≥ 98%

3.3. Characterization techniques

3.3.1. *Powder X-ray diffraction*

Powder X-ray diffraction (XRD) patterns were collected using a Bruker D8 Discover diffractometer using Cu Kα radiation, in the scattering angle 2θ range 15–90°. About 0.5 g power samples were used for XRD analysis.

3.3.2. *UV–visible absorbance*

UV–visible absorbance spectra of the pollutant and catalyst solutions were collected using a Shimadzu 1700 UV–Vis spectrophotometer operating in the wavelength range 190–800 nm. The scan speed was selected as high speed.

3.3.3. *Scanning electron microscope*

A Zeiss Supra 55VP scanning electron microscope (SEM) (10 kV) was used to examine the morphology and elemental composition of the catalysts. The electron high tension (EHT) was 15 kV and the Ext I Monitor was 125.2 μA.

3.3.4. *Zeta potential values*

Zeta potential values were measured using 50 mg of catalyst in 100 mL of 1 mM KCl solution at different pH. Samples were pre-equilibrated for 48 h. Zeta potential values were determined using a Nano-ZS Zeta-seizer (Malvern Instruments Limited, UK, and Model: ZEN3600). The pH values were adjusted using 0.1-1 M HNO_3 or NaOH as required. Zeta potential was measured three times at each pH (50 scans each time) and the average and standard deviation was calculated.

3.4. Quantitative determination by LC-MS/MS

3.4.1. Sample preparation in water and wastewater

All experiments were conducted in a cylindrical reactor filled with 200 mL of PFOA solution (50 mg L^{-1}) and mixed continuously using magnetic stirring. The concentration of 50 mg L^{-1} was comparatively high, compared with the concentrations of PFOA occurring in the most contaminated water; it was also used as the initial concentration in a previous study (Chen et al., 2015b). PFOA aqueous solution was

prepared by diluting the stock solution in the beaker. The diluting water could be ultra-pure water or real water samples (influent and effluent) taken from a municipal sewage treatment plant in Sydney, Australia. The catalysts were added and stirred for 0.5 h under darkness to achieve adsorption-desorption equilibrium. After the treatment of photolysis, the samples were taken out by syringe and went through the filter (Whatman, FP 30/0.2 μm), then stored in a vial for instrument analysis.

3.4.2. Instrumental analysis and quantification

A triple quadrupole ultra-high-performance liquid chromatography tandem mass spectrometer (UHPLC-MS/MS; LC/MS 8060, Shimadzu) equipped with a binary pump and Shim-pack column (1.6 μm, 2.0 mm × 50 mm) was used for the quantitative qualitative analysis of PFOA and its degradation products (PFHpA, PFHxA, PFPeA, PFBA, PFPrA, TFA). The LC and MS/MS setup conditions were provided in **Table 3-2**.

Table 3-2

General UHPLC and MS/MS source conditions.

LC and MS/MS source	Set
Analytical column	Kinetex EVO C18 5 μm 100 × 2.1 mm
Column Temperature	30 ℃
Sample Temperature	5 ℃
Injection Volume	1 μL
Mobile Phase A	Milli-Q water
Mobile Phase B	Methanol
Polarity	Negative
Nebuilizing Gas Flow	3.0 L min^{-1}
Drying Gas Flow	10.0 L min^{-1}
Heating Gas Flow	10.0 L min^{-1}
Interface	ESI
Interface Temperature	300 ℃
Q1 Pre-rod Bias	5.0 V
Q3 Pre-rod Bias	5.0 V

The mobile phase A was Milli-Q water with and mobile phase B was methanol. The flow rate was 0.4 ml min^{-1} and the injection volume was 1 μL. The elution gradient of PFOA analysis method was initiated with 50% B for 2.5 min, then 100% B for the next

1 min, followed by 50% B for another 1.5 min. The total method run time was 5 min as shown in **Table 3-3**. Similarly, the elution gradient of simultaneously 8 PFAS analysis method was presented in **Table 3-4**. The mass spectrometer source was operated using electrosprayionization in negative mode (-ve ESI). Nitrogen was used as the nebulizing and dissolvating gas. Argon was used as the collision gas. The system was operated in the multiple reaction monitoring mode (MRM) and under optimized mass spectrometry parameters. For PFOA, m z^{-1} 169.1 and m z^{-1} 219.0 are used as the qualitative ions and m z^{-1} 99 369.0 is used as the quantitation ion to avoid mass interference (Hansen et al., 2001; Martin et al., 2004). The tandem mass spectrometry operating conditions of the target 7 compounds are listed in **Table 3-5**. In addition, the MRM mass chromatograms of the 7 PFAS were exhibited in **Fig. 3-1**. Quantification was performed using internal standard method with a five point calibration curve spanning the range of anticipated analyte concentrations in samples.

Table 3-3

LC time program of PFOA method.

Time (min)	Mobile Phase A (%)	Mobile Phase B (%)	Flow rate (µL min^{-1})
0.25	50	50	0.4
2.50	0	100	0.4
3.50	0	100	0.4
3.51	50	50	0.4
5.00	–	–	–

Table 3-4

LC time program of simultaneously seven PFAS method.

Time (min)	Mobile Phase A (%)	Mobile Phase B (%)	Flow rate (µL min^{-1})
0.20	50	50	0.4
0.30	30	70	0.4
2.30	10	80	0.4
2.50	0	100	0.4
5.50	0	100	0.4
5.60	50	50	0.4
7.00	–	–	–

Table 3-5

The target compounds of PFAS analysed, and their MS/MS parameters.

Acronym	Name	Formula	MS/MS mass transition	Cone voltage (V)	Collision energy (eV)
PFOA	Perfluorooctanoic acid	$C_7F_{15}COOH$	412.90 → 369.00	20	10
PFHpA	Perfluoroheptanoic acid	$C_6F_{13}COOH$	363.00 → 319.00	2.6	22
PFHxA	Perfluorohexanoic acid	$C_5F_{11}COOH$	313.00 → 269.00	2.6	8.4
PFPeA	Perfluoropentanoic acid	C_4F_9COOH	262.55 → 219.10	2.6	8.4
PFBA	Perfluorobutyric acid	C_3F_7COOH	212.20 → 169.10	2.6	10.0
PFPrA	Pentafluoropropionic acid	C_2F_5COOH	162.9 → 118.8	12.0	7.0
TFA	Trifluoroacetic acid	CF_3COOH	112.9 → 68.9	12.0	7.0

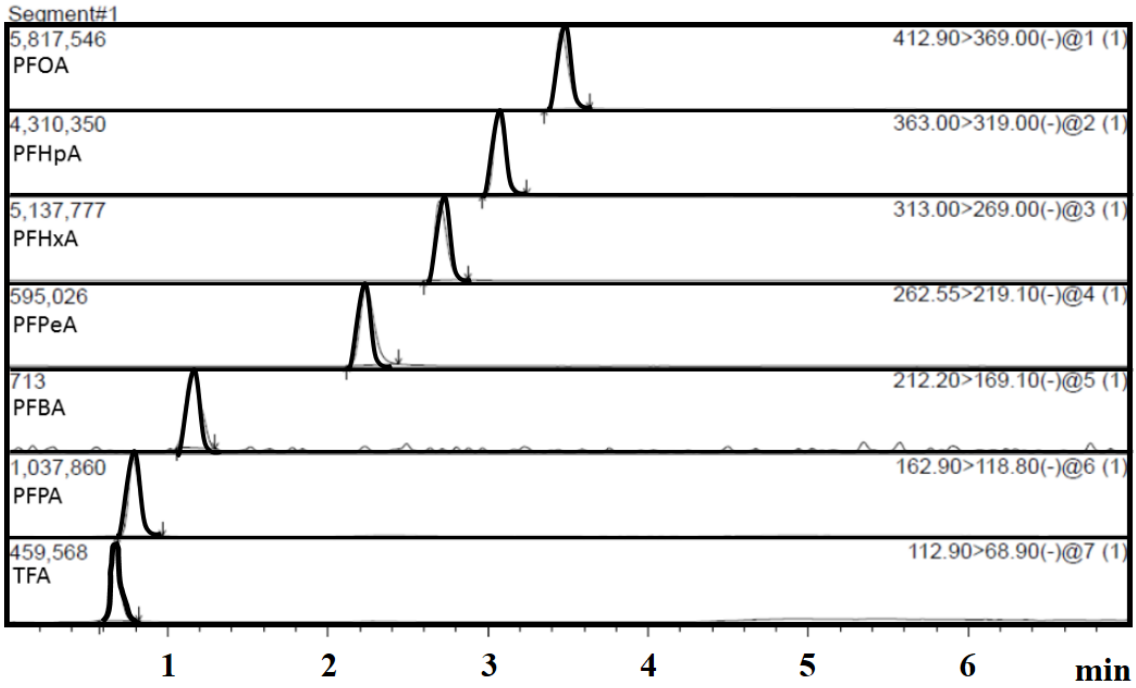

Fig. 3-1. Chromatography of seven PFAS detected by UHPLC-MS/MS.

The pH condition would affect the intensity of the peaks during the PFAS determination by LC-MS/MS. As shown in **Fig. 3-2**, the peak intensity of PFOA was very low at pH 2, while increased sharply at pH 3, and kept stable at comparatively high level at the pH ranging from 3 to 10. Similar situations were also found in the quantification of other PFAS, i.e. PFHpA, PFNA, and PFDA by LC-MS/MS. The peak intensity was

increased with the pH increasing from 2 to 5 and did not change obviously during pH 5–10. Thus, PFAS got lower intensity at extreme acid and higher intensity over pH 5.

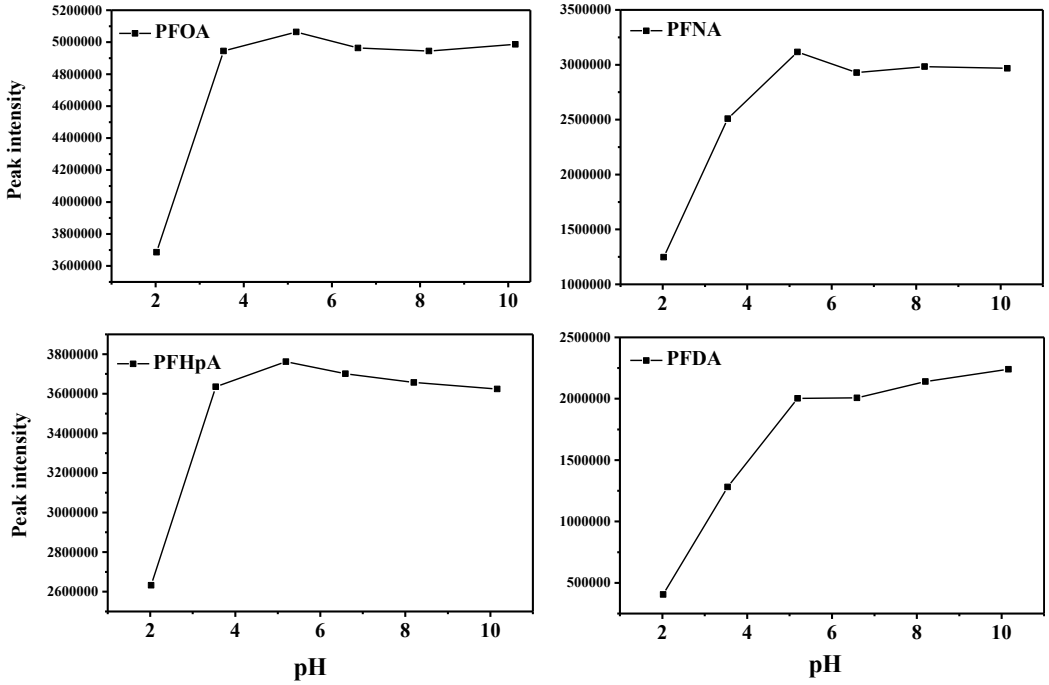

Fig. 3-2. The peak intensity of PFAS under different pH conditions by LC-MS/MS analysis.

3.4.4. *Limitation, accuracy and recovery of the analytical method*

The minimum value was selected as 2 μg L^{-1} with a signal/noise (S/N) value exceeding 25 and the upper limit of linearity was determined to be 50 μg L^{-1} for PFOA analysis. Thus, its linear range of PFOA analysis was 2–50 μg L^{-1} (2, 5, 10, 20, and 50 μg L^{-1}) and the calibration curve regression coefficient consistently exceed 0.99. And LOD and LOQ for PFOA analysis in LC-MS/MS were 0.23 and 0.77 μg L^{-1}, respectively. Similarly, the other 13 PFAS conditions are presented in **Table 3-6**.

Besides, PFOA standard recoveries were used to calaulate the accuracy of the analytic method. Deionized water was evaluated as matrix for the calibration of liquid materials. Three levels of concentrations (2, 10, and 50 μg L^{-1}) of PFAS were injected

into the matrix. After pre-treatment and quantitation by LC-MS/MS, the recoveries were achieved by comparing the value of directly injection of PFAS standards at the same concentration. The results of five repeating recovery experiments suggests that all the recoveries in deionized water reached more than 90% and RSD were less than 5%. Therefore, recoveries of 95-105% in this study should be considered to be adequate accuracy for PFOA determination from environmental samples.

A further investigation of inter-day precision, calculated as the relative standard deviation (RSD) of 25 repeated injection of PFOA calibration, were conducted and the range was from 5% to 8%. In addition, intraday precision (within-run), calculated as the RSD of 5 repeated injection of three concentration PFOA standards, respectively, within one day, ranged from 3.6% to 5.4%. Besides, using the LC-MS/MS detection method for PFOA analysis, the replicate analyses of PFOA standards with the concentration of 2, 5, 10, 20, and 50 μg L^{-1} and the data were conducted over a one-month period to assess the ruggedness and reliability of the method. The linearity slopes in each day ranged from 90% to 110%, with the RSD less than 5%. Thus, the results proved that the analytic method by LC-MS/MS was sufficiently sensitive, accurate, and precise for PFOA determination.

Table 3-6

Analytical data for PFAS standards using UHPLC-MS/MS method.

Compound	Working range (μg L^{-1})	r^2	LOD (μg L^{-1})	LOQ (μg L^{-1})
PFOA	2—50	0.9991	0.23	0.77
PFHpA	2—50	0.9983	0.41	1.38
PFHxA	2—50	0.9986	0.29	0.95
PFPeA	2—50	0.9990	0.44	1.65
PFBA	2—50	0.9981	0.58	1.94
PFPrA	2—50	0.9926	0.44	1.45
TFA	2—50	0.9935	0.59	1.98

3.4.3. *Elimination of the background contamination*

However, PFOA could be found existing in the HPLC system, such as solvent delivery tubing, filters, fittings, online degassers, pump heads and injection valve components, while trace levels of PFOA can leach out. In addition, the contamination was also generated from the mobile phase and fluid tank (Rogatsky et al., 2017). Thus, this problem should be taken into consideration during the quantitation of PFAS with HPLC systems. In this study, rinsing HPLC system with solvents for a long time is used as a significant method to control the background contamination. **Fig. 3-3** indicates that after 12 h rising with methanol at the flowrate of 1.0 mL min^{-1}, the peak from background PFOA (pure water injection) has obviously decreased compared with the conditions before rising. And the peak intensity of blank was stable during a batch of sample injections, which was lower than 10^4. Thus, the concentration of PFOA caused by HPLC systems could be ignored due to the high intensity of PFOA in samples. Other PFAS were not obviously affected by HPLC system and the optimal chromatograms of 12 PFAS are shown in **Fig. 3-1**, with clearly peak of each compound.

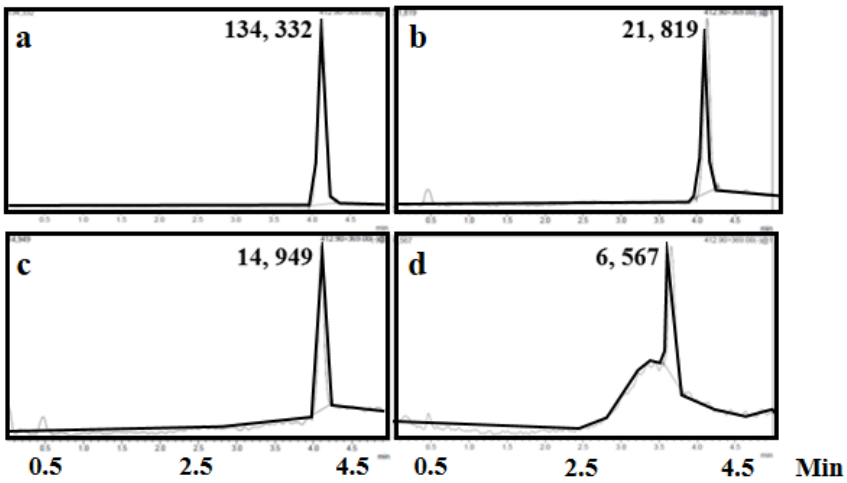

Fig. 3-3. The peak of POFA reduced after rinse several times. (a) – (d) was rinsed from the beginning to 3 h, 6 h and 10 h, respectively.

3.5. Experimental reactor and light sources

A cylindrical reactor vessel was filled with PFOA aqueous solution of 200 mL and different initial PFOA concentrations (50 ng L^{-1}, 50 µg L^{-1}, 50 mg L^{-1}) at room temperature. The solid catalysts were dispersed in PFOA solution, to which PMS was then added to initiate the reaction with continuous stirring for 30 min under darkness. The effect of solution pH on PFOA photodegradation was assessed by repeating experiments at pH 3, 5, 7 and 10. Light irradiation was provided by three separate lamps: UV light (wavelength = 254 nm) from a 32 W low-pressure UV lamp (Cnlight Co. Ltd., Shanghai, China), UV light (wavelength = 185 nm) from a 32 W low-pressure UV lamp (Cnlight Co. Ltd., Shanghai, China), and visible light (wavelength = 400–800 nm) from a 300 W xenon lamp (Nbet Co. Ltd., Beijing, China). The irradiation intensity of UV light (254 nm) was 1.71 mW cm^{-2} as measured by an UV intensity meter (ST-512). The centre of the reactive solutions was 829.6 mW cm^{-2} for the xenon light source as measured by a light intensity meter (HSX-F500). The wavelength spectrums of UV light (254 and 185 nm) and visible light were exhibited in **Figs 3-4**, **3-5** and **3-6**, respectively.

During photodegradation, the lamps were placed 5 cm above the liquid surface of the reactor and the solution was well mixed by magnetic stirring. At regular time intervals, aliquots of the sample were taken using a syringe and filtered through a filter (Puradisc syringe filter, 0.2 µm, Whatman) before analysis. All experiments were conducted in triplicate. **Fig. 3-7** represents the overall process of the experiments.

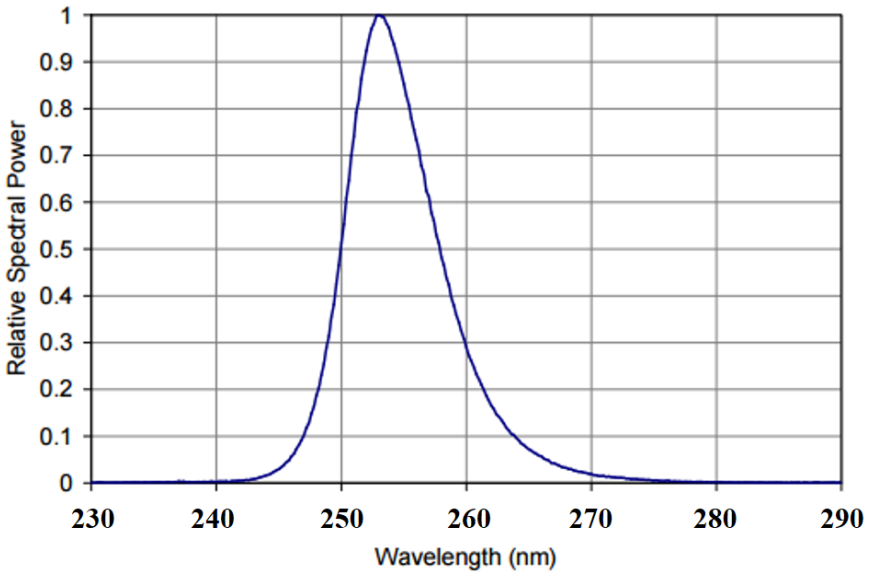

Fig. 3-4. Wavelength spectrum of UV light (254 nm) from a 32 W low-pressure UV lamp (Cnlight Co. Ltd., Shanghai, China).

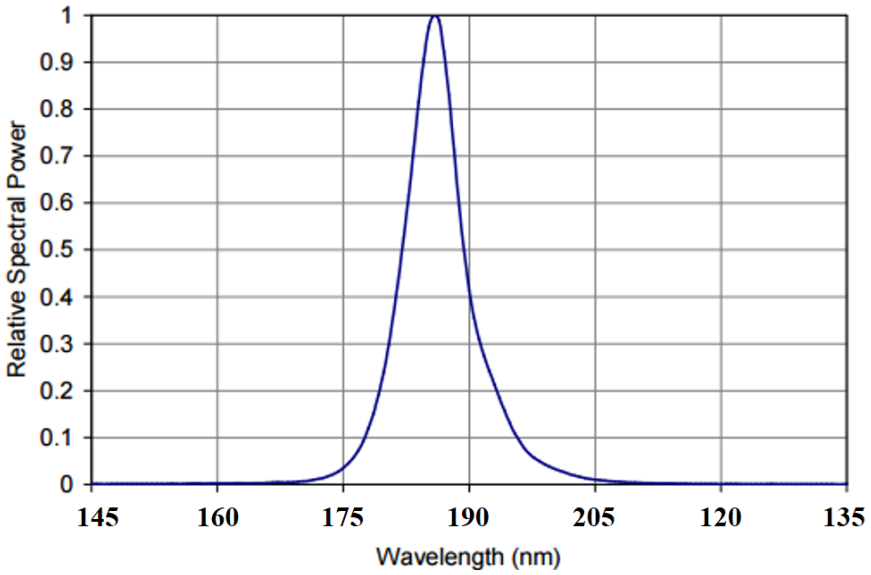

Fig. 3-5. Wavelength spectrum of UV light (185 nm) from a 32 W low-pressure UV lamp (Cnlight Co. Ltd., Shanghai, China).

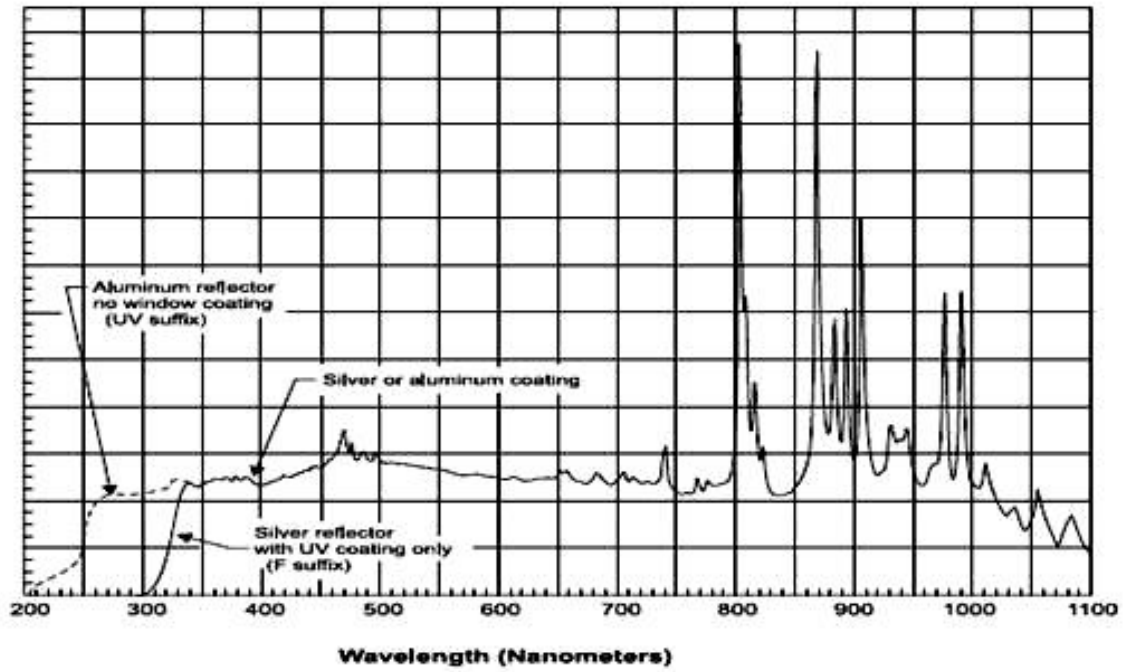

Fig. 3-6. Wavelength spectrum of visible light from 300 W xenon lamp (Nbet Co. Ltd., Beijing, China).

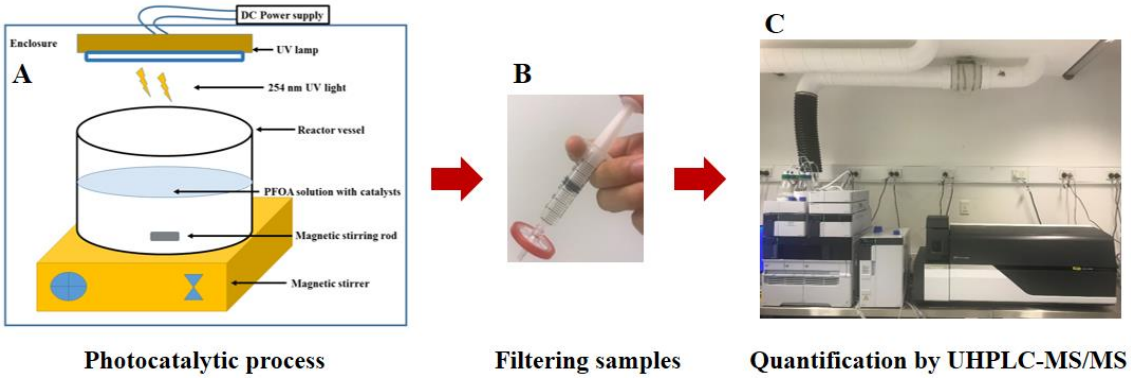

Fig. 3-7. The schematic diagram of the overall experimental process. (A) The photocatalytic process in the reactor. (B) Filtering the liquid samples before quantification. (C) Quantification by UHPLC-MS/MS.

3.6. Auxiliary laboratory equipment

Total organic carbon (TOC) was measured by a Multi N/C 3100 Analytikjena total organic carbon (TOC) analyser. $P\text{-}PO_4^{3-}$ and $N\text{-}NH_4^{+}$ were analysed using a DR 3900 Hach (Germany) spectrophotometer. TDS was using an EC/TDS Hanna

spectrophotometer. pH readings were obtained using Hach pH meter. The pH meter was calibrated using three buffer solutions with pH 4.01, 7.01 and 10.01.

Chapter 4. Photocatalysis of PFOA by five commercial catalysts under UV irradiation

4.1. Introduction

Five commercial materials are commonly used as catalysts for photolysis as follows: TiO_2 (P25), In_2O_3, Ga_2O_3, cerium dioxide (CeO_2) and cadmium sulfide (CdS) (Cao et al., 2017; Chen et al., 2017c; Magdalane et al., 2017; Moreira et al., 2018; Zhou et al., 2017b). Notably, P25 TiO_2 nanoparticles are considered to be the classical one which have been applied in wastewater treatment, photoinduced hydrophilic coatings, degradation of organic pollutants, and production of hydrogen fuel (Kommireddy et al., 2005; Yasuda et al., 2017). **Fig. 4-1** presents the cost of each material (Sigma-Aldrich, Australia) and the price sequence from cheap to expensive is listed as follows: TiO_2 < CdS < CeO_2 < Ga_2O_3 < In_2O_3. TiO_2 has a comparatively lower cost material than others, which makes it popular to be used in industry (Xu et al., 2017a). It has been reported that PFOA could be effectively removed by TiO_2 catalyst under UV irradiation (Gomez-Ruiz et al., 2018; Panchangam et al., 2018). Ga_2O_3 is a semiconductor with a band gap of 4.68 eV. After absorption of photon energy equal or more than the band gap, photogenerated holes (h^+) in the valence band and photogenerated electrons (e^-) in the conduction band are formed. The redox ability of the photoexcited hole-electron pairs make it potentially suitable for the light energy conversion and pollutant degradation (Chen et al., 2015a). Besides, CeO_2, In_2O_3 and CdS have also been applied to pollutant photocatalysis and were found to be effective (Bai et al., 2006; Li et al., 2013b; Liu et al., 2004).

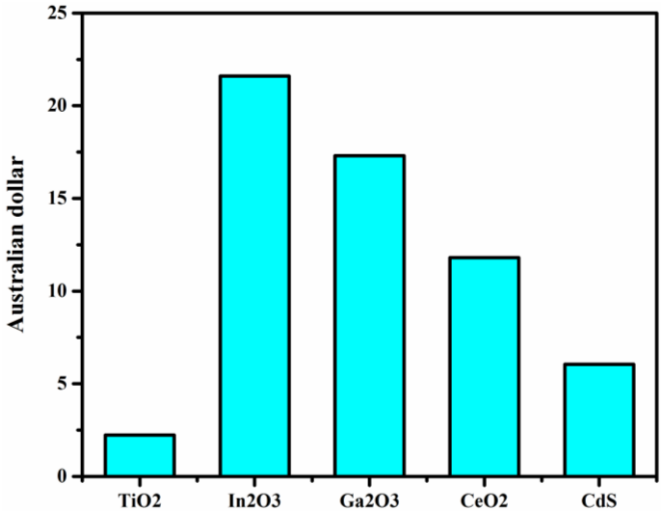

Fig. 4-1. Price of each commercial catalysts (i.e. TiO_2, In_2O_3, Ga_2O_3, CeO_2 and CdS) according to the quote from Sigma-Aldrich, Australia.

PFAS, which are anthropogenic compounds, have drawn great attentions due to their wide use in industrial and their persistent and bioaccumulative nature in the environment (Kotthoff et al., 2015; Rappazzo et al., 2017). As a well-known type of PFAS, PFOA has been widely detected in the aquatic environment at the concentration from ng L^{-1} to mg L^{-1} (Pignotti et al., 2017; Valsecchi et al., 2015). Up to now, there have been several publications on the photocatalysis for PFAS degradation (Gatto et al., 2015; Song et al., 2012). However, insufficient evidence has provided to prove which material is more suitable for this technology with fewer energy cost and no secondary pollutant generation. In this study, five commercial catalysts, i.e. TiO_2, CdS, CeO_2, Ga_2O_3 and In_2O_3 were investigated under the condition and their degradation performance was compared to evaluate the photocatalytic ability. Furthermore, the influence of solution pH, photon energy absorption, band gap energy and interaction reaction between chemical bonds and radicals were explored to explain the photocatalysis mechanism. All these were necessary to be conducted and the results would be the significant foundation for further research

and could be instructive for real wastewater treatment. The main process during photocatalysis was shown in **Fig. 4-2**.

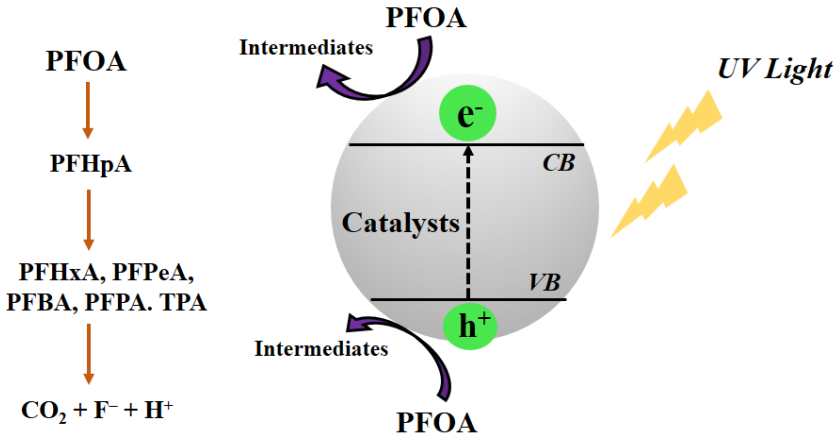

Fig. 4-2. The approximately process of photocatalysis degradation for PFOA.

4.2. Methodology

A catalyst (e.g. Ga_2O_3, TiO_2, CeO_2, In_2O_3 and CdS) was added in the solution individually with a concentration of 0.5 g L^{-1}. After stirring for 0.5 h under darkness to achieve adsorption-desorption equilibrium, the mixed solution was exposed to UV light irradiation without any pH adjustment. The UV light source was provided by a 32 W low-pressure UV lamp (Cnlight Co. Ltd., Shanghai, China) positioned 5 cm above the liquid surface of the reactor. The irradiation intensity of UV light was 1.71 mW cm^{-2} as measured by an UV intensity meter (ST-512). The mixed depth of the water column was 1.3 cm and light intensity was considered as evenly distribution in each part of the water column ideally for convenient calculation. At regular time intervals, aliquots of the sample were taken using a syringe and filtered through a filter (Puradisc syringe filter, 0.2 µm, Whatman) before analysis. To avoid the possible impact of filter adsorption on PFOA concentration, the first 3 mL filtrate was discarded. All experiments were conducted in triplicate.

4.3. Results and discussion

4.3.1. *Characterization of different catalysts*

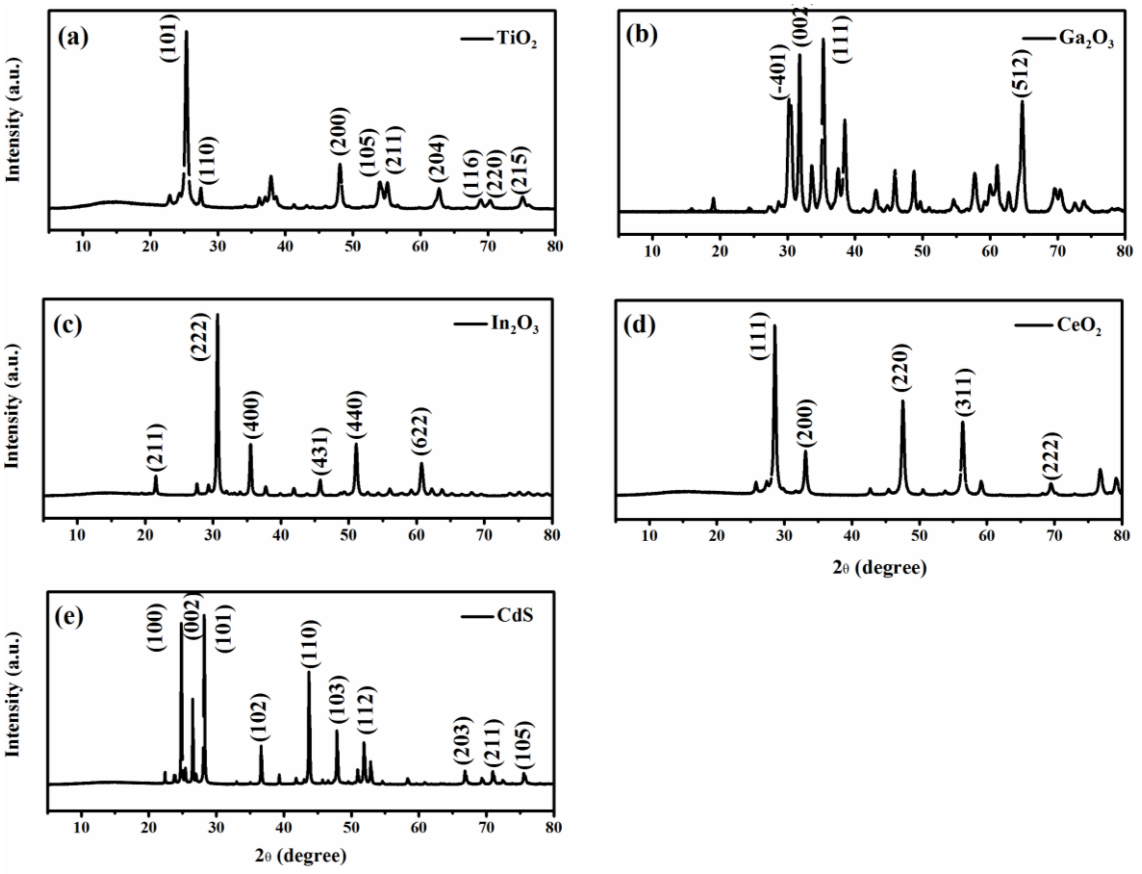

Fig. 4-3. XRD patterns of catalysts TiO_2, Ga_2O_3, CeO_2, In_2O_3 and CdS.

The XRD patterns of TiO_2, Ga_2O_3, In_2O_3, CeO_2 and CdS used in the study are shown in **Fig. 4-3**. Specifically, strong diffraction peaks as shown in **Fig. 4-3 (a)** indicates TiO_2 only in anatase phase (~80%) and rutile phase (~20%) (JCPDS No. 71-1166) (Sacca et al., 2005). **Fig. 4-3 (b)** indicates that all of the diffraction peaks are in agreement with those of monoclinic phase of beta-Ga_2O_3 (JCPDS No. 41–1103) and the sharp diffraction peaks reveal that the samples has a high crystalline quality (Wang et al., 2015a). **Fig. 4-3 (c)** shows that most of the XRD peaks are consistent with those of cubic In_2O_3 (JCPDS No. 06-041) (Huang et al., 2018). Besides, the peaks observed in the XRD patterns of commercial CeO_2 and CdS both match with those from the standard joint committee on

the power diffraction standards card of cubic CeO_2 (JCPDS No. 34–0394) and hexagonal CdS (JCPDS No. 41-1049), respectively as shown in **Fig. 4-3 (d)** and (**e)** (Bai et al., 2006; Shao et al., 2003). The morphologies of these commercial catalysts were investigated by SEM. At the same magnification, Ga_2O_3 has a larger size than that of the others by comparison (**Fig. 4-3**). SEM images of TiO_2 and CeO_2 both present aggregated nanoparticles while Ga_2O_3 shows to be rods with clear boundaries. Besides, In_2O_3 has smaller size of the particles in nm than the others and the CdS particles are observed to be decentralized in the field of vision with different particle size as shown in **Fig. 4-4**.

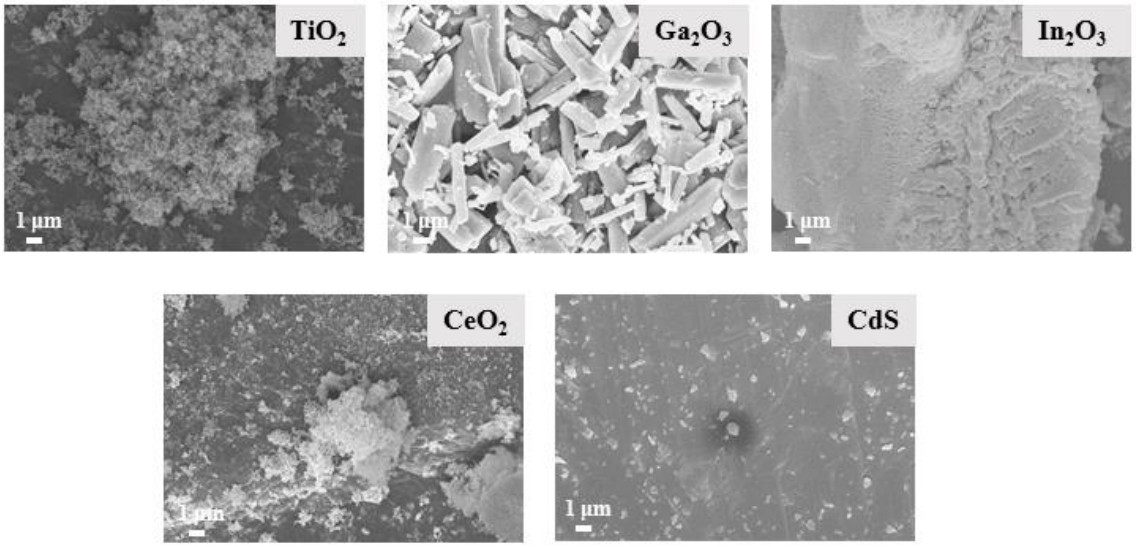

Fig. 4-4. SEM images of catalysts TiO_2, Ga_2O_3, In_2O_3, CeO_2 and CdS.

4.3.2. Photocatalytic performance

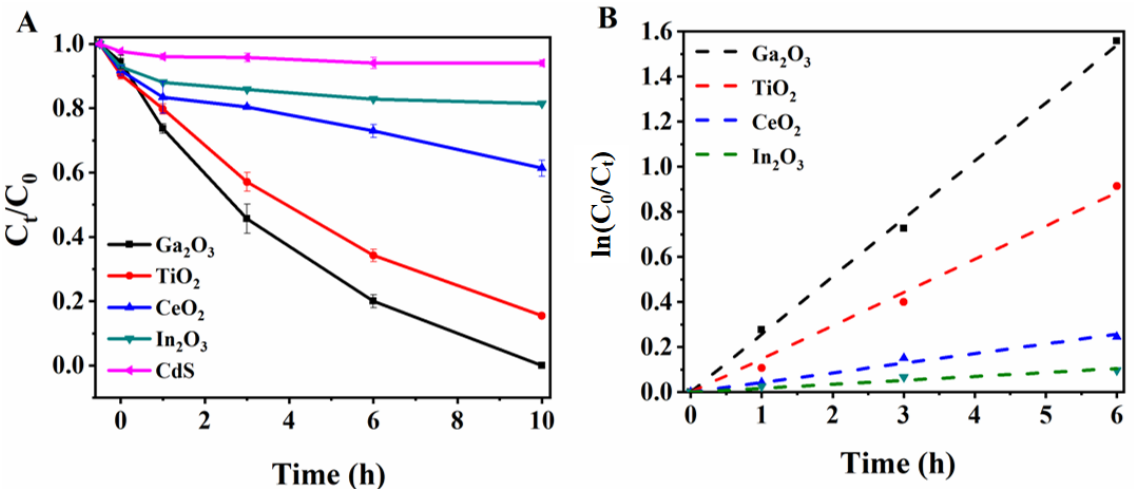

Fig. 4-5. Degradation rate of PFOA by catalysts (i.e. TiO_2, Ga_2O_3, CeO_2, In_2O_3 and CdS) under UV 254-nm irradiation within 10 h.

Comparative experiments were conducted to investigate the photocatalytic ability for PFOA removal from water by catalysts of TiO_2, Ga_2O_3, CeO_2, In_2O_3 and CdS. To ensure strict comparison, the initial PFOA concentration (50 mg L^{-1}) and the other conditions (i.e. room temperature, initial pH, a UV lamp of 254 nm) were identical with all experiments being conducted in the same reactor under continuous stirring. For easy comparison, the catalyst doses were all of 0.25 g L^{-1} and the initial pH was 3.0 ± 0.2 without pH adjustment. As shown in **Fig. 4-5A**, under UV irradiation within 10 h, almost 100% PFOA was degraded by Ga_2O_3 followed by about 84% of PFOA removed by TiO_2. Also, CeO_2 and In_2O_3 degraded only approximately 40% and 20% PFOA, respectively, while CdS had caused almost no PFOA degradation. Additionally, the kinetics of the photodegradation of PFOA fitted well to the pseudo-first-order model (R^2 > 0.90) described as follows (**Fig. 4-5B**):

$$\ln(C_0/C_t) = k\,t \qquad (4.1)$$

where k is the rate constant (min^{-1}), C_0 and C_t are the concentrations of PFOA ($mg\ L^{-1}$) in solution at irradiation time 0 and t, respectively. As a result, except CdS, the rate constant for PFOA degradation (k_t) of these selected catalysts were 0.257, 0.147, 0.043 and 0.017 h^{-1}, respectively. Therefore, the photocatalytic capability for PFOA degradation decreased as $Ga_2O_3 > TiO_2 > CeO_2 > In_2O_3 > CdS$.

Furthermore, the fluence-based first-order rate constant (k_f, $cm^2\ mJ^{-1}$) and the half-life ($\tau_{1/2}$, h) were investigated to compare with the efficacy by other treatment as shown in **Table 4-1**. k_f ($cm^2\ mJ^{-1}$) is calculated as: $k_f = \frac{k_t}{I}$, where I is the light intensity of 1.71 $mW\ cm^{-2}$. $\tau_{1/2}$ (h) is described as $\tau_{1/2} = \frac{In2}{k_t}$. Notably, k_f of TiO_2 doped with Pd and Ag under 125 nm UV light was 2.30×10^{-5} and 7.00×10^{-6} $cm^2\ mJ^{-1}$, respectively (Li et al., 2016), both lower than the value of commercial Ga_2O_3. While TiO_2-Pd could degrade almost all PFOA (60 $mg\ L^{-1}$) within 7 h, which was quicker than that of Ga_2O_3 in this study with 100% removal of 50 $mg\ L^{-1}$ PFOA within 10 h. Besides, TiO_2 doped with Cu, Fe and Pb degraded 80%, 60% and almost 100% PFOA at 50 $mg\ L^{-1}$ (Chen et al., 2015b; Chen et al., 2016), compared with about 80% removal by commercial Ga_2O_3 within 6 h. However, metal-doped technology needs specific conditions. For example, Pd-TiO_2 was prepared under 400 ℃ with $PdCl_2$ addition and the synthesis process commonly cost more than 5 h. On the contrary, the commercial catalysts used in this study could be directly utilized in photocatalytic system after purchased, avoiding the complex synthesis process. Overall, these findings concluded that commercial Ga_2O_3 was preferable for PFOA photodegradation with comparatively high degradation efficacy.

Table 4-1

Comparison of Photocatalytic conditions for PFOA removal by TiO_2/PMS in this study and other catalysts in the literature.

Catalyst	Catalyst dosage ($g\ L^{-1}$)	Light source	Light intensity ($mW\ cm^{-2}$)	C_0 (PFOA) ($mg\ L^{-1}$)	Removal (reaction period)	k_t (h^{-1})	k_f ($cm^2\ mJ^{-1}$)	$\tau_{1/2}$ (h)	Reference
Ga_2O_3	0.05	32 W, λ=254 nm	1.71	50	100% (10 h)	0.257	4.18×10^{-5}	2.70	this study
TiO_2	0.05	32 W, λ=254 nm	1.71	50	84% (10 h)	0.147	2.39×10^{-5}	4.71	this study
CeO_2	0.05	32 W, λ=254 nm	1.71	50	40% (10 h)	0.043	7.00×10^{-6}	16.12	this study
In_2O_3	0.05	32 W, λ=254 nm	1.71	60	20% (10 h)	0.017	2.76×10^{-6}	40.76	this study
TiO_2 with Pd	0.5	125 W, λ=365 nm	5.3	60	98% (7 h)	0.438	2.30×10^{-5}	1.58	(Li et al., 2016)
TiO_2 with Ag	0.5	125 W, λ=365 nm	5.3	60	45% (7 h)	0.126	7.00×10^{-6}	5.50	(Li et al., 2016)
TiO_2 with Cu	0.5	400 W, λ=254 nm	–	50	80% (6 h)	0.186	–	–	(Chen, et al., 2015b)
TiO_2 with Fe	0.5	400 W, λ=254 nm	–	50	60% (6 h)	0.090	–	–	(Chen, et al., 2015b)
TiO_2 with Pb	0.5	400 W, λ=254 nm	–	50	98% (6 h)	0.516	–	–	(Chen et al., 2015b)

4.3.3. Initial pH effect on the photocatalysis

Different pH conditions could affect the photodegradation of aqueous PFOA under UV irradiation by catalysts in previous reports (Shang et al., 2018; Zhao et al., 2012). One significant reason was related to the bonding between PFOA and catalysts by Coulombic attraction. Notably, the p*K*a of aqueous PFOA is about 2.8, which indicates that PFOA stays in a protonated form ($C_7F_{15}COOH$) at pH < 2.8 and anionic form ($C_7F_{15}COO^-$) at pH > 2.8. In addition, zeta potential of these catalysts (Ga_2O_3, TiO_2, CeO_2, In_2O_3 and CdS) were presented in **Fig. 4-6** and the points of zero charge were 8.6, 5.6, 6.95, 3.8 and < 0. This suggests at a pH 3-4 condition, these catalysts were all positive charged except CdS. The solution pH with PFOA and catalysts addition were 3 ± 0.2 without any pH adjustment. Thus, at pH 3 ± 0.2, the selected catalysts except CdS could closely combine with PFOA because of the Coulombic attraction. Therefore, the poor degradation by CdS was significantly attributed to the pH. While the different degradation performance by Ga_2O_3, TiO_2, CeO_2 and In_2O_3 was not related to the initial solution pH. In addition, the mechanism of the reasons about the photocatalytic mechanism of these four common materials was further investigated to explain their various abilities for PFOA removal.

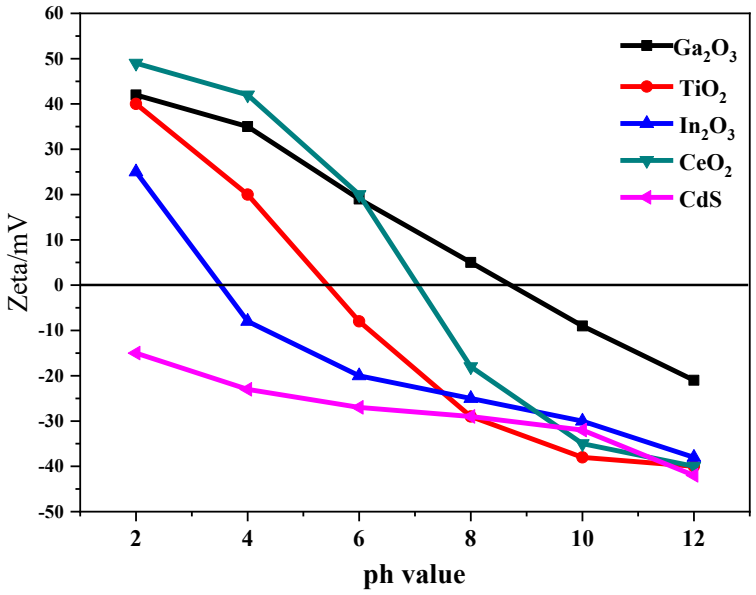

Fig. 4-6. Zeta potential of Ga_2O_3, TiO_2, In_2O_3, CeO_2 and CdS.

4.3.4. Photon energy absorbed by catalysts

The energy of one photon energy (E_0) is calculated as follows:

$$E_0 = \frac{hc}{\lambda} \qquad (4.2)$$

where h is Planck's constant of 6.63×10^{-34} J·s, c is light speed of 3×10^8 m s^{-1}, λ is the wavelength of UV light, which is 254 nm, and thus E_0 is calculated of 7.8×10^{-19} J. For one mole of photon, the energy (Em) is as follows:

$$Em = eE_0 \qquad (4.3)$$

From this calculation, one Einstein of 254 nm photons has an energy of (E_m) 4.7×10^5 J. In addition, light intensity (I) is 1.71 mW cm^{-2} in this study, and also is 1.71 mJ cm^{-2} s^{-1} (mW = mJ s^{-1}). Consequently, the quantity of photon (Ep) generated by UV light irradiation could be calculated as follows:

$$E_p = I / E_m \qquad (4.4)$$

As a result, *E*p is 3.6×10^{-9} Einstein cm^{-2} s^{-1}. Furthermore, the quantum yield (Φ), defined as moles of PFOA degraded per Einstein of photons absorbed by certain amount of catalysts, was estimated as follows:

$$\Phi = \frac{Total\ number\ (moles) of\ PFOA\ degraded}{Total\ number\ (moles)\ of\ photons\ absorbed\ in\ the\ system} \quad (4.5)$$

The degradation rate constant (k_{Δ}) during the photocatalytic process could be used for the calculation of quantum yield as follows:

$$\Phi = \frac{k_{\Delta}}{I_a} \quad (4.6)$$

where $k_{\Delta} = d(C_0\text{-}C_t)/dt$ (mg L^{-1} h^{-1}), and I_a is the photon numbers absorbed by the catalysts, which can be calculated by Eq. 4.7:

$$I_a = \frac{E_p \times \left(1-10^{-2\cdot(\alpha(\lambda)\cdot C)\cdot z}\right)}{z} \times \frac{A1-A0}{A1} \quad (4.7)$$

where *C* is the concentration of the catalyst solution (mM) and *z* is the mixed depth of the water column (1.3 cm). In addition, A is the amount of light absorbed by the catalyst at a wavelength of 254 nm, which was detected by the spectrophotometer as shown in **Table 4-2**. $\alpha(\lambda)$ is the light attenuation coefficient of the catalysts which is calculated as:

$$\alpha(\lambda) = \frac{A}{Cl} \quad (4.8)$$

where *l* is the distance that light travels through the solution (1 cm). All the equations mentioned above are from the book (Schwarzenbach et al., 2016). Based on the data summarized in **Table 4-3**, quantum yield by the catalysts of Ga_2O_3, TiO_2, CeO_2 and In_2O_3, under UV light (254 nm) were 0.0032, 0.0075, 0.0041 and 0.0005 mol $Einstein^{-1}$, respectively during the photocatalysis of PFOA. Owing to the poor degradation performance, the value for

CdS was not calculated. Accordingly, quantum yield was sequenced as TiO_2 > CeO_2 > Ga_2O_3 > In_2O_3, which may not be the main reason attributed to their photocatalytic ability for PFOA removal.

Table 4-2

The band gap energy of commercial In_2O_3, Ga_2O_3, TiO_2, CeO_2 and CdS.

Commercial materials	Band gap energy (eV)	References
In_2O_3	2.80	(Li et al., 2012a)
Ga_2O_3	4.68	(Shao et al., 2013a)
TiO_2	3.14	(Pu et al., 2018)
CeO_2	2.93	(Zang et al., 2018)
CdS	2.42	(Liu et al., 2004)

Table 4-3

The key experimental parameters and their values in this study.

Parameter	Symbol	Value	Detection method
Rate constant	K	0.0156 min^{-1}	Calculated
Light intensity	I	1.71 mW cm^{-2}	UV intensity meter
PFOA concentration in solution	C_1	0.12 mM	Calculated
Catalyst concentration in solution (Ga_2O_3)	C_2	1.3 mM	Calculated
Catalyst concentration in solution (TiO_2)	C_2	3.1 mM	Calculated
Catalyst concentration in solution (In_2O_3)	C_2	0.9 mM	Calculated
Catalyst concentration in solution (CeO_2)	C_2	1.5 mM	Calculated
Light absorbed by PFOA solution at 254-nm Ga_2O_3	A	0.201	spectrophotometer
Light absorbed by PFOA solution at 254-nm TiO_2	A	0.321	Spectrophotometer
Light absorbed by PFOA solution at 254-nm In_2O_3	A	0.127	Spectrophotometer
Light absorbed by PFOA solution at 254-nm CeO_2	A	0.215	Spectrophotometer
Mixed depth of the water column	z	1.3 cm	Measured
Distance of light passage through solution	l	1 cm	Measured

4.3.5. Photocatalytic mechanism

The band gap energy is a critical factor to decide the photocatalytic performance. Calculated from the data of UV-vis spectrum, the band gap energy of these catalysts used in this study is similar to the values reported in the previous literature (**Table 4-2**) (Li et

al., 2012a; Liu et al., 2004). As a result, the band gap energy decreased as Ga_2O_3 = 4.68 eV> TiO_2 = 3.14 eV > CeO_2 = 2.93 eV > In_2O_3 = 2.80 eV > CdS = 2.42 eV. Viewing on the photocatalytic mechanism, catalyst absorbs a photon with energy of 7.8×10^{-19} J (E_0 as calculated in the previous section) and only if E_0 was equal to or greater than its band gap energy, the photoinduced hole and electron pairs could be generated for the photodegradation. Specifically, based on the equation of 1 eV = 1.6×10^{-19} J and the data in **Table 4-2**, the band gap energy of Ga_2O_3, TiO_2, CeO_2, In_2O_3 and CdS were 7.3×10^{-19} J, 5.0×10^{-19} J, 4.7×10^{-19} J, 4.5×10^{-19} J and 3.9×10^{-19} J, respectively. Hence, these catalysts with same amount could be activated by UV light to produce similar quantity of hole and electron pairs as their band gap energy were all less than the photon energy. While the oxidation-reduction ability of photogenerated hole and electron pairs decreases with the narrowing of the band gap. Accordingly, the photocatalytic capability of these catalysts should be Ga_2O_3 > TiO_2 > CeO_2 > In_2O_3 > CdS, which exactly matched the photodegradation performance from good to poor in this study. Thus, Ga_2O_3 outperformed the other common catalysts because its band gap energy was more suitable than the others due to the stronger redox ability of photogenerated hole and electron pairs. Additionally, the wavelength spectrum of each material overlayed with the lamp spectral output were exhibited in **Fig. 4-7**, indicating that all the materials had high absorbance of 254 nm UV light.

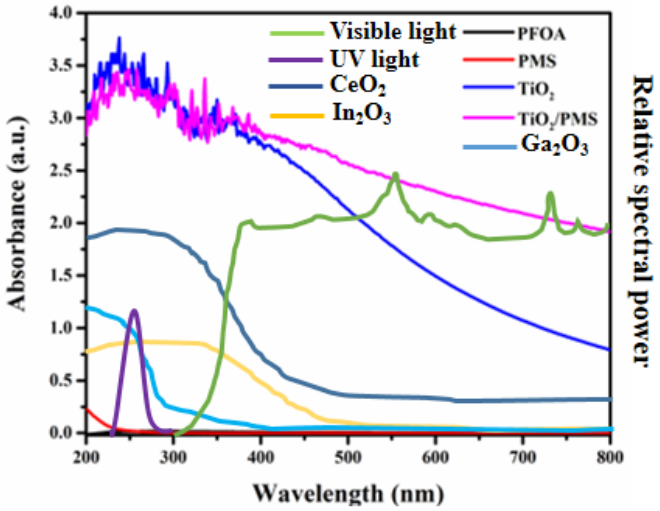

Fig. 4-7. The wavelength spectrum of each material overlayed with the lamp spectral output.

It is well know that photogenerated hole and electrons played the main roles with redox ability to degrade PFOA during photocatalysis process (Merino et al., 2016; Xu et al., 2017a). In this study, Ga_2O_3, TiO_2, CeO_2 and In_2O_3 all could be irradiated by 254 nm UV light to generate holes and electrons and they had the various degradation efficacies. Disodium ethylenediaminetetraacetate (EDTA-Na_2), as a scavenger of holes, was introduced to the photocatalytic system to check the function of photogenerated holes or electrons. Consequently, **Fig. 4-8** indicates that EDTA-Na_2 obviously affected the degradation efficiency of TiO_2, CeO_2 and In_2O_3, while only slight increase of the degradation efficacy was observed in Ga_2O_3 photocatalytic system between the EDTA-Na_2 addition or not. This proved that photogenerated holes played main roles when TiO_2, CeO_2 and In_2O_3 were the catalysts and on the contrary, photogenerated electrons were the main reactants when Ga_2O_3 was used for the degradation.

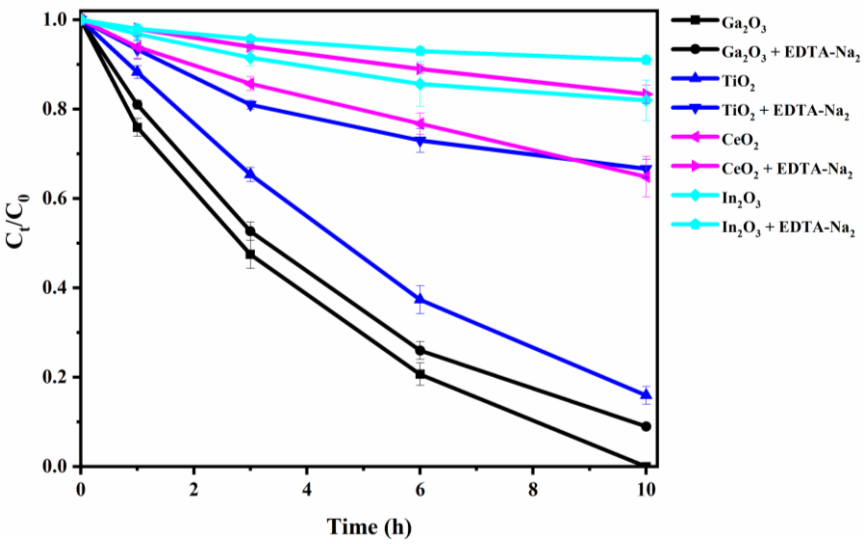

Fig. 4-8. Degradation rate of PFOA by catalysts (i.e. TiO_2, Ga_2O_3, CeO_2, In_2O_3 and CdS) with and without EDTA-Na_2 addition.

Moreover, degradation of PFOA undergoes two pathways upon reaction with holes or electrons as shown in **Fig. 4-9**. As previously reported, the α-position C-F bond was more easily to break up by photogenerated electrons than the bonds in other positions (Song et al., 2013). Thus, when the reduction ability of electrons was more than the bond energy of α-position C-F, the degradation process will go through in route (a) as shown in the **Fig. 4-9**. As a result, the fluorine atom rather than carbon reacts with electron, escaping from molecular state to become free fluorine ion. Due to the large band gap energy, PFOA photocatalysis by Ga_2O_3 occurred in route (a). Nevertheless, when the electrons were not able to reduce the fluorine atom, PFOA would be decomposed in route (b), namely oxygen atom in the carboxyl is oxidized by photogenerated holes to form C_7F_{15}• radicals and CO_2. In_2O_3, TiO_2 and CeO_2, as the comparatively low band gap energy, degraded PFOA in route (b). Consequently, PFOA proceeds in a step-by-step mode to shorter chain intermediates such as PFHpA, PFHxA, PFPeA, PFBA, PFPA, and TPA, and finally turns to CO_2 and H_2O as reported in the literature (Li et al. 2012a; Sansotera et al. 2014).

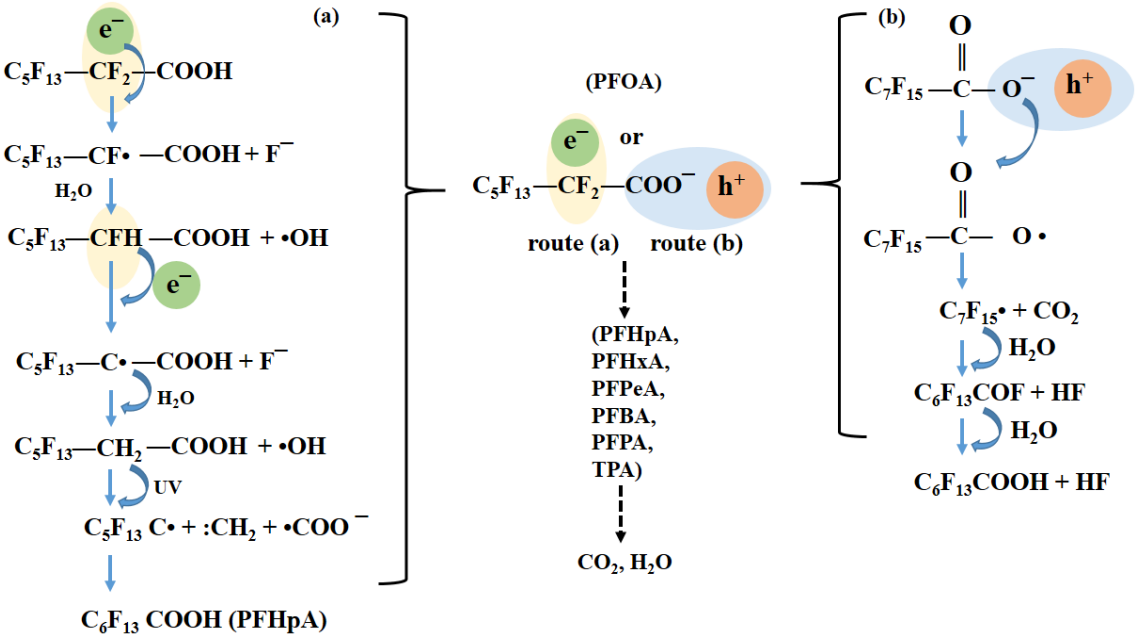

Fig. 4-9. Degradation mechanism of PFOA in route (a) by photogenerated electrons and in route (b) by photogenerated holes.

4.4. Conclusions

In summary, the commercial catalysts of Ga_2O_3, TiO_2, CeO_2 and In_2O_3 were able to degrade PFOA within 10 h and Ga_2O_3 had best performance with 100% PFOA removal. However, CdS showed almost no ability for PFOA photodegradation probably due to the initial pH. In addition, the quantum yield during the UV irradiation were 0.0032, 0.0075, 0.0041 and 0.0005 mol Einstein^{-1}, respectively by the catalysts of Ga_2O_3, TiO_2, CeO_2 and In_2O_3. And their band gap energy of $Ga_2O_3 = 7.3 \times 10^{-19}$ J > $TiO_2 = 5.0 \times 10^{-19}$ J > $CeO_2 = 4.7 \times 10^{-19}$ J > $In_2O_3 = 4.5 \times 10^{-19}$ J > CdS = 3.9×10^{-19} J. In the reaction, photogenerated electrons played the main role when using Ga_2O_3/UV, while photogenerated holes were more important by TiO_2, CeO_2 and In_2O_3 under UV light. Notably, photogenerated holes played main roles when TiO_2, CeO_2 and In_2O_3 were the catalysts and on the contrary, photogenerated electrons were the main roles when Ga_2O_3 was used for the degradation.

PFOA was degraded into shorter carbon chain stepwise and finally turned to CO_2 and H_2O.

Chapter 5. Improved photocatalysis of perfluorooctanoic acid in water and wastewater by Ga_2O_3/UV system assisted by peroxymonosulfate

5.1. Introduction

PFAS, anthropogenic compounds characterised by their fully fluorinated hydrophobic carbon and a hydrophilic end group, have been applied in many industrial, commercial and domestic products and as the key ingredient in aqueous film-forming foams since the 1950s (Bräunig et al., 2019). Due to the highly stable carbon-fluorine bond with a bond energy of 544 kJ mol^{-1} (Saleh et al., 2019), PFAS are ubiquitous in the environment and globally detected in many environmental matrices and even in human tissues (Jian et al., 2018; Mazzoni et al., 2019). For example, the Williamtown site from Sydney, Australia was found to contain more than 1 mg L^{-1} level of PFOA and PFOS, two kinds of well-known PFAS, over the past decades (www.health.nsw.gov.au/environment). Both substances worked their way through the surface water or soil to the groundwater underneath the site, leading to the land contamination close to the site (Anderson et al., 2019; Janda et al., 2019). Until now, these chemicals have been reported to be linked to many human diseases such as kidney cancer (Mulabagal et al., 2018), thyroid disease (Blake et al., 2018), testicular cancer (Mastrantonio et al., 2017) and pregnancy-induced hypertension (Apelberg et al., 2007; Holtcamp, 2012). Therefore, as a precautionary approach, new technologies with strong degradation ability for PFAS removal is urgently needed to mitigate PFAS contamination.

PMS (commercial name of Oxone®, $2KHSO_5 \cdot KHSO_4 \cdot K_2SO_4$) is an environmentally friendly oxidant (Khan et al., 2017b; Lin et al., 2016). It can be activated by UV light to produce sulfate radicals ($SO_4^{\bullet -}$) which have strong oxidizing ability (Gao et al., 2016). A recent study used persulfate-assisted photocatalytic ozonation, and their results revealed 99.2% removal of PFOA (Wu et al., 2018). Nevertheless, such significant research is limited, and still there is a research gap in the kinetics and mechanistic study of PFOA degradation in complex systems. Based on the previous chapter 4, Ga_2O_3

performed better than the other catalysts. Thus, in the present study, Ga_2O_3 assisted with PMS was firstly used as the mixed catalysts for PFOA photodegradation under UV irradiation. Experimental factors such as catalyst amount and solution pH were evaluated by comparative experiments to explore the optimum conditions. The intermediates generated during the process and active species in charge of PFOA degrading were analysed to derive the possible photocatalytic mechanism in PMS/Ga_2O_3/UV system. The main chemical process during photocatalysis of Ga_2O_3/PMS was shown in **Fig. 5-1**.

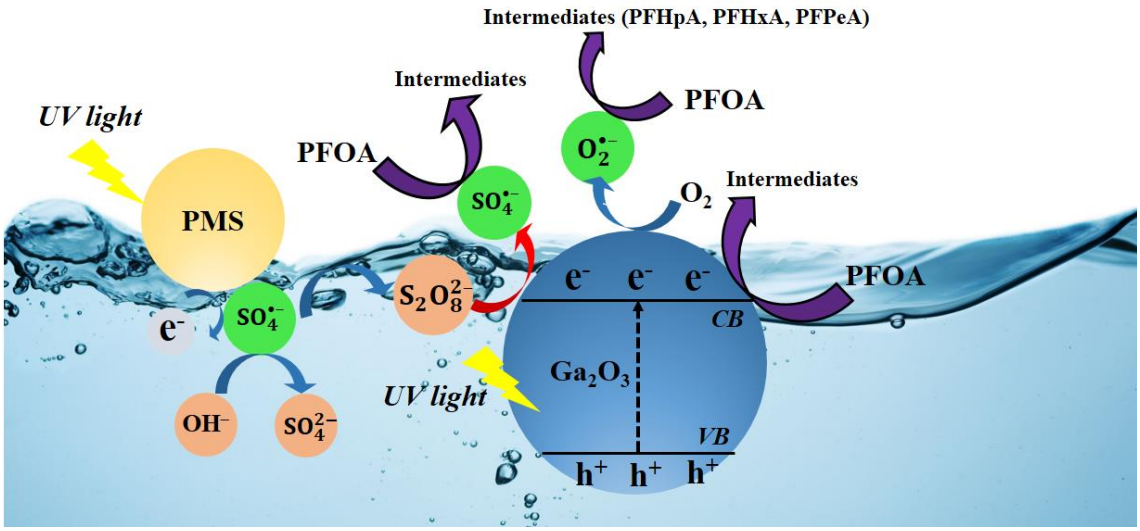

Fig. 5-1. The main chemical process during photocatalysis of Ga_2O_3/PMS (Xu et al., 2019).

5.2. Methodology

A cylindrical reactor vessel was filled with PFOA aqueous solution of 200 mL and different initial PFOA concentrations (50 ng L^{-1}, 50 µg L^{-1}, 50 mg L^{-1}) at room temperature. The concentration of 50 mg L^{-1} was comparatively high, compared with the concentrations of PFOA occurring in the most contaminated water; it was also used as the initial concentration in a previous study (Chen, et al., 2015b). The solid catalyst of Ga_2O_3 was dispersed in PFOA solution, to which PMS was then added to initiate the reaction with continuous stirring for 30 min under darkness. The effect of solution pH on

PFOA photodegradation was assessed by repeating experiments at pH 3, 5, 7 and 10. Light irradiation was provided by three separate lamps: UV light (wavelength = 254 nm) from a 32 W low-pressure UV lamp, UV light (wavelength = 185 nm) from a 32-W low-pressure UV lamp, and visible light (wavelength = 400–800 nm) from a 50-W xenon lamp. The irradiation intensity of UV light (254 nm) was 0.37 mW cm^{-2} as measured by an UV intensity meter (ST-512). During photodegradation, the lamps were placed 5 cm above the liquid surface of the reactor and the solution was well mixed by magnetic stirring (Li et al., 2016; Zhao et al., 2015). At regular time intervals, aliquots of the sample were taken using a syringe and filtered through a filter (Puradisc syringe filter, 0.2 μm, Whatman) before analysis. All experiments were conducted in triplicate.

5.3. Results and Discussion

5.3.1. *Photocatalytic ability of Ga_2O_3/PMS*

In order to improve the catalytic efficacy, Ga_2O_3 was mixed with PMS in the PFOA solution as the catalysts for the PFOA degradation under UV light (254 nm). For the convenient comparison, the initial concentration of Ga_2O_3 was 0.25 g L^{-1} and PMS was 0.41 g L^{-1} so the molar ratio between Ga_2O_3 and PMS was 1:1. **Fig. 5-2A** shows that PFOA was completely degraded within 120 min by the catalysts of Ga_2O_3 mixed with PMS. However, when only PMS or Ga_2O_3 was used as the catalysts under the same condition, 18% and 58.3% of PFOA was degraded, respectively within 180 min. Thus, the photocatalytic ability decreased as Ga_2O_3/PMS > Ga_2O_3 > PMS. Meanwhile, the kinetics of the photodegradation of PFOA fitted well to the pseudo-first-order model (R^2 > 0.90) described as follows:

$$\ln(C_0/C_t) = k\,t \qquad (5.1)$$

where k is the rate constant (min^{-1}), C_0 and C_t are the concentrations of PFOA ($mg\ L^{-1}$) in solution at irradiation time 0 and t, respectively. Based on the results in **Fig. 5-1A**, the rate constant for PFOA degradation according to system configuration or the type of catalyst used in the reactor (single or mixed catalyst) was found to be 0.0041 min^{-1}, 0.0013 min^{-1} and 0.0156 min^{-1}, for Ga_2O_3, PMS and Ga_2O_3/PMS, respectively. A catalyst combination of PMS/Ga_2O_3 significantly promoted the photocatalytic ability, resulting in 3.8 and 12 times higher rate constant than that of single Ga_2O_3 and PMS, respectively. Therefore, the results imply that sulfate radicals ($SO_4^{\bullet-}$) generated by PMS significantly enhanced the catalytic ability of Ga_2O_3 targeting on the PFOA degradation under UV irradiation. As the PMS/Ga_2O_3 system for PFOA photodegradation has not been studied before, their photocatalytic kinetics and mechanism were further investigated.

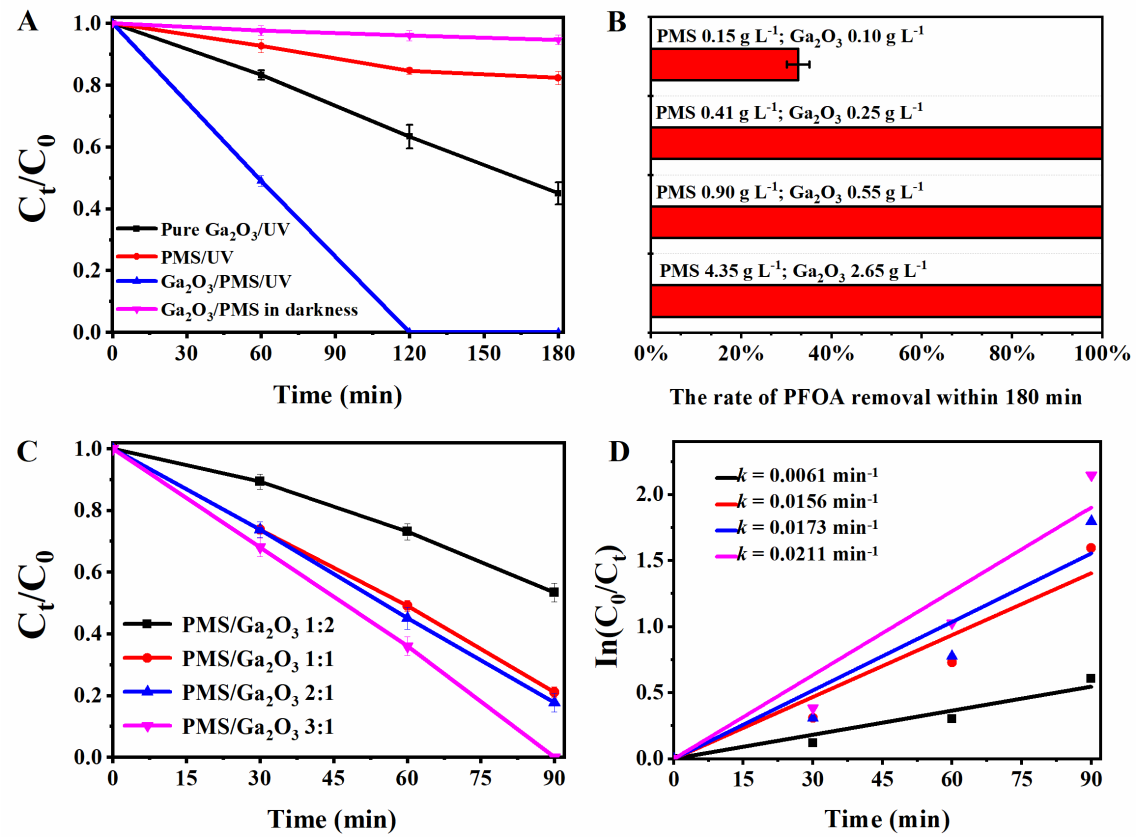

Fig. 5-2. (A) Comparison of photocatalytic performance for PFOA removal among Ga_2O_3, PMS and Ga_2O_3/PMS under UV 254-nm. (B) Degradation rate of PFOA by different

amounts of PMS (0.16, 0.41, 0.90, 4.35 g L^{-1}) and Ga_2O_3 (0.10, 0.25, 0.55, 2.65 g L^{-1}). (C) Photocatalytic performance by different PMS/Ga_2O_3 ratios (1:2, 1:1, 2:1, 3:1) under UV 254-nm. (D) The fitting of degradation curves and rate constant (*k*) derived.

5.3.2. *Effect of catalyst loading*

Many previous studies have shown that the amount of catalyst has a positive effect on photocatalytic efficacy (Carbajo et al., 2018; Xu et al., 2017a). Because the number of reactive sites increase with the increase of the catalyst amount that promote the rate of oxidation. However, a high concentration of catalyst would make the solution turbid, and reduce the photo permeability of UV light, with a negative effect on the photocatalytic degradation rate. In this study, under the 1:1 molar ratio of PMS to Ga_2O_3, different amounts of PMS/Ga_2O_3 (PMS at 4.35, 0.90, 0.41 and 0.16 g L^{-1}, Ga_2O_3 at 2.65, 0.55, 0.25 and 0.10 g L^{-1}) were used to assess the performance in PFOA removal. **Fig. 5-2B** shows that PMS ranging from 0.41 to 4.35 g L^{-1} and Ga_2O_3 ranging from 0.25 to 2.65 g L^{-1} generated identical results that 100% PFOA was degraded within 180 min. However, when the amount of PMS and Ga_2O_3 was decreased to 0.16 and 0.10 g L^{-1}, respectively, the degradation process was significantly inhibited, as only about 33% PFOA was removed during 180 min. This may be attributed to the insufficient active groups produced in the system with a low concentration of Ga_2O_3 and PMS, which was also mentioned in a previous study (Carbajo et al., 2018). Compared with the previous study, 0.5 g L^{-1} TiO_2 doped with Pb could degrade almost 100% PFOA (50 mg L^{-1}) within 480 min at rate constant of 0.0086 min^{-1} (Chen et al., 2016), which was lower than that of Ga_2O_3/PMS (0.41 and 0.25 g L^{-1}) which has a rate constant of 0.0156 min^{-1} in this study. Following the principle of low cost and high efficacy, the dosage of 0.41 g L^{-1} of PMS

and 0.25 g L^{-1} of Ga_2O_3 were preferable under 1:1 molar ratio between PMS and Ga_2O_3 to obtain the most effective photodegradation.

Fig. 5-2C depicts the photocatalytic degradation process of aqueous PFOA in the presence of PMS/Ga_2O_3 with different PMS/Ga_2O_3 molar ratios such as 1:2, 1:1, 2:1 and 3:1 within 90 min. The dose of Ga_2O_3 was kept constant at 0.25 g L^{-1} while the amount of PMS was varied at 0.21, 0.41, 0.82, and 1.23 g L^{-1} for easy comparison. When the ratio was 3:1, the results showed that 100% PFOA was removed within 90 min. While lower ratio of PMS and Ga_2O_3 (i.e. 2:1, 1:1 and 1:2) resulted in lower PFOA degradation (i.e. 82%, 79% and 47%). Furthermore, the pseudo-first-order kinetics were used to evaluate the degradation of PFOA with different ratio of persulfate addition. The rate constant increased with the increasing ratio of PMS/Ga_2O_3 in the system as follows: $k_{3:1} = 0.0211$ $min^{-1} > k_{2:1} = 0.0173$ $min^{-1} > k_{1:1} = 0.0156$ $min^{-1} > k_{1:2} = 0.0061$ min^{-1}. The findings therefore suggest that $SO_4^{\bullet-}$ played a significant role in PMS/Ga_2O_3/UV system for PFOA degradation and a sufficient dose of PMS could boost the degradation efficacy during the photocatalytic process. Thus, increasing the molar ratio between PMS and Ga_2O_3 from 1:2 to 3:1 would be better than increasing their individual amounts for PFOA removal.

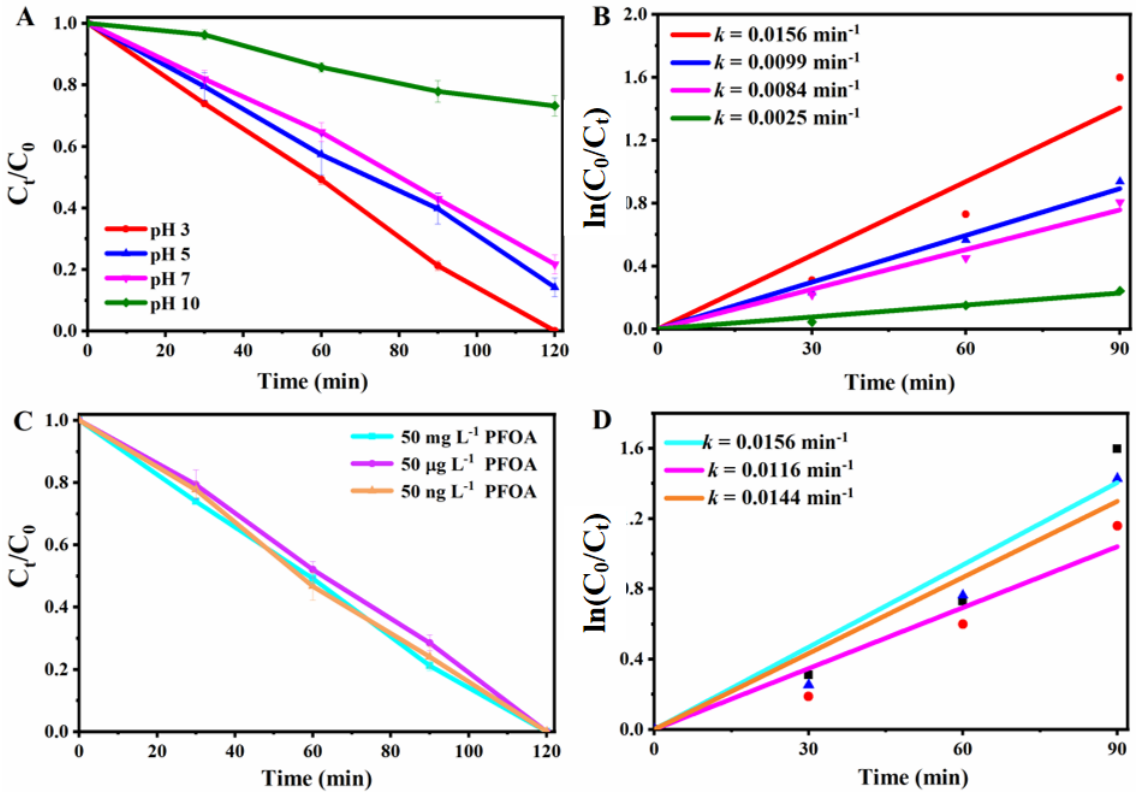

Fig. 5-3. (A) Photocatalytic performance under different initial pH conditions (i.e. pH 3, pH 5, pH 7 and pH 10) activated in PMS/Ga_2O_3/UV system within 120 min ([PFOA] = 50 mg L^{-1}, [PMS] = 0.41 g L^{-1}, [Ga_2O_3] = 0.25 g L^{-1}) and (B) the fitting of degradation curves within 90 min and the rate constant (*k*) derived. (C) Photocatalytic performance with initial PFOA concentration of 50 mg L^{-1}, 50 µg L^{-1} and 50 ng L^{-1} in PMS/Ga_2O_3/UV system within 120 min ([PMS] = 0.41 g L^{-1}, [Ga_2O_3] = 0.25 g L^{-1}) and (D) the fitting of degradation curves within 90 min and the rate constant (*k*) derived.

5.3.3. *Effect of solution pH*

The photodegradation of PFOA was evaluated at various initial solution pH (pH 3, 5, 7 and 10) as shown in **Fig. 5-3A**. Under UV irradiation for 120 min, PFOA exhibited almost 100% removal at pH 3 which was decreased to 86% and 78% when pH was increased to 5 and 7, respectively. The removal of PFOA further dropped significantly to 27% under the basic condition of pH 10. Moreover, the degradation results followed the

pseudo-first-order kinetic profile during the photocatalytic process under UV irradiation, with the rate constant decreasing as k_{pH3} = 0.0156 min^{-1} > k_{pH5} = 0.0099 min^{-1} > k_{pH7} = 0.0084 min^{-1} > k_{pH10} = 0.0025 min^{-1} (**Fig. 5-3B**). Hence, the degradation efficiency increased with decreasing solution pH. This could be attributed to the reaction between sulfate radicals ($SO_4^{\bullet-}$) and OH^- ions forming hydroxyl radicals (•OH) as shown in Eq. 5.2 (Liang et al., 2007):

$$SO_4^{\bullet-} + OH^- \rightarrow SO_4^{2-} + \bullet OH \qquad (5.2)$$

As previously reported, the hydroxyl radicals have poorer reactivity with PFOA in aqueous solution compared with $SO_4^{\bullet-}$ or photogenerated hole and electron pairs (Hori et al., 2004); thus, hydroxyl radicals production in the reaction system could slow down the PFOA degradation. Such a conclusion was also drawn from the research by (Lee et al., 2009). In addition, in basic solution, abundant OH^- ions would react with •OH, which further inhibited the reaction of PFOA degradation following Eq. 5.3:

$$\bullet OH + OH^- \rightarrow O^{\bullet-} + H_2O \qquad (5.3)$$

On the other hand, the pH also affects the dissociation of ionizable chemicals such as PFOA in solution and consequently, influences their photocatalytic performance. As the pK_a of PFOA is about 2.8 (Burns et al., 2008), in the aqueous solution it is mainly in the protonated form ($C_7F_{15}COOH$) at pH < 2.8 and the anionic form ($C_7F_{15}COO^-$) at pH > 2.8 based on Eq. 5.4 and 5.5:

$$C_7F_{15}COOH \rightleftharpoons H^+ + C_7F_{15}COO^- \qquad (5.4)$$

$$pKa = pH - \log\frac{C_7H_{15}^-}{C_7H_{15}COOH} \qquad (5.5)$$

The zeta potential of Ga_2O_3 continuously decreased with the increased solution pH and the points of zero charge (pH_{pzc}) was 8.6 as measured (**Fig. 5-4**), which is in accordance with the previous research (Zhao et al., 2015a). This suggests that when the solution pH was lower than 8.6, the surface of Ga_2O_3 was positively charged due to the protonation;

while over pH 8.6, the surface of Ga_2O_3 was negatively charged. In addition, compounds adsorption on catalyst is a significant step during the photocatalytic process. The lower the pH value is, the more positive the Ga_2O_3 surface will be. Therefore, comparatively high amount of PFOA was adsorbed on the surface of Ga_2O_3 at pH 3 due to the Coulombic attraction, promoting the photodegradation efficacy.

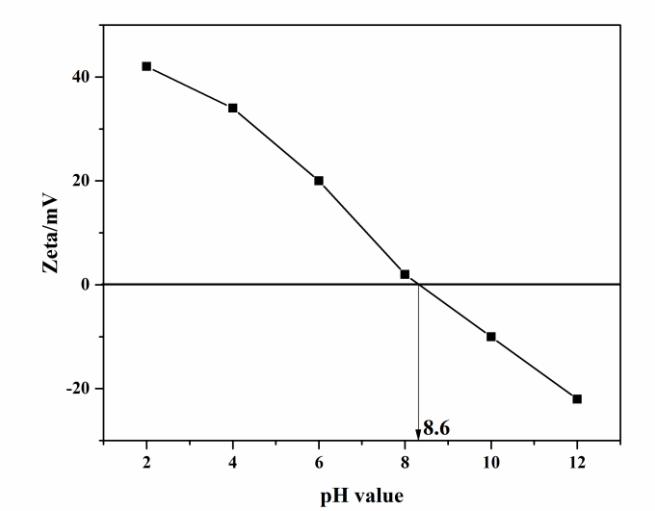

Fig. 5-4. Zeta potential of Ga_2O_3.

5.3.4. *Effect of initial PFOA concentration*

Initial PFOA concentration might affect the degradation rate (Hamid and Li, 2018; Tian and Gu, 2018). This study investigated three initial PFOA concentrations: 50 mg L^{-1}, 50 µg L^{-1} and 50 ng L^{-1}, to cover its likely levels in the aquatic environment. In the solution, PMS and Ga_2O_3 were set at 0.41 g L^{-1} and 0.25 g L^{-1}, respectively and the solution pH was adjusted to 3 to achieve the best performance of PFOA degradation. **Fig. 5-3C** shows that all three levels of concentration have similar degradation efficacy with similar rate constant at 0.0144–0.0156 min^{-1} (**Fig. 5-3D**), demonstrating that the photodegradation performance was relatively independent of initial PFOA concentrations. The results are due to the fact that 0.41 g L^{-1} of PMS and 0.25 g L^{-1} of Ga_2O_3 provided sufficient active sites and radicals, which completely degraded PFOA ranging from 50 ng

L^{-1} to 50 mg L^{-1} at the similar degradation rate. Therefore, PMS/Ga_2O_3/UV system provided very effective treatment of PFOA whether at trace level (ng L^{-1}) or high level (mg L^{-1}), with great potential for decontaminating water and wastewater with varying degrees of pollution.

5.3.5. *Effect of light sources*

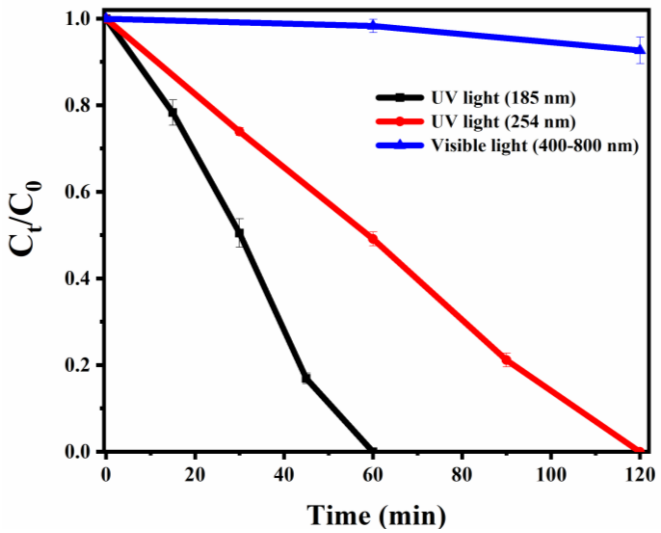

Fig. 5-5. Photocatalytic performance by PMS/Ga_2O_3 under UV light (185 nm, 254 nm) and visible light (400-800 nm) ([PMS] = 1.23 g L^{-1}, [Ga_2O_3] = 0.25 g L^{-1}).

To explore the effect of light sources on the efficacy, photodegradation of PFOA (50 mg L^{-1}) under the optimum conditions (1.23 g L^{-1} PMS, 0.25 g L^{-1} Ga_2O_3, pH 3) were conducted with both UV light (185 nm and 254 nm) and visible light (400–800 nm). **Fig. 5-5** presents that Ga_2O_3 with PMS under 185 nm UV light has higher degradation efficacy, as 100% PFOA was removed within 60 min. While under 254 nm UV light, the time spent for complete removal increased to 120 min. Furthermore, under visible light (400-800 nm), PFOA could only be degraded to a smaller extent. The results show that PMS/Ga_2O_3 absorption of 185 nm UV light was higher than that of 254 nm UV light, which in turn was significantly higher than that of visible light.

Notably, nanostructured In_2O_3 such as nanocubes, nanoplates and porous microsphere were synthesized previously (Li et al., 2012a; Li et al., 2013b). Until now, these synthesized catalysts showed better performance of PFOA degradation under UV light (15 W, 254 nm) compared with other synthesized catalysts (i.e. Cu-TiO_2, TiO_2 nanotube arrays, Pb-$BiFeO_3$/RGO) in previous studies (Chen et al., 2015a; Shang et al., 2018; Wu et al., 2016). They could remove all PFOA (30 mg L^{-1}) within 30, 60 and 120 min, respectively. However, such catalysts need many precursors and a solvothermal process for their synthesis, hence high cost. In this study, PMS/Ga_2O_3/UV system prepared by mixing the commercial Oxone and Ga_2O_3 at a molar ratio (e.g. 3:1) under UV irradiation (32 W, 254 nm, 1.71 mW cm^{-2}) achieved comparatively high efficacy with complete removal of 50 mg L^{-1} PFOA in 90 min. Moreover, when the wavelength of UV light was changed to 185 nm, the degradation time was shortened to 60 min by PMS/Ga_2O_3. Therefore, PMS/Ga_2O_3/UV system has the advantages of being easily prepared, low cost and high degradation efficiency, hence demonstrating significant potential to be applied for PFAS removal in the aquatic environment.

5.3.6. *Calculation of quantum yield*

The results were analysed in terms of not only the first-order kinetic model, but also the explicit effect of photon absorption. The quantum yield (Φ), defined as moles of PFOA degraded per Einstein of photons absorbed by certain amount of catalysts, was estimated by Eq. 5.6:

$$\Phi = \frac{Total\ number\ (moles) of\ PFOA\ degraded}{Total\ number\ (moles)\ of\ photons\ absorbed\ in\ the\ system} \quad (5.6)$$

The photocatalytic rate constant of the PFOA, *k*, under UV light (254 nm) can be used for the calculation of the reaction quantum yield as shown in Eq. 5.7:

$$\Phi = \frac{k_{\Delta}}{I_a} \quad (5.7)$$

where k_{Δ} = d(C_0-C_t)/dt (0.43 mg L^{-1} min^{-1}), and I_a is the photon numbers absorbed by the catalysts, which can be calculated by Eq. 5.8:

$$I_a = \frac{E_p \times \left(1-10^{-2\cdot(\alpha(\lambda)\cdot C)\cdot z}\right)}{z} \times \frac{A1-A0}{A1} \quad (5.8)$$

where E_p is the average photon intensity (1.71 mW cm^{-2}), C is the concentration of the catalyst solution (2.8 mM) and z is the mixed depth of the water column (1.3 cm). In addition, A is the amount of light absorbed by the catalyst at wavelength 254 nm, which was detected by the spectrophotometer. $\alpha(\lambda)$ is the light attenuation coefficient of the catalysts which is calculated as:

$$\alpha(\lambda) = \frac{A}{Cl} \quad (5.9)$$

where l is the distance that light travels through the solution (1 cm). Based on the data summarized in **Table 5-1**, the quantum yield by the catalysts of PMS/Ga_2O_3 (0.41 g L^{-1} and 0.25 g L^{-1}, respectively) under UV light (254 nm) was 0.009 mol $Einstein^{-1}$. The details of calculation are presented as follows:

Table 5-1

The key experimental parameters and their values in this study.

Parameter	Symbol	Value	Detection method
Rate constant	K	0.0156 min^{-1}	Calculated
Light intensity	I	1.71 mW cm^{-2}	UV intensity meter
PFOA concentration in solution	C_1	0.12 mM	Calculated
Catalyst concentration in solution (Ga_2O_3+PMS)	C_2	2.8 mM	Calculated
Light absorbed by PFOA solution at 254-nm	A_0	0.002	spectrophotometer
Light absorbed by mixed solution (PFOA+Ga_2O_3+PMS) at 254-nm	A_1	0.212	spectrophotometer
Mixed depth of the water column	z	1.3 cm	Measured
Distance of light passage through solution	l	1 cm	Measured

$$One\ photon\ energy\ (E_0) = \frac{hc}{\lambda} \qquad (5.10)$$

$E_0 = 6.63 \times 10^{-34}$ J·s × 3×10^8 m·s^{-1} / (254×10^{-9} m) = 7.8×10^{-19} J

For one mole of photon, the energy is $E_m = eE_0$

I = 1.71 mW cm^{-2} = 1.71 mJ cm^{-2} s^{-1}

$E_p = I / E_m$ (5.11)

= 1.71×10^{-3} / [(6.02×10^{23}) (7.8×10^{-19})] Einstein cm^{-2} s^{-1}

= 3.6×10^{-9} Einstein cm^{-2} s^{-1}

$A_1 - A_0 = \alpha(\lambda)Cl$ (5.12)

Catalyst: $\alpha(\lambda) = (A_1 - A_0) / (Cl)$

= 0.210 / (0.0028 M × 1 cm) = 75.0 M^{-1} cm^{-1}

The photo number absorbed by catalyst:

$$I_a = \frac{E_p * \left(1 - 10^{-2*(\alpha(\lambda)*C2)*z}\right)}{z} * \frac{A1 - A0}{A1}$$ (Einstein cm^{-3} s^{-1})=1.98×10^{-9} Einstein cm^{-3} s^{-1}

(5.13)

$k_\Delta = d(C_0 - C_t)/t$=0.4274 mg L^{-1} min^{-1} (5.14)

$$\Phi = \frac{k_\Delta}{1000 I_a} \qquad (5.15)$$

= (0.4274/(1000 × 60 × 414.07) mol L^{-1} s^{-1}) / (1000 × 1.98 ×10^{-9} Einstein cm^{-3} s^{-1})

= 0.009 mol Einstein^{-1}

5.3.7. *Photocatalysis mechanism*

5.3.7.1. Intermediates analysis

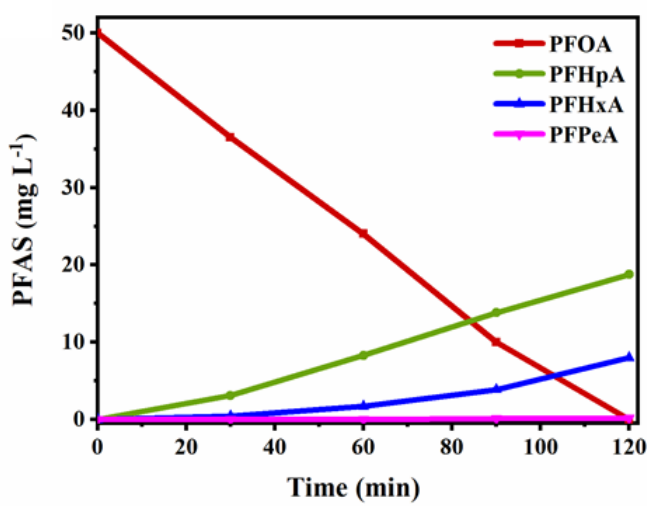

Fig. 5-6. Evolution of PFOA and shorter-chain intermediates during PFOA degradation in PMS/Ga_2O_3/UV system within 120 min.

Intermediates during PFOA photocatalytic process were identified and quantified with UHPLC-MS/MS, which were the shorter-chain PFAS including PFHpA, PFHxA, PFPeA, PFBA, PFPA and TFA as shown in **Fig. 3-1**. **Fig. 5-6** presents the time-dependence of the intermediates during the photodegradation process over PMS/Ga_2O_3 under 254 nm UV light irradiation. PFHpA increased slowly to about 18.77 mg L^{-1} within 120 min, with the target pollutant PFOA decreasing from 50 mg L^{-1} to nearly zero. The amount of PFHxA was gradually increased to 7.98 mg L^{-1} within 120 min and PFPeA was firstly detected at 90 min and slightly increased to 0.175 mg L^{-1} at 120 min. While species with shorter chains (i.e. PFBA PFPA and TFA) had the low concentrations (below limit of quantification). This phenomenon suggests that PFOA was degraded stepwise into shorter chain intermediates such as PFHpA, PFHxA and PFPeA, which was consistent with the previous study (Lee et al., 2009).

5.3.7.2. Analysis of active species

In PMS/Ga_2O_3/UV system, five types of active species including sulfate radicals ($SO_4^{\bullet-}$), photoinduced holes (h^+) and electrons (e^-), hydroxyl radicals (•OH), and

superoxide radical anions ($O_2^{\bullet-}$), could be produced during the photocatalytic process as shown in eqs 5.16-5.19 (Chen et al., 2016):

$$HSO_5^- + hv \rightarrow SO_4^{\bullet-} + \bullet OH \quad (5.16)$$

$$Ga_2O_3 + hv \rightarrow Ga_2O_3\ (h^+ + e^-) \quad (5.17)$$

$$h^+ + H_2O \rightarrow \bullet OH + H^+ \quad (5.18)$$

$$e^- + O_2 \rightarrow O_2^{\bullet-} \quad (5.19)$$

To confirm which active species take the lead in the photocatalytic reaction, *t*-BuOH, EDTA-Na_2 and BQ were added to the system, which were used as scavengers of •OH, holes and $O_2^{\bullet-}$, respectively. Degradation by Ga_2O_3 only was used to simulate the condition of adding the scavenger of $SO_4^{\bullet-}$ radicals. **Fig. 5-7** shows the scavengers effect on the photocatalysis in PMS/Ga_2O_3/UV system and the rate constants were provided during 90 min of the photocatalytic process. When no scavengers were added, 100% PFOA could be degraded within 120 min with the rate constant of 0.156 min^{-1}. However, during the degradation by Ga_2O_3 only (equivalent to the scavenging of $SO_4^{\bullet-}$), the degradation rate dropped to 47%, and the rate constant decreased to 0.0081 min^{-1}. The results suggested that $SO_4^{\bullet-}$ produced by PMS was a critically important oxidant for PFOA degradation in the photocatalytic system. In addition, *t*-BuOH added in the solution resulted in 63% PFOA removal with the rate constant of 0.0068 min^{-1}. The findings indicated that •OH radicals should be a secondary active species compared with $SO_4^{\bullet-}$ and $O_2^{\bullet-}$ radicals reacting with PFOA under UV irradiation. Additionally, when EDTA-Na_2 was added in the system, only a slight decrease was observed on the degradation rate compared with that of no scavenger addition, as 80% PFOA was degraded within 120 min and the rate constant could reach 0.0087 min^{-1}. Such findings suggest that photogenerated electrons rather than photogenerated holes were the main factor promoting the photocatalytic efficacy, which are consistent with the previous study (Zhao

et al., 2015a). When BQ was added in the PFOA solution, the degradation rate was significantly reduced to 38% and the rate constant was 0.0037 min^{-1}, indicating that $O_2^{\bullet-}$ radicals generated by electrons had obvious effect on the PFOA degradation. As shown in Eq. 5.19, the generation of superoxide from the conduction band electrons reduces the quantity the electrons. BQ inhibited the generation of superoxide, which indirectly increased the quantity of electrons. While the electron has well degradation capability for the degradation. Thus, when BQ was added to the solution, the degradation rate was reduced mainly due to the loss of $O_2^{\bullet-}$ radicals in the reaction, proving that $O_2^{\bullet-}$ radicals was essential for the PFOA photodegradation. Conclusively, the results proved that the $SO_4^{\bullet-}$ radicals produced by PMS, $O_2^{\bullet-}$ radicals, and photogenerated electrons (e^-) played major roles in degrading PFOA in the PMS/Ga_2O_3/UV system. The •OH radicals are of secondary importance while photogenerated holes have little effect on the degradation efficacy.

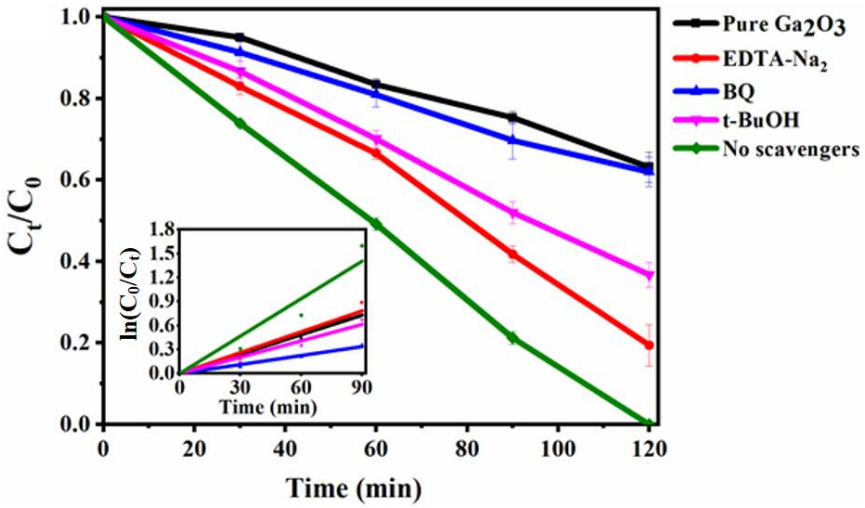

Fig. 5-7. Effects of different scavengers (i.e. Pure Ga_2O_3, EDTA-Na_2, BQ, *t*-BuOH, no scavengers) on the PFOA degradation in PMS/Ga_2O_3/UV system within 120 min. Insert showing the fitting of degradation curves within 90 min and degradation rate constant (*k*) derived (D).

5.3.7.3. Photocatalytic process

According to the intermediates presence and main active species photogenerated electrons (e^-), $SO_4^{\bullet-}$ and $O_2^{\bullet-}$ radicals during the photocatalytic process as mentioned above, the PFOA degradation process can be described as follows. First, the fluorine atom was more preferable than the carbon atom to react with photo-induced electron (e^-), leading to the cleavage of C-F bonds, similar to previous studies on perfluorocarboxylates photodegradation (Qu et al., 2010; Song et al., 2013). Moreover, the α-position C-F bond was more easily attacked by e^- due to the inductive effect of the carboxyl in PFOA. Thus, fluorine was eliminated from PFOA to form $C_7F_{13}H_2COOH$:

$$C_7F_{15}COOH + e^- \rightarrow \bullet C_7F_{14}COOH + F^- \quad (5.20)$$

$$\bullet C_7F_{14}COOH + H_2O \rightarrow C_7F_{14}HCOOH + \bullet OH \quad (5.21)$$

$$C_7F_{14}HCOOH + e^- \rightarrow \bullet C_7F_{13}COOH + F^- \quad (5.22)$$

$$\bullet C_7F_{13}COOH + H_2O \rightarrow C_7F_{13}H_2COOH + \bullet OH \quad (5.23)$$

$C_7F_{13}H_2COOH$ was excited by UV irradiation to generate C_6F_{13} radical, COOH radical and CH_2 carbene. Then C_6F_{13} and COOH radical could recombine to form PFHpA ($C_6F_{13}COOH$):

$$C_7F_{13}H_2COOH \rightarrow \bullet C_6F_{13} + :CH_2 + \bullet COOH \quad (5.24)$$

$$\bullet C_6F_{13} + \bullet COOH \rightarrow C_6F_{13}COOH \text{ (PFHpA)} \quad (5.25)$$

Consequently, PFHpA was decomposed into PFHxA and PFPeA, and theoretically, it would continue degradation to form PFBA, PFPA and TPA in the same way and finally become mineralized to CO_2 and fluoride ions in the stepwise manner as reported (Li et al., 2013c).

In the Ga_2O_3/UV system, when the adsorption of photon energy is equal or more than the band gap energy of Ga_2O_3, holes and electrons are generated on the surface of Ga_2O_3 particles due to the irradiation of UV light. Notably, the photo-induced electrons

were the main active species for PFOA degradation as mentioned in the previous section, which were also reported (Trojanowicz et al., 2018). However, the recombination of the photo-induced hole and electron could seriously reduce the photocatalytic efficiency (Li et al., 2018). In the PMS/Ga_2O_3/UV system, sulfate radical anions ($SO_4^{\bullet-}$) and $O_2^{\bullet-}$ can oxidize PFOA into perfluorinated alkyl radicals (•C_7F_{15}):

$$SO_4^{\bullet-} + C_7F_{15}COOH \rightarrow SO_4^{2-} + \bullet C_7F_{15}COOH^+ \quad (5.26)$$

$$\bullet C_7F_{15}COOH^+ \rightarrow \bullet C_7F_{15} + CO_2 + H^+ \quad (5.27)$$

$$C_7F_{15}COOH + O_2^{\bullet-} \rightarrow \bullet C_7F_{15} + CO_2\uparrow + HO_2^- \quad (5.28)$$

Then formed C_7F_{15} radical react with water to form $C_6F_{13}COF$ after H^+ and F^- elimination:

$$\bullet C_7F_{15} + H_2O \rightarrow C_7F_{15}OH + H \quad (5.29)$$

$$C_7F_{15}OH \rightarrow C_6F_{13}COF + HF \quad (5.30)$$

By hydrolysis, $C_6F_{13}COF$ is converted into PFHpA ($C_6F_{13}COOH$) with CF_2 units reduced and followed by a stepwise degradation of PFOA to form shorter chain PFAS:

$$C_6F_{13}COF + H_2O \rightarrow C_6F_{13}COOH\ (PFHpA) + HF \quad (5.31)$$

Furthermore, the excited e^- could activate MPS to produce $SO_4^{\bullet-}$ radicals, which have been demonstrated in a previous study (Liu et al., 2017). These processes could explain that photodegradation efficiency was much better in PMS/Ga_2O_3/UV system than by sole Ga_2O_3 or PMS:

$$S_2O_8^{2-} + 2e^- \rightarrow 4SO_4^{\bullet-} \quad (5.32)$$

Overall, the mechanism during the photocatalysis process of PFOA degradation in the PMS/Ga_2O_3/UV system is postulated in **Fig. 5-8**.

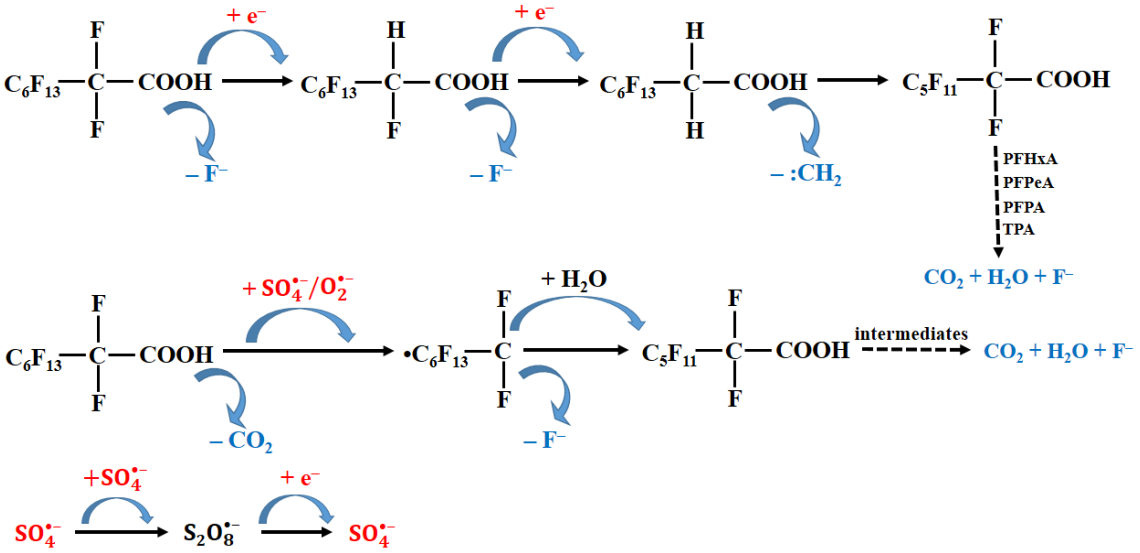

Fig. 5-8. The mechanism of PFOA degradation during the photocatalytic process in PMS/Ga_2O_3/UV system. The active species are marked in red, and the ion or compounds removed during degradation are marked in blue.

5.4. Conclusions

PFOA removal from aqueous solution was studied by UV photocatalysis using Ga_2O_3 and further enhanced in the presence of PMS. Specifically, the application of 1.23 g L^{-1} of PMS and 0.25 g L^{-1} of Ga_2O_3 was able to degrade 100% PFOA in aqueous solution within 90 min under UV 254 nm and 60 min under UV 185 nm. Furthermore, acidic condition at pH 3 was favourable for PFOA degradation in PMS/Ga_2O_3/UV system. Such degradation was not affected by the initial concentration of PFOA ranged from 50 ng L^{-1} to 50 mg L^{-1}. The quantum yield during photocatalysis by PMS/Ga_2O_3 under UV light (254 nm) was 0.009 mol $Einstein^{-1}$. Through the analysis of intermediates, PFOA was gradually degraded from long chian species into short chain intermediates. Scavenger experiments proved that $SO_4^{\bullet-}$ radicals, $O_2^{\bullet-}$ radicals and photogenerated electrons were the most important active species contributing to the PFOA photodegradation. Overall,

the PMS/Ga_2O_3/UV system has great potential to be applied in the photodegradation of PFOA and other similar organic pollutants in water and wastewater.

Chapter 6. Visible and UV photocatalysis of aqueous perfluorooctanoic acid by TiO_2 and peroxymonosulfate: Process kinetics and mechanistic insights

6.1. Introduction

PFAS have been extensively used in industry and consumer products since the 1950s (Janousek et al., 2019). The chemical structure of common PFAS were exhibited in **Fig. 1-1**. Consequently, some PFAS, particular PFOA, are widely reported in the aquatic environment to reach μg L^{-1} and even up to mg L^{-1}. For instance, it was reported that the concentration of PFOA in the surface water of Bormida River, Italy ranged from 0.253 to 6.468 μg L^{-1}, with the mean value of 1.613 μg L^{-1} (Valsecchi et al., 2015). In studying PFAS occurrence in surface water within a 10 km radius from a mega-fluorochemical industrial park, it was found that PFOA was in a severe contamination level with the concentration ranging from 0.0386 to 1707.29 μg L^{-1} (Liu et al., 2016). These levels constitute human health risks, which may lead to growth and reproduction toxicity, liver injury and even cancer from PFOA exposure (Bassler et al., 2019; Behr et al., 2018; Hurley et al., 2018). In February 2019, United States, Environmental Protection Agency (US, EPA) built a multi-media, multi-program, national communication and research plan to address an emerging environmental challenge like PFAS (https://www.epa.gov/pfas). Therefore, it is increasingly urgent to develop novel technologies with high efficacy and low cost for PFAS degradation.

TiO_2 has proven to be one of the promising semiconductors for heterogeneous catalyst due to its wide band gap (3.14 eV), nontoxicity and long-term photostability (Yoo et al., 2018; Zhang et al., 2019). Meanwhile, it has some obvious drawbacks such as the recombination of photo-generated charge carriers, which reduces the overall quantum efficiency and usually inability to be activated under visible light (Cao et al., 2016; Pan et al., 2013). Hence, TiO_2 is widely used as co-catalyst synthesized with other materials during the photocatalytic process (Wang and Zhang, 2011). For example, the accelerated TiO_2 photodegradation of Acid orange 7 (AO7) were investigated under visible light

mediated by peroxymonosulfate (PMS) (Chen et al., 2012). PMS, as an environmentally friendly oxidant, could produce sulfate radicals ($SO_4^{\bullet-}$) in the solution and has a remarkable synergistic effect in the combined TiO_2/PMS system (Feng et al., 2018; Jo et al., 2018). As a consequence, AO7 was fully degraded by TiO_2/PMS within 1.5 h, while only about 60% AO7 was removal by TiO_2 only (Chen et al., 2012). In another instance, it was found that TiO_2/PMS could efficiently degrade lindane by visible light with 100% removal within 4 h (Khan et al., 2017a).

The aims of this work were to investigate the degradation efficacy of PFOA removal by TiO_2 with PMS under different light resources and to explore the possibility for the degradation under visible light. The effect of catalysts dosage and initial solution pH were also investigated. The reaction intermediates of PFOA in the Vis/TiO_2/PMS system were identified and a possible degradation pathway is proposed according to the scavenger experiments.

6.2. Methodology

All experiments were conducted in a cylindrical reactor vessel filled with 200 mL of PFOA solution (50 mg L^{-1}) and mixed continuously using magnetic stirring. The concentration of 50 mg L^{-1} was comparatively higher than that in the most contaminated water, which was also used as the initial concentration in the previous literature (Panchangam et al., 2009). PFOA aqueous solution was prepared by diluting the stock solution in the beaker. The catalysts were added and stirred for 0.5 h under darkness to achieve adsorption-desorption equilibrium. The effect of solution pH on PFOA photodegradation was assessed by varying solution pH at 3, 5, 7 and 10.

The powerful visible light source was provided by a 300 W Xenon lamp (HSX-F500, NBeT Company, China) positioned 38 cm above the liquid surface inside the

reactor. A cut off was used to remove wavelengths shorter than 400 nm so the wavelength of the light source ranged from 400–770 nm. The electric current was 20 A and light intensity in the centre of the reactive solutions was 829.6 mW cm^{-2} for the Xenon light source as measured by a light intensity meter (HSX-F500). While the general visible light source was emitted by a 30 W Xenon lamp (NBeT Company, China) and the light intensity was detected of 3.65 mW cm^{-2}. In addition, two 32 W low-pressure UV lamp (Cnlight Co. Ltd., Shanghai, China) with wavelengths of 254 nm and 185 nm, respectively were also used. The irradiation intensity of UV light at 254 nm wavelength was 3.7 mW cm^{-2} as measured by a UV intensity meter (ST-512). At regular time intervals, aliquots of the sample were taken using a syringe and filtered through a filter (Puradisc syringe filter, 0.2 μm, Whatman) before analysis. To avoid the possible impact of filter adsorption on PFOA concentration, the first 3 mL filtrate was discarded. All experiments were conducted in triplicate.

6.3. Results and discussion

6.3.1. *Catalyst characterization*

The XRD pattern of the commercial TiO_2 (P25) was exhibited in **Fig. 6-1** and the experimental XRD pattern agrees with the JCPDS card no. 21-1272 (anatase TiO_2) (Xu et al., 2015). The strong diffraction peaks at 25°, and 48° confirms the TiO_2 (~80%) anatase and (~20%) rutile structure and the broad diffraction peaks indicate very small size crystallite (Hussain et al., 2010). Also, **Fig. 6-2** gave the UV-vis diffuse reflection absorption spectra of aqueous PFOA, PMS, TiO_2 and TiO_2/PMS. PFOA and PMS show negligible absorbance for all the light resources. Comparatively, TiO_2 has the increasing absorbance ability of the light resource with the decreasing of the light wavelength from 800 to 250 nm, which proves that TiO_2 has a certain ability for visible light absorption

(400–800 nm) but worse than that for UV light (< 400 nm). However, when TiO_2 was mixed with PMS in the solution, promoted light absorbance was observed in the range of visible light resource (400–800 nm). This is probably because, in the mixed suspension, some visible-light absorbing complexes on TiO_2 surface was formed with the addition of PMS. A previous study investigated the activation of PMS with TiO_2 on visible light irradiation and claimed that surface charge-transfer complex ($Ti\text{-}OOSO_3^-$) was produced through the reaction (i.e. $>TiO_2 + HSO_5^- \rightarrow > Ti\text{-}OOSO_3^- + H_2O$), which was responsible for the visible light absorption in TiO_2/PMS suspensions (Jo et al., 2018).

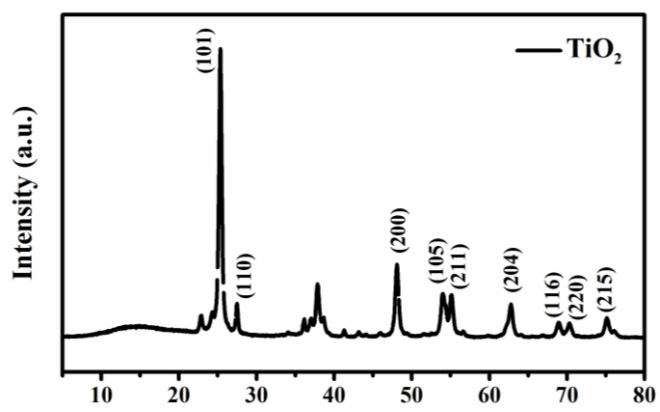

Fig. 6-1. XRD pattern of TiO_2 catalyst.

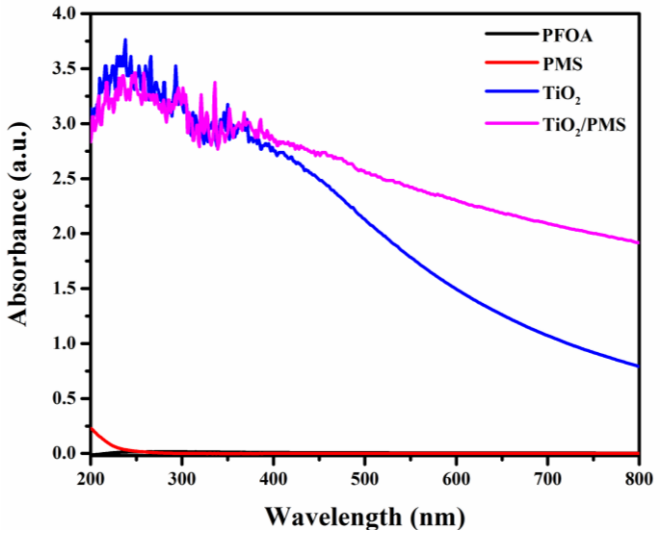

Fig. 6-2. UV-vis absorption of PFOA, PMS, TiO_2 and TiO_2/PMS.

6.3.2. *Degradation performance of PFOA under visible light*

Comparative experiments with different catalysts (PMS, TiO_2, and TiO_2/PMS) were conducted to explore the synergistic effect of TiO_2 and PMS under powerful visible light irradiation (300 W, 400-770 nm wavelength). Some same experiments were conducted under both darkness and general visible light (30 W) for the comprehensive analysis. The initial concentration of PFOA was 50 mg L^{-1}, which could be the level in some seriously contaminated water. The catalysts of PMS and TiO_2 were 0.72 g L^{-1} and 0.25 g L^{-1}, respectively, in either the separate system or the TiO_2/PMS system. While a different amount of the catalysts would be further investigated in the next section. No other solution was added to adjust the pH value, and the initial pH of the solution was 3.0 ± 0.2.

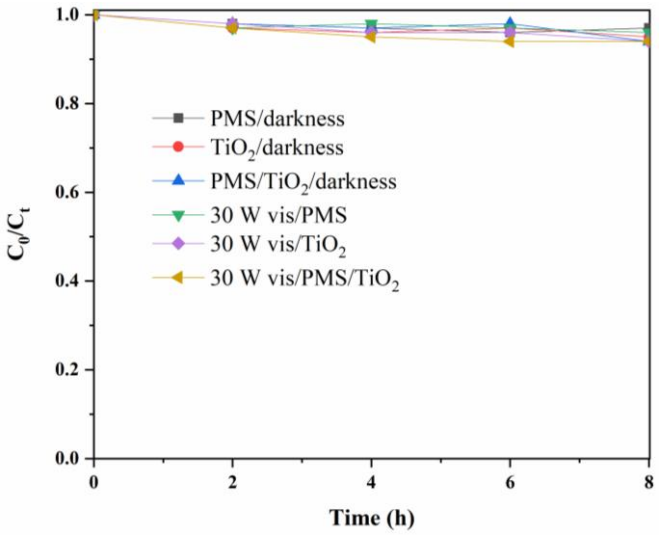

Fig. 6-3. Photodegradation of PFOA by TiO_2 and PMS under darkness and 30 W visible light.

As a result, **Fig. 6-3** presents that all the catalysts (i.e. PMS, TiO_2, and TiO_2/PMS) showed almost no catalytic ability for aqueous PFOA removal under darkness and 30 W visible light, which indicates that PFOA couldn't be largely absorbed by PMS or TiO_2

and these catalysts were not able to be activated under general visible light, respectively. Nevertheless, when the light source was changed to a more powerful visible light (300 W), the degradation performance was obviously promoted by PMS/TiO_2 that almost 100% of PFOA was degraded within 8 h. This might be attributed to the increasing light intensity which could activate TiO_2 under visible light (400-700 nm). In theory, one photon energy (E_0) is calculated as: $E_0 = \frac{hc}{\lambda}$, where h is Planck's constant of 6.63 × 10^{-34} J·s, c is light speed of 3 × 10^8 m s^{-1}, λ is the wavelength of UV light, which is 400 nm, and thus E_0 is calculated of 5.0 × 10^{-19} J. In addition, the band gap of TiO_2 is 3.14 eV or 5.0 × 10^{-19} J (1 eV = 1.6 × 10^{-19} J), which was approximately equal to E_0. Thus, low powerful visible light provided insufficient photons with the energy of 1.6 × 10^{-19} J to activate TiO_2 producing photogenerating hole and electron pairs. While increasing the light intensity to a certain level (300 W, 829.6 mW cm^{-2} in this study), TiO_2 could work under visible light. In the previous studies, TiO_2 was modified with other materials to be utilized under visible light. For example, it was claimed that nitrogen-doped TiO_2 (N-doped TiO_2) exhibited broad absorption in the visible region, allowing the utilization of a large part of the solar spectrum for photocatalytic degradation of organic pollutants. Further investigation should be focused on the N-doped TiO_2 with PMS under general visible light (about 30 W) or solar irradiation (Ansari et al., 2016) .

On the other hand, under powerful visible light, the degradation of PFOA with the sole PMS was negligible, which means the sulfate radicals ($SO_4^{\bullet-}$), responsible for the PFOA degradation, may not be activated by visible light as shown in Eq. 6.1 (Wang et al., 2015b):

$$HSO_5^- + hv \rightarrow SO_4^{\bullet-} + \bullet OH \qquad (6.1)$$

Comparably, sole TiO_2 showed only about 20% PFOA removal, while TiO_2/PMS has an obvious better catalytic performance for PFOA removal than sole PMS or TiO_2 as shown in **Fig. 6-4A**. The reason might be that holes and electrons could be generated on the surface of TiO_2 irradiated by powerful visible light as mentioned previously (Grilla et al., 2019) and HSO_5^- could react with photogenerated electrons to form sulfate radicals($SO_4^{\bullet-}$) as Eq. 6.2 (Shao et al., 2017). Thus, under powerful visible light, TiO_2/PMS outperformed than TiO_2 or PMS in degrading PFOA. Further reasons are discussed in the following section 3.3.

$$HSO_5^- + e^- \rightarrow SO_4^{\bullet-} + OH^- \qquad (6.2)$$

In addition, the kinetics of the PFOA degradation fitted well to the pseudo-first-order model ($R^2 > 0.90$) described as Eq. 6.3:

$$\ln (C_0/C_t) = k\,t \qquad (6.3)$$

where k is the rate constant (h^{-1}), C_0 and C_t (mg L^{-1}) are the concentrations of PFOA in the solution at irradiation time 0 and t (h), respectively. In the case of TiO_2/PMS, the rate constant was found to be 0.310 h^{-1}, which was almost 11 times higher than that of TiO_2 catalyst, which was only 0.028 h^{-1}. Nevertheless, until now, no previous study has been reported to achieve PFOA photocatalysis under visible light. Thus, the degradation of 50 mg L^{-1} aqueous PFOA within 8 h at the rate constant of 0.310 h^{-1} under 300 W visible light irradiation could be the reference of degradation efficiency for future investigations on the PFOA photocatalysis under the similar conditions to this study.

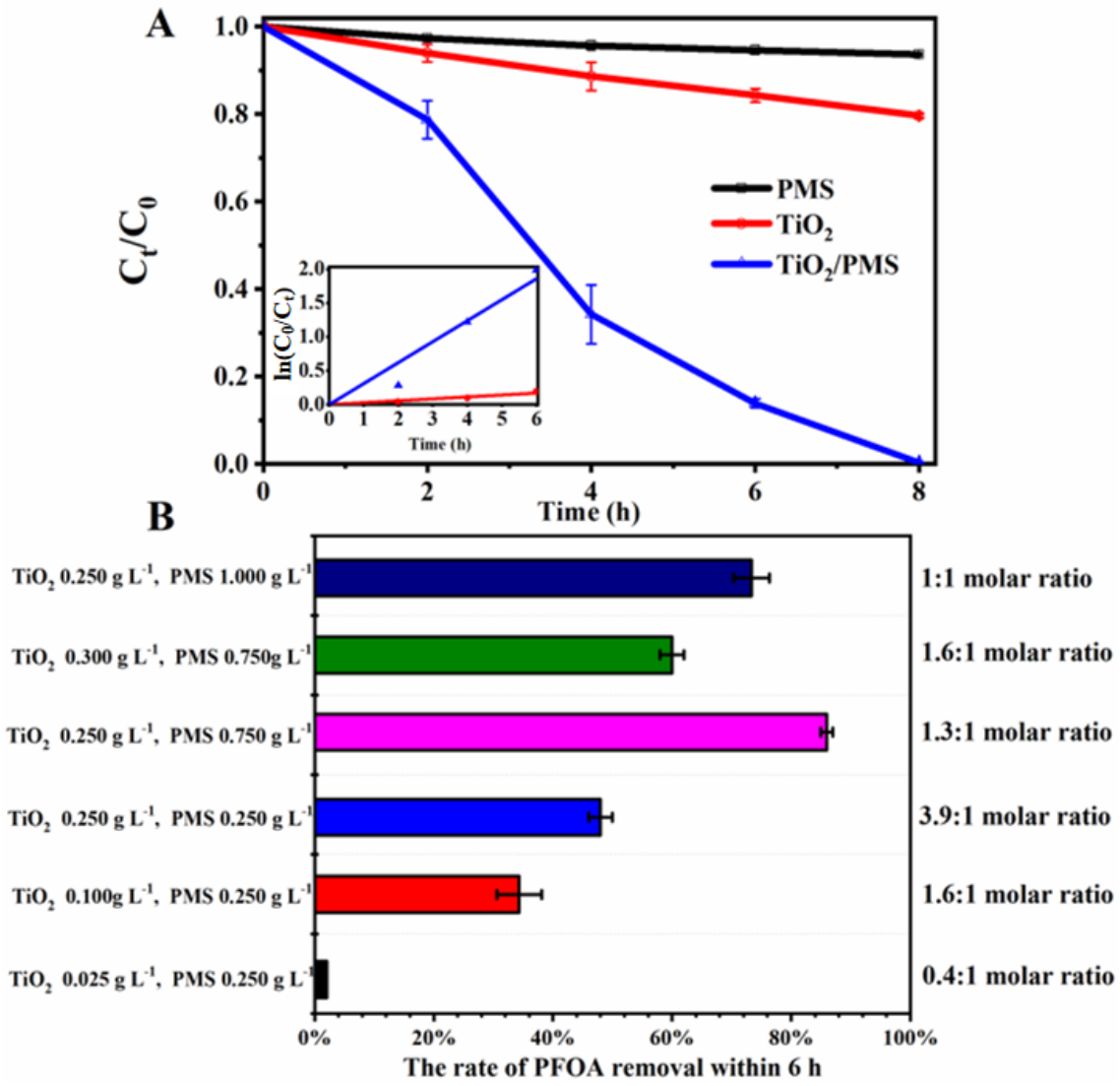

Fig. 6-4. (A) Degradation rate of PFOA in the system of PMS, TiO_2 and TiO_2/PMS, respectively under 300 W visible light irradiation within 8 h ([PFOA] = 50 mg L^{-1}, [PMS] = 0.75 g L^{-1}, and [TiO_2] = 0.25 g L^{-1}). Enlarged view of degradation curves within 6 h and the histogram of each degradation rate constant (k) was also provided. (B) Degradation rate of PFOA by different amount of TiO_2/PMS (300 W visible light, [PFOA] = 50 mg L^{-1}).

6.3.3. *Effects of catalyst dosage*

To select appropriate catalysts dosage, different amounts of PMS and TiO_2 were added in PFOA solution, the PFOA removal in a photocatalysis process under visible light irradiation within 6 h is presented in **Fig. 6-4B**. When the dose of TiO_2 and PMS were 0.025 and 0.25 g L^{-1} with the ratio between them of 0.4:1, almost no PFOA was reduced by the photocatalysis. Because the low amount of TiO_2 could not provide sufficient active species such as photogenerated holes (h^+) and electrons (e^-) for PFOA degradation during the reaction process. However, increasing the molar ratio of TiO_2/PMS from 0.4:1 to 1.6:1, together with PMS constant of 0.25 g L^{-1} (namely [TiO_2] = 0.1 g L^{-1}, [PMS] = 0.25 g L^{-1}), the degradation was increased to 34%. Further, the degradation of PFOA reached 48% when the molar ratio was increased to 3.9:1 (namely [TiO_2] = 0.25 g L^{-1}, [PMS] = 0.25 g L^{-1}). Thus, at 0.25 g L^{-1} PMS, increasing the ratio of TiO_2 could indeed improve the degradation effect. Also, when TiO_2 was kept at 0.25 g L^{-1}, but with the increase concentration of PMS from 0.25 to 0.75 g L^{-1} (the molar ratio of TiO_2/PMS decreased from 3.9:1 to 1.3:1), the degradation of PFOA increased obviously from 48% to 86%. Because the increasing ratio of PMS was able to produce more sulfate radicals (Eq. 6.2), which has oxidative power for the PFOA degradation. Nevertheless, when PMS concentration continually increased to 1.0 g L^{-1} (the ratio of TiO_2/PMS decreased to 1:1), the removal of PFOA did not increase further as expected. The reason could be that the excessive sulfate radicals were quenched to produce sulfate groups. Therefore, excessive ratio of PMS would instead inhibit the photodegradation process. Similarly, when PMS was kept as 0.75 g L^{-1}, and TiO_2 concentration increased from 0.25 to 0.30 g L^{-1}, the degradation of PFOA slightly decreased from 86% to 73%. This might be attributed to that high concentration of TiO_2 would make the solution turbid, which reduced the photo permeability of visible light, leading to a negative effect on the

degradation rate. Similar conclusion was also provided in the previous literatures (Aoudjit et al., 2019; Wang et al., 2014). Hence, on the treatment of 50 mg L^{-1} aqueous PFOA, the preferable amounts of catalyst were 0.25 g L^{-1} TiO_2 and 0.75 g L^{-1} PMS and the suitable molar ratio of TiO_2/PMS was 1.3:1.

6.3.4. *Effects of solution pH*

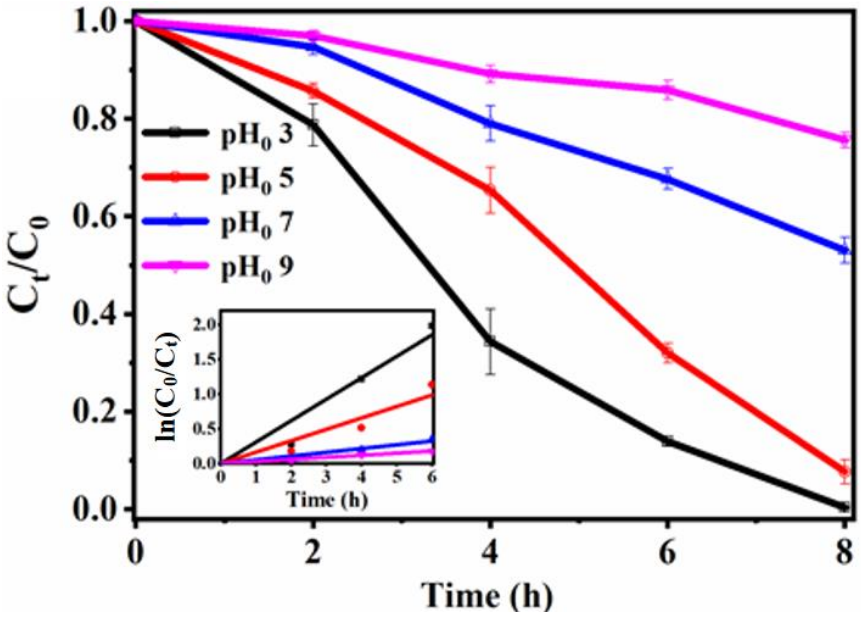

Fig. 6-5. Effect of different initial solution pH conditions (i.e. pH_0 3, 5, 7 and 9) on PFOA degradation in 300 W Vis/TiO_2/PMS system. Insert showing the fitting of degradation curves within 6 h and degradation rate constant (k) derived.

Fig. 6-5 shows the impact of initial pH (pH_0) on the catalytic performance for PFOA degradation in Vis/TiO_2/PMS system. In detail, at pH_0 3 the degradation of PFOA was almost 100% under Vis/TiO_2/PMS photodegradation for 8 h, which was the best performance compared with the other pH conditions. With the increase of pH_0 to 5 and 7, within 8 h the degradation of PFOA was 90% and 45%, respectively. However, the removal of PFOA further dropped significantly to 24% at pH 9. In addition, the degradation rate increased with time and all followed the pseudo-first-order kinetic model

under different pH_0 conditions. Moreover, the rate constant decreased with increase of initial solution pH in the order: $k_{pH3} = 0.310\ h^{-1} > k_{pH5} = 0.165\ h^{-1} > k_{pH7} = 0.054\ h^{-1} > k_{pH9} = 0.030\ h^{-1}$. The results indicate that the degradation efficacy of PFOA in Vis/TiO_2/PMS was higher and faster when the solution pH was low.

Two reasons might explain such a phenomenon. First one was the reaction between the sulfate radical and OH^- ion to form hydroxyl radicals (•OH) as shown in Eq. 6.4 (Liang et al., 2007)

$$SO_4^{\bullet-} + OH^- \rightarrow SO_4^{2-} + \bullet OH \qquad (6.4)$$

Nevertheless, hydroxyl radicals have poor reactivity with PFOA, so the replacement of $SO_4^{\bullet-}$ by •OH would slow down the PFOA degradation (Hori et al., 2004; Lee et al., 2009).

The second reason is related to the Coulombic attraction between the catalysts and pollutants. The surface zeta potential of TiO_2 (**Fig. 6-6**) continuously decreased with the increased of solution pH and the points of zero charge was 5.6. This means that when the solution pH was lower than 5.6, the surface of TiO_2 was positively charged in the form of ($TiOH_2^+$) due to the protonation (Xu et al., 2003), and negatively charged in the form of TiO^- in the solution when pH was above 5.6. On the other hand, the pK_a of PFOA is 2.8 (Burns et al., 2008). Therefore, when solution pH is more than 2.8, PFOA can become deprotonated form ($C_7F_{15}COO^-$) based on the reaction Eq. 6.5:

$$C_7F_{15}COOH \rightleftharpoons H^+ + C_7F_{15}COO^- \qquad (6.5)$$

Thus, as shown in **Fig. 6-7**, when the solution pH was below 5.6 but over 2.8, PFOA could strongly interact with the TiO_2 by electrostatic interaction, leading to the accelerating photodegradation efficacy. However, at pH 6 to 10, the surfaces of the catalysts were negatively charged due to the deprotonation (based on zeta potential value) resulting in an electrostatic repulsion between PFOA (neutral or negatively charged PFOA) and the catalysts (negatively charged). Therefore, acidic conditions (especially

initial of pH 3 in this study) were the most beneficial for PFOA photodegradation in our system of Vis/TiO_2/PMS.

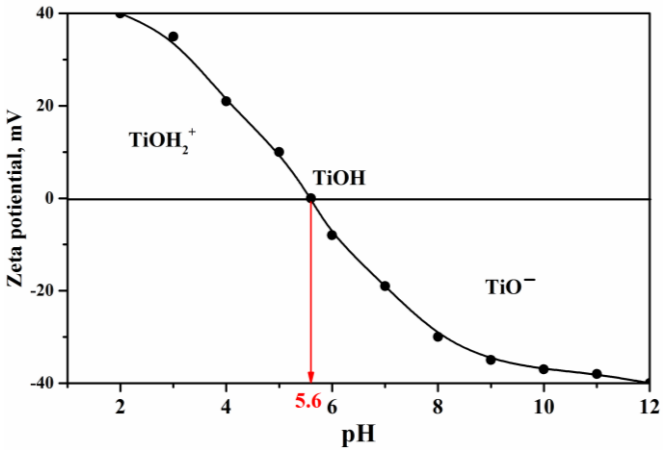

Fig. 6-6. Zeta potentials of TiO_2.

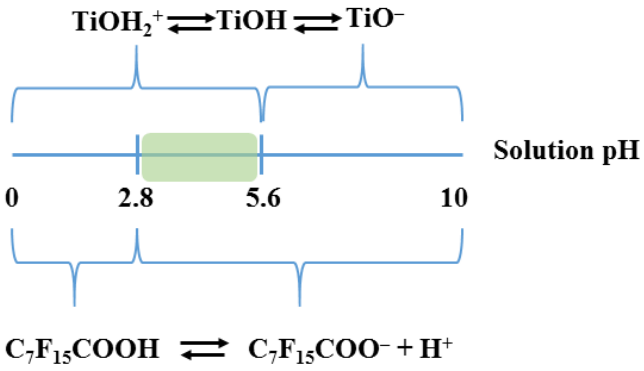

Fig. 6-7. Schematic diagram of Coulombic attraction between TiO_2 and PFOA influenced by the solution pH.

6.3.5. *Effects of light sources*

The photocatalysis of aqueous PFOA was also evaluated by TiO_2/PMS under UV light with the two different wavelengths of 254 and 185 nm, compared with the performance in Vis/TiO_2/PMS. 50 mg L^{-1} PFOA solution was treated by 0.5 g L^{-1} TiO_2 together with 0.15 g L^{-1} PMS without pH adjustment. As shown in **Fig. 6-8**, the degradation efficiencies were almost similar for both wavelengths of 254 and 185 nm and

their degradation was both almost 100% within 1.5 h. Thus, UV light irradiation significantly promoted the degradation rate as the reaction time was 8 h for 100% PFOA removal under visible light, which was more than 5 times longer than that under UV light. The reason might be related to the absorbance ability of different light resources by the catalysts. As shown in **Fig. 6-2**, the absorbance intensity was higher in UV wavelength (< 400 nm) than that in visible light wavelength (400-700 nm), and therefore more quantity of photons was absorbed in the system for the photodegradation. Also, the photons of UV light have higher energy than visible light, which could irradiate more quantity of photoinduced hole and electron pairs, leading to a stronger redox ability for PFOA degradation. Such reasons were also discussed in previous research (Giri et al., 2012). Therefore, TiO_2/PMS have the stronger photocatalytic ability under UV light (both 254 and 185 nm UV light resources) than visible light, but may need more energy cost from UV light.

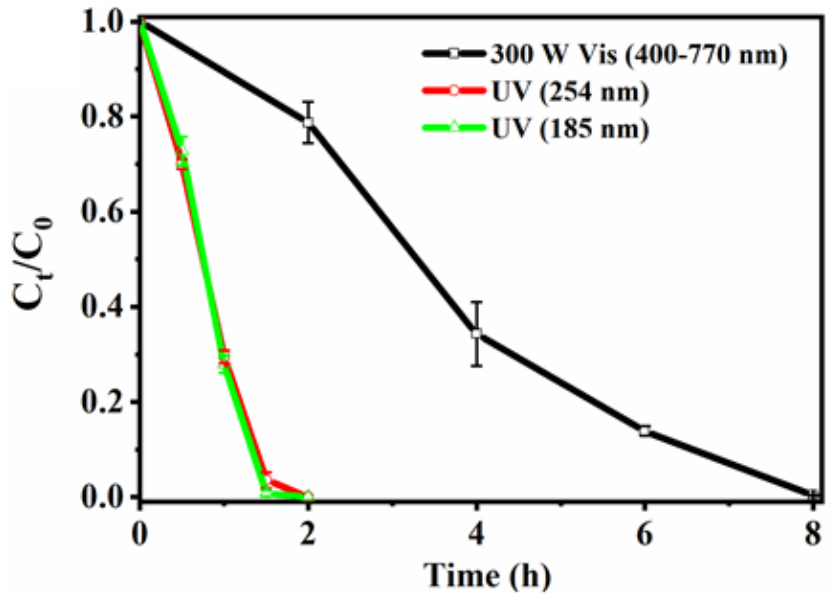

Fig. 6-8. Effect of different light source on PFOA degradation by TiO_2/PMS. Visible light (300 W, 400-770 nm) was produced by a Xenon lamp, and 254 nm and 185 nm UV light

were from two types of low-pressure UV lamps, respectively ([PFOA] = 50 mg L^{-1}, [PMS] = 0.75 g L^{-1}, and [Ga_2O_3] = 0.25 g L^{-1}).

6.3.6. *Advantages of photocatalysis by TiO_2/PMS*

When compared with other materials in the previous studies (**Table 6-1**) (Li et al., 2016; Panchangam et al., 2009), the catalyst of TiO_2/PMS firstly investigated in this study presents excellent advantages on the treatment for aqueous PFOA. Initially, TiO_2/PMS utilized as catalyst under visible light irradiation could degrade PFOA from the solution and 100% PFOA was removal within 8 h. This finding provides the basic knowledge of solar application on the treatment of water containing PFAS, which could be an ideal technology with low energy consumption. Secondly, TiO_2/PMS have comparatively high degradation ability under UV light irradiation compared with other findings as shown in **Table 6-1**. The fluence-based first-order rate constant (k_f, cm^2 mJ^{-1}) and the half-life ($\tau_{1/2}$, h) were introduced to make a comprehensive comparison among different catalytic systems (Zhang et al., 2017). Notably, k_f of TiO_2/PMS under 254 nm UV light was 8.18 × 10^{-4} cm^2 mJ^{-1}, higher than that of all the other catalysts except In_2O_3 PNPs under UV light. The $\tau_{1/2}$ value was found to increase as: $\tau_{1/2}$ (UV/In_2O_3 PNPs = 0.07 h) < $\tau_{1/2}$ (UV/β-Ga_2O_3 Nanorods = 0.27 h) < $\tau_{1/2}$ (UV/TiO_2/PMS = 0.64 h) < the other conditions. Finally, yet importantly, TiO_2/PMS was easy to be prepared by simply mixing the commercial TiO_2 and PMS powders in the solution. However, In_2O_3 PNPs and β-Ga_2O_3 Nanorod with shorter $\tau_{1/2}$ value need more complex synthesizing process than the preparation for TiO_2/PMS. For example, In_2O_3 porous nanoplates (PNPs) were synthesized by ethylenediamine-assisted hydrothermal process, which needs to be maintained at 180 °C for 16 h and 270 °C for 2 h in the air (Li et al., 2014). β-Ga_2O_3 Nanorods were obtained by microwave irradiation hydrothermal synthesis procedure from the precursor of

$Ga(NO_3)_3•H_2O$ (Zhao et al., 2015b). Overall, TiO_2/PMS should be considered as the potential catalyst applied for the photocatalysis of PFOA no matter under visible light for energy saving or UV light for the high degradation efficiency.

Table 6-1

Comparison of Photocatalytic conditions for PFOA removal by TiO_2/PMS in this study and other catalysts in the literature.

Catalyst	Catalyst dosage ($g\ L^{-1}$)	Light source	Light intensity ($mW\ cm^{-2}$)	C_0 (PFOA) ($mg\ L^{-1}$)	Removal (reaction period)	k_t (h^{-1})	[a]k_f ($cm^2\ mJ^{-1}$)	[b]$\tau_{1/2}$ (h)	Reference
TiO_2 with PMS	0.25/0.75	300 W, λ=400–770 nm	129.6	50	100% (8 h)	0.310	6.64×10^{-6}	2.24	This study
TiO_2 with PMS	0.25/0.75	32 W, λ=254 nm	3.7	50	98% (1.5 h)	1.09	8.18×10^{-4}	0.64	This study
TiO_2 with $HClO_4$	0.7	16 W, λ=254 nm	0.45	50	86% (7 h)	0.282	1.74×10^{-4}	2.46	(Panchangam et al. 2009)
TiO_2 with Pt	0.5	125 W, λ=365 nm	5.3	60	100% (5 h)	0.726	0.38×10^{-4}	0.95	(Li et al., 2016)
TiO_2 with Pd	0.5	125 W, λ=365 nm	5.3	60	98% (7 h)	0.438	0.23×10^{-4}	1.58	(Li et al., 2016)
TiO_2 with Ag	0.5	125 W, λ=365 nm	5.3	60	45% (7 h)	0.126	0.07×10^{-4}	5.50	(Li et al., 2016)
β-Ga_2O_3 Nanorod	0.5	50 W, λ=254 nm	35	10	100% (1.5 h)	2.58	0.20×10^{-4}	0.27	(Zhao et al., 2015b)
In_2O_3 PNPs	0.5	15 W, λ=254 nm	3.2	30	100% (0.5 h)	9.48	8.23×10^{-4}	0.07	(Li et al., 2014)

[a]The fluence-based first-order rate constant k_f ($cm^2\ mJ^{-1}$) is calculated as follows: $k_f = \frac{k_t}{I}$, where I is the light intensity.

[b]The half-life ($\tau_{1/2}$) of the reactants is described as: $\tau_{1/2} = \frac{ln2}{k_t}$.

6.3.7. *Proposed degradation mechanism*

6.3.7.1. Intermediates analysis

Intermediates such as PFHpA, PFHxA, PFPeA, PFBA, PFPA and TFA during PFOA photocatalytic process in the TiO_2/PMS system were identified and quantified by UHPLC-MS/MS as shown in **Fig. 3-1**. The $m\ z^{-1}$ ratio of individual compound and the other MS/MS parameters were listed in **Table 3-6**. Thereupon, the time dependence of PFOA and these intermediates were described in **Fig. 6-9A**. Clearly, PFHpA was first produced, and its concentration was increased to the maximum of 0.5 mg L^{-1} within 6 h and then decreased. PFHxA was initially to be detected after 2 h and continuously increased to 1.0 mg L^{-1} within 8 h. PFPeA increased during the time from 4 to 8 h reaction course. However, the concentrations of shorter chains such as PFBA PFPA and TFA were below the limit of quantification. This observation indicates that the photocatalytic process of PFOA proceeds in a step-by-step mode from PFOA to shorter chain intermediates (i.e. PFHpA, PFHxA, and PFPeA) as reported in the literature (Li et al., 2016; Wu et al., 2018).

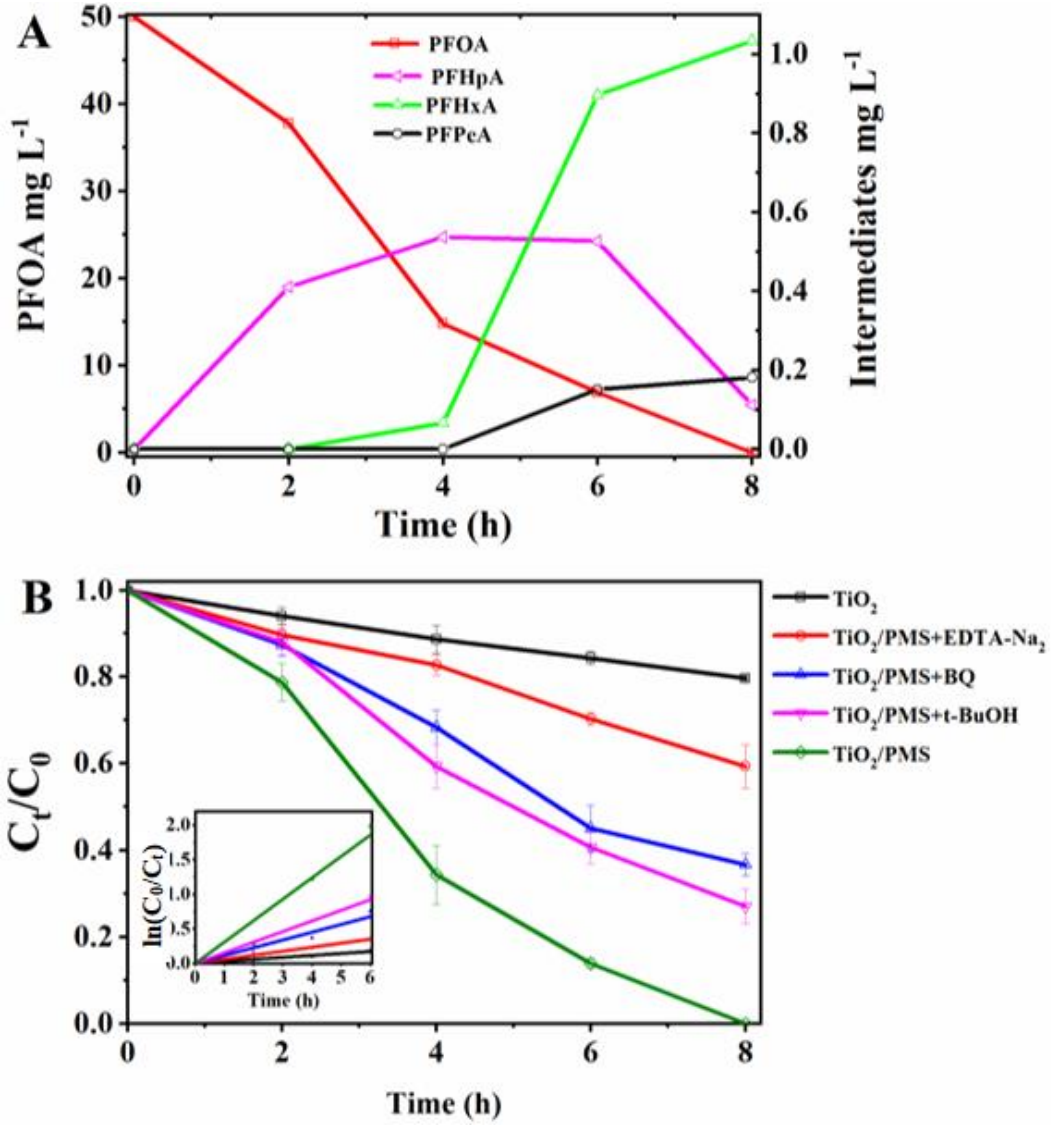

Fig. 6-9. (A) Time dependence of PFOA and its shorter-chain PFAS intermediates. (B) Effects of different scavengers (i.e. Pure TiO_2, EDTA-Na_2, BQ, *t*-BuOH, and no scavengers) on the PFOA degradation in Vis/TiO_2/PMS system within 8 h (300 W visible light, [PFOA] = 50 mg L^{-1}, [PMS] = 0.15 g L^{-1}, [TiO_2] = 0.05 g L^{-1}). Insert showing the fitting of degradation curves within 6 h and degradation rate constant (*k*) derived.

6.3.7.2. Actives species analysis

During the photocatalytic process in Vis/TiO_2/PMS system, four types of active species, including photoinduced holes (h^+) and electrons (e^-), hydroxyl radical (•OH),

sulfate radicals ($SO_4^{\bullet-}$) and superoxide radical ($O_2^{\bullet-}$) are supposed to be generated as shown in Eq.6.2, 6.4 and 6.7, which own the oxidative and reduction ability contributing the PFOA degradation.

$$TiO_2 (h^+) + H_2O \rightarrow TiO_2 + \bullet OH + H^+ \qquad (6.6)$$

$$TiO_2 (e^-) + O_2 \rightarrow O_2^{\bullet-} \qquad (6.7)$$

To prove the degradation ability of these four species, tertbutanol (*t*-BuOH), disodium ethylenediaminetetraacetate (EDTA-Na_2) and benzoquinone (BQ) were added into the system, which was used as scavengers of •OH, holes and $O_2^{\bullet-}$, respectively. Degradation by TiO_2 only was used to simulate the condition of adding the scavenger of $SO_4^{\bullet-}$ radicals. As shown in **Fig. 6-9B**, it is easily observed that degradation by only TiO_2 has the poorest photodegradation performance that only 20% PFOA was removal within 8 h, which proves that $SO_4^{\bullet-}$ radicals play the essential roles in Vis/TiO_2/PMS system for PFOA degradation. Secondly, the addition of EDTA-Na_2 in the reaction solution caused only 40% PFOA removal, which indicates that the photoinduced holes, rather than electrons, could largely react with the absorbed PFOA molecules directly and played the main role in degrading PFOA in the photocatalytic system. While the scavengers of BQ and *t*-BuOH have less negative effect for the degradation efficacy compared with the others. When BQ was added, 63% PFOA was degraded, which suggests that PFOA photodegradation was less influenced by $O_2^{\bullet-}$ radicals generated. Furthermore, when *t*-BuOH was added in the system, 77% PFOA removal was observed on the degradation rate. This suggests that that hydroxyl radical (•OH) owns the worst degradation ability for PFOA than the other species, and it is consistent with the theory that •OH has poor reactivity with PFOA as mentioned in the section 3.2.3. On the other hand, based on degradation curves of different scavengers within 6 h photocatalysis, the rate constant ranked from highest to

lowest was as follows: $k_{(\text{No addition})} = 0.310\ h^{-1} > k_{(\text{t-BuOH})} = 0.154\ h^{-1} > k_{(\text{BQ})} = 0.112\ h^{-1} > k_{(\text{EDTA-Na2})} = 0.058\ h^{-1} > k_{(\text{Only TiO2})} = 0.028\ h^{-1}$. Thus, it means that the active species produced during the photocatalytic process from most important to least for PFOA degrading was followed by: $SO_4^{\bullet-}$ radicals > photoinduced holes (h^+) > $O_2^{\bullet-}$ radicals > •OH. Besides, in the Vis/TiO_2/PMS system, photoinduced holes (h^+) rather than electrons (e^-) played the main role in PFOA degradation.

6.3.7.3 Possible degradation pathway

Based on the intermediates and active species analysis during the photocatalytic process, the primary degradation mechanism occurring in Vis/TiO_2/PMS would be proposed as the following equations (6.8–6.16):

Part of PFOA in the solution could exist as an anionic compound ($C_7F_{15}COO^-$) and was absorbed on the surface of TiO_2 (Chen, et al., 2015a).

$$C_7F_{15}COOH + H_2O \rightarrow C_7F_{15}COO^- + H_3O^+ \quad (6.8)$$

Then, $C_7F_{15}COO^-$ reacts with sulfate radicals ($SO_4^{\bullet-}$) or photoinduced holes (h^+) to form perfluoroperoxy radicals ($C_7F_{15}COO\bullet$) (Wu et al., 2016).

$$C_7F_{15}COO^- + SO_4^{\bullet-} \rightarrow C_7F_{15}COO\bullet + SO_4^{2-} \quad (6.9)$$

$$C_7F_{15}COO^- + h^+ \rightarrow C_7F_{15}COO\bullet \quad (6.10)$$

While the $C_7F_{15}COO\bullet$ is quite unstable and then spontaneously undergo Kolbe decarboxylation to form $C_7F_{15}\bullet$ radicals (Chen et al., 2015a).

$$C_7F_{15}COO\bullet \rightarrow C_7F_{15}\bullet + CO_2\uparrow \quad (6.11)$$

Then formed $C_7F_{15}\bullet$ reacts with water to form $C_6F_{13}COF$ after H+ and F^- elimination (Nohara et al., 2001).

$$C_7F_{15}\bullet + H_2O \rightarrow C_7F_{15}OH + H \quad (6.12)$$

$$C_7F_{15}OH \rightarrow C_6F_{13}COF + HF \quad (6.13)$$

By hydrolysis, $C_6F_{13}COF$ is converted into PFHpA ($C_6F_{13}COOH$) with F^- reduced (Hori et al., 2008b).

$$C_6F_{13}COF + H_2O \rightarrow C_6F_{13}COOH\ (PFHpA) + HF \qquad (6.14)$$

Furthermore, PFHpA was decomposed into PFHxA, and PFPeA proved in this study, and would continually change to PFBA, PFPA and TPA in the same way and finally mineralized to CO_2 and fluoride ions in the stepwise manner as reported by previous literature (Liu et al., 2019). Consequently, the excellent synergistic effect between TiO_2 and PMS for PFOA removal was attributed to that both sulfate radicals (produced by PMS) and photoinduced holes (produced by TiO_2) had the strong photocatalytic ability for PFOA degradation (as shown in Eq. 6.9 and 6.10). Besides, photoinduced electrons (e^-) could both reacted with PMS (HSO_5^-) and peroxydisulfate ($S_2O_8^{2-}$) to form sulfate radicals (as shown in Eq. 6.2 and 6.15), which not only increased the quantity of sulfate radicals in the solution but also inhibited the recombination of photoinduced holes and electrons (Eq. 6.16) as the electrons were consumed in the reaction of Eq. 6.2 and 6.15. Thus, the amount of photoinduced holes and sulfate radicals was primarily increased during the photocatalytic reaction in Vis/TiO_2/PMS, leading to a higher degradation efficiency than that in sole PMS or TiO_2 system.

$$S_2O_8^{2-} + 2e^- \rightarrow 4SO_4^{\bullet -} \qquad (6.15)$$

$$h^+ + e^- \rightarrow \text{recombination} \qquad (6.16)$$

Besides, as shown in **Fig. 6-2**, TiO_2/PMS have higher visible light absorbance than TiO_2 and PMS, which also contributes to the fact that Vis/TiO_2/PMS outperformed Vis/TiO_2 and Vis/PMS in PFOA photocatalysis degradation. The main photocatalytic mechanism were presented in **Fig. 6-10**.

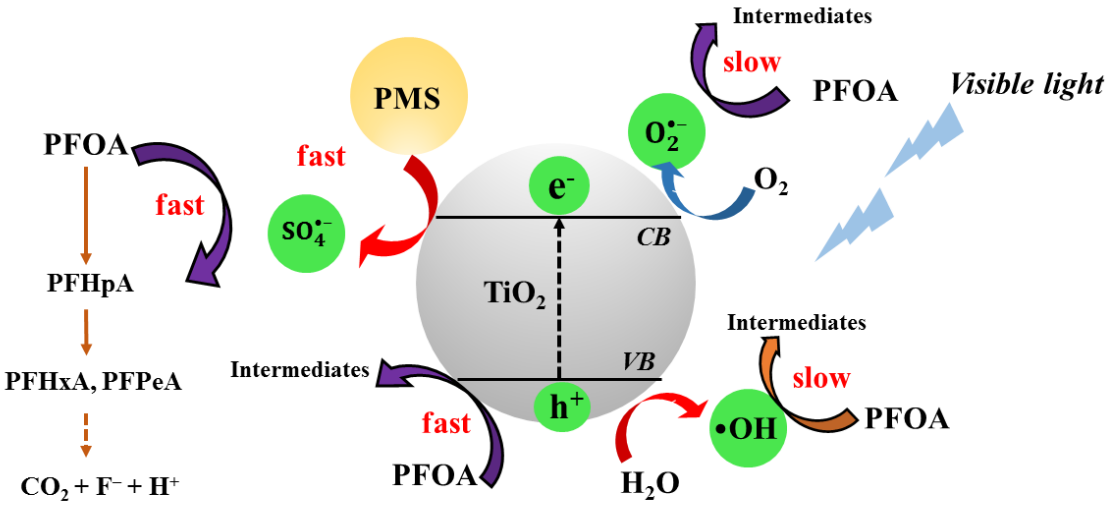

Fig. 6-10. The main photocatalysis by TiO_2/PMS for PFOA degradation (Xu et al. 2020).

6.4. Conclusions

In summary, 300 W Vis/TiO_2/PMS could degrade 100% of PFOA (50 mg L^{-1}) within 8 h, which was better than sole PMS or TiO_2 under same conditions. Taken the influence factors into consideration, 0.25 g L^{-1} TiO_2 and 0.75 g L^{-1} PMS added in the reaction solution with the initial pH 3 showed better performance than on the other conditions studied in this study. Furthermore, under UV light irradiation at 254 and 185 nm wavelengths, TiO_2/PMS both achieved excellent degradation efficacy of PFOA (almost 100%) within 1.5 h. According to the analysis of intermediates, PFOA was gradually from the long chain into shorter chain species during the photocatalytic process. Scavenger experiments proved that $SO_4^{\bullet-}$ radicals and photogenerated holes were the most important active species contributing to the PFOA photodegradation. Overall, TiO_2/PMS under powerful visible light could potentially be applied to the PFAS photocatalysis in water and wastewater.

Chapter 7. Comparison of Ga_2O_3 and TiO_2 with PMS and potential application

7.1. Introduction

Over the years, heterogeneous photocatalysis to be applied for PFAS treatment have drawn significant attention by scientists (Xu et al., 2018). For example, graphene oxide/TiO_2 nanotubes array were synthesized as catalysts irradiated by UV light and achieved 83% PFOA degraded within 4 h (Park et al., 2018). ZnO-reduced graphene oxide was used for PFOA degradation combined with persulfate oxidation under UV light irradiation and observed that almost 100% PFOA was removed within 4 h (Wu et al., 2018). However, such methods have some potential drawbacks in relation to real world applications. Firstly, these catalysts are commonly synthesized under certain conditions (i.e. high temperature and specific precursors), which unavoidably increase the energy cost and operation difficulty. Secondly, UV light was often the indispensable light source in the photocatalytic system to activatee the catalysts degrading pollutants (Hao et al., 2019). At ground level, 44% of the sunlight energy is in the visible range, with only 3% in the ultraviolet range. Thus, it is difficult to utilize UV light from sunlight as photodegradation energy source, and the extra UV energy has to be provided for PFAS degradation, with UV-based treatment technologies. As previous studies, Ga_2O_3 or TiO_2 with PMS both have well performance for PFOA degradation under UV light. Moreover, TiO_2 with PMS also has the photocatalytic ability for PFOA removal under 300 W visible light. Thus, these founding provides the possibility of aqueous PFOA degradation on water and wastewater treatment.

7.2. Methodology

Two real wastewater samples were collected from a wastewater treatment plant in Sydney, Australia. The diluting water was ultra-pure water or real water samples (influent and effluent) taken from a municipal sewage treatment plant in Sydney, Australia. The

influent went through physical settlement and biodegradation and discharged as effluent. Some foundation factors of these water samples were measured as follows: $N\text{-}NH_4^+$ and $P\text{-}PO_4^{3-}$ concentrations were measured using Merck cell test and spectrophotometer (Spectroquant NOVA 60; Merck, Germany). TOC was measured by Multi N/C 3100 Analytikjena total organic carbon (TOC) analyser. TDS was using an EC/TDS Hanna spectrophotometer. The PFOA concentration in the wastewater samples was under detection limit and then 50 mg L^{-1}

PFOA was injected into these samples for the photocatalysis. Ga_2O_3/PMS and TiO_2/PMS were added into the solution, respectively and went through the light resources of 185 and 254 nm UV light and 300 W visible light irradiation.

7.3. Results and discussion

7.3.1. *Real wastewater treatment by Ga_2O_3/PMS under Visible or UV light*

Table 7-1

Characteristics of the wastewater taken from a municipal wastewater plant in Sydney, Australia.

Effluent		Influent	
Parameter	Value	Parameter	value
PFOA	<LOQ[a]	PFOA	<LOQ
TOC	10.64 mg L^{-1}	TOC	14.41 mg L^{-1}
TDS	693 mg L^{-1}	TDS	659 mg L^{-1}
$N\text{-}NH_4^+$	0.7 mg L^{-1}	$N\text{-}NH^{4+}$	1.0 mg L^{-1}
$P\text{-}PO_4^{3-}$	6.8 mg L^{-1}	$P\text{-}PO_4^{3-}$	6.7 mg L^{-1}
pH	6.15	pH	6.17

[a] Limit of quantitative

Wastewater samples were taken from the influent and effluent of a municipal sewage treatment plant in Sydney, Australia, to prepare 50 mg L^{-1} of PFOA solution. The

characteristics of the influent and effluent samples are listed in **Table 7-1.** When the PFOA and catalysts was added, the pH was changed to 3.0±0.2 without pH adjustment. Hereupon, photodegradation of PFOA under the optimum conditions (1.23 g L^{-1} PMS, 0.25 g L^{-1} Ga_2O_3, pH 3) were conducted with both UV light (185 nm and 254 nm). As shown in **Fig. 7-1A,** under 254 nm UV irradiation, 100% PFOA in wastewater was degraded by Ga_2O_3/PMS within 120 min with the rate constant of 0.012 min^{-1}, which was similar to that obtained in pure water. Under 185 nm UV irradiation, 60-75% PFOA in wastewater was removal at 30 min, and totally degraded within 60 min, which was also equal to the efficacy during treatment in pure water. Such findings indicated that photocatalysis by Ga_2O_3/PMS under UV light irradiation (254 and 185 nm) was highly stable and not easily disturbed by other organic compounds in the real wastewater. Besides, total organic carbon (TOC) was also analyzed before and after the treatment. As shown in **Fig. 7-1B**, in the effluent sample, 75% TOC was removed under 254 UV light whereas 32% TOC was removed under 185 nm UV light. Similarly, in the influent sample, 85% TOC removal was observed under 254 nm UV, which was higher than 54% TOC removal under 185 nm UV. Thus, TOC could be significantly removed after the treatment under 254 nm UV light, which was better than that under 185 nm UV light. The reason might be related to fact that 185 nm UV does not transmit as well through water as does 254 nm UV (Imoberdorf and Mohseni, 2011). 254 nm UV light is fairly well transmitted as water molecules do not absorb the energy corresponding to this wavelength, while 185 nm intensity drops because it is absorbed by water molecules. Thus, 185 nm UV light is more powerful than 254 nm but poor transmitted in water, leading to the different degradation removal of TOC and PFOA in water and wastewater.

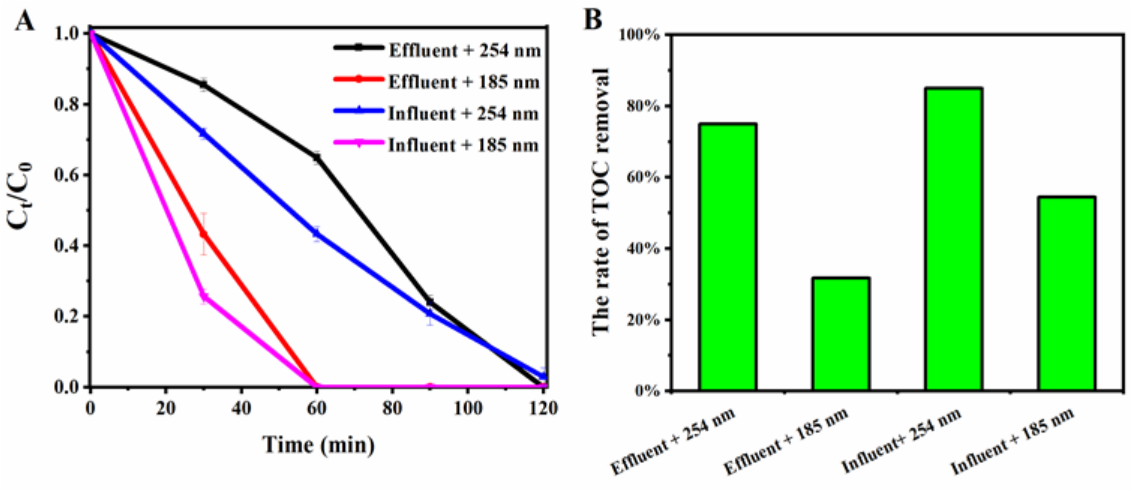

Fig. 7-1. (A) Degradation of PFOA in wastewater samples including influent and effluent from a wastewater treatment plant under UV 254 nm and 185 nm. (B) The rate of TOC removal by Ga_2O_3/PMS under 254 nm and 185 nm UV light. ([PFOA] = 50 mg L^{-1}, [PMS] = 0.45 g L^{-1}, [Ga_2O_3] = 0.25 g L^{-1}).

7.3.2. *Real wastewater treatment by TiO_2/PMS under Visible or UV light*

As the coexisting compounds may reduce the degradation efficacy (Beltran et al., 2008), the influent and effluent samples taken from a municipal sewage treatment plant in Sydney, Australia was investigated to validate the feasibility of TiO_2/PMS photocatalysis to degrade PFOA in the real wastewater. The characteristics of these water samples were listed in **Table 7-1**. The original pH of wastewater samples were 6.15 to 6.17. When PFOA and the catalysts of TiO_2/PMS were added in, the pH of the suspension was changed to 3.0 ± 0.2 without pH adjustment. Herein, 50 mg L^{-1} PFOA in the samples (influent and effluent samples) were prepared with 0.25 g L^{-1} TiO_2 and 0.75 g L^{-1} PMS for the catalysis under 300 W Visible light, 254 and 185 nm UV light irradiation, respectively. As a result, **Fig. 7-2A** presents that in the powerful visible light system, 65-82% PFOA was degraded within 8 h by TiO_2/PMS in influent and effluent samples and their rate constant was 0.136 and 0.070 h^{-1}, respectively, which were both lower than that

in pure water (k = 0.310 h^{-1}). This was probably due to the adverse impacts of coexisting organic matters in these sewage water samples, leading to the reduced performance for PFOA removal (Shao et al., 2013). However, in the UV light system, the degradation performance in the wastewater was as good as in pure water, reflecting the stable photocatalytic ability of TiO_2/PMS under UV light irradiation (both in 254 and 185 nm), which was not easily disturbed by other organic compounds in the real wastewater samples.

Total organic carbon (TOC) was another important index reflecting the degradation effect, so the changes of TOC with time were also measured in this study. As it can be deduced from **Fig. 7-2B**, in the influent sample, 65% TOC was removed in 254 nm UV/TiO_2/PMS system, whereas 34% TOC diminished in 185 nm UV/TiO_2/PMS system and in 300 W Vis/TiO_2/PMS the removal of TOC was 26%. Similarly, in the effluent sample, the rate of TOC removal decreased in the order as 254 nm UV/TiO_2/PMS (69%) > 185 nm UV/TiO_2/PMS (53%) > 300 W Vis /TiO_2/PMS (44%). Because 254 nm UV light is fairly well transmitted as water molecules do not absorb the energy corresponding to this wavelength, while 185 nm intensity drops as it is absorbed by water molecules (Imoberdorf and Mohseni, 2011). Thus, although 185 nm UV light is more powerful than 254 nm, it is does not transmit as well through water as 254 nm, leading to the various degradation performance between TOC and PFOA removal in the real wastewater.

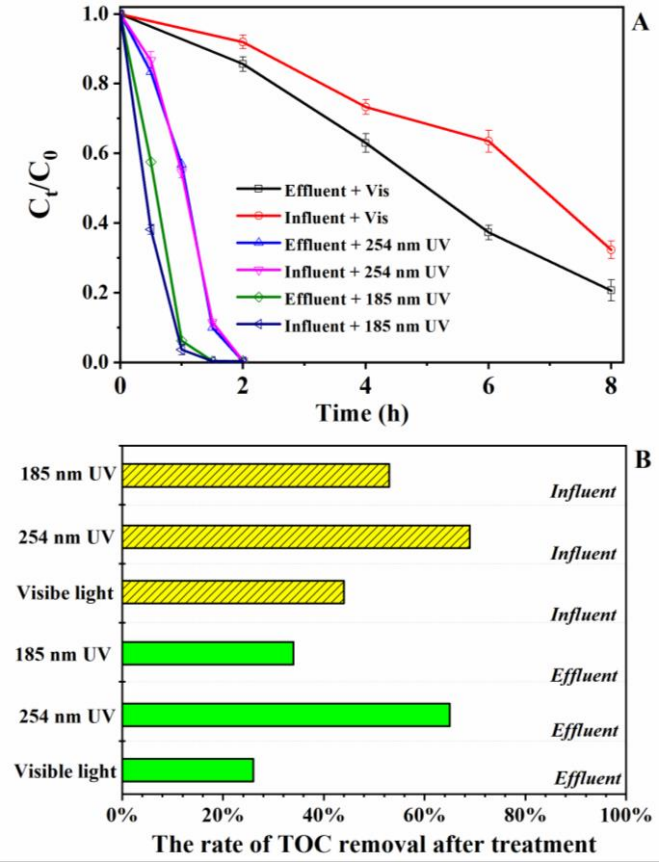

Fig. 7-2. (A) Degradation of wastewater samples including influent and effluent from a wastewater treatment plant and (B) the rate of TOC removal by TiO_2/PMS under 300 W visible light, 254 nm and 185 nm UV light.

7.3.3. *Comparison of Ga_2O_3/PMS and TiO_2/PMS for PFOA removal*

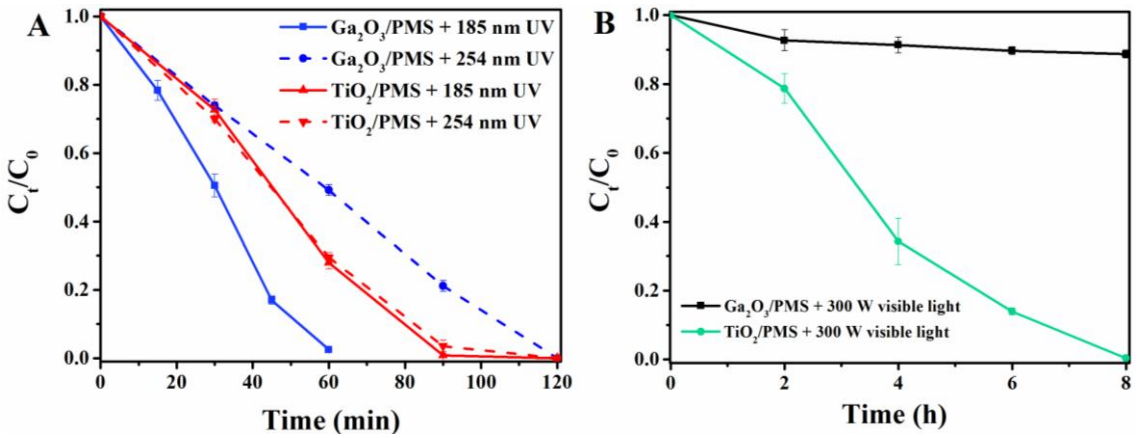

Fig. 7-3. (A) Comparison between Ga_2O_3/PMS and TiO_2/PMS for PFOA removal in pure water under 185 nm, 254 nm UV light and (B) 300 W visible light.

Previous study proved that Ga_2O_3 with PMS was good at PFOA degrading under 254 and 185 nm UV irradiation. Meanwhile, TiO_2 with PMS was able to degrade PFOA under both UV light and 300 W visible light. In detail, Ga_2O_3/PMS performed best under the conditions of 0.25 g L^{-1} Ga_2O_3, 1.23 g L^{-1} PMS, and initial pH of 3 ± 0.2. In addition, TiO_2/PMS outperformed under the conditions of 0.25 g L^{-1} TiO_2, 0.75 g L^{-1} PMS and initial pH of 3 ± 0.2. As shown in **Fig. 7-3A**, Ga_2O_3/PMS under 185 nm UV could most efficiently degrade 100% PFOA within 60 min, followed by TiO_2/PMS under 185 nm UV or 254 nm UV, which both degraded completely PFOA within 90 min. While Ga_2O_3/PMS under 254 nm UV was able to remove 100% PFOA within 120 min, which was longer than that of previous conditions. However, under 300 W visible light irradiation, TiO_2/PMS could degrade 100% PFOA within 8 h, while Ga_2O_3/PMS had almost no ability for PFOA removal (**Fig. 7-3B**). This might be related to the difference of light absorption between Ga_2O_3 and TiO_2. The band gap of Ga_2O_3 was 4.68 eV, which was higher than that of TiO_2 with 3.14 eV, indicating that 300 W visible light was difficult to active the electron from valence band to conduction band in the surface of Ga_2O_3.

Therefore, TiO_2/PMS could potentially be utilized with solar for the PFOA photodegradation.

Based on the performance of PFOA in real wastewater treatment as shown in **Fig. 7-1** and **7-2**, Ga_2O_3/PMS and TiO_2/PMS could both degrade 100% PFOA within 60 min under 185 nm UV light and 254 nm UV light, respectively, suggesting that under UV light, their photocatalytic ability for PFOA removal in the wastewater was similar. While TiO_2/PMS could also deal with PFOA in wastewater under 300 W visible light. Additionally, Ga_2O_3/PMS and TiO_2/PMS both have the similar ability for TOC removal in wastewater treatment and the results indicate that the under 254 nm UV light, the removal rate of TOC was higher than that under 185 nm UV light and visible light.

7.4. Conclusions

Overall, Ga_2O_3/PMS was able to degrade almost PFOA in wastewater within 60 min under 185 nm UV light and 90 min under 254 nm UV light, respectively. Meanwhile, TiO_2/PMS owned the similar photocatalytic ability for PFOA removal in wastewater. In addition, Ga_2O_3/PMS and TiO_2/PMS could remove 75% and 65% TOC in wastewater under 254 nm UV light irradiation, respectively. While under 185 nm and 300 W visible, the removal rate was reduced by both Ga_2O_3/PMS and TiO_2/PMS. For PFOA removal in both pure and wastewater, the degradation efficiency was similar by Ga_2O_3/PMS and TiO_2/PMS under UV light. The different presented on the performance under 300 W visible light that TiO_2/PMS was able to degrade PFOA in both pure water and wastewater while Ga_2O_3/PMS could not.

Chapter 8. Conclusions and recommendations

8.1. Summary

The research mainly aimed to develop the advanced treatment for aqueous PFOA degradation under UV or visible light irradiation. The effectiveness of common catalysts such as Ga_2O_3, TiO_2, CeO_2, In_2O_3 and CdS were investigated under the same conditions and Ga_2O_3 and TiO_2 were proved to be better catalysts for PFOA removal. The use of PMS mixed with TiO_2 and Ga_2O_3 was also examined. PFOA removal from aqueous solution was studied by UV photocatalysis using Ga_2O_3 and further enhanced in the presence of PMS. Moreover, under 300 W visible light and UV light irradiation, TiO_2 with PMS assisted achieved well performance for PFOA removal in water and wastewater, satisfying the objective that visible light could be utilized on the treatment of aqueous PFOA. In summary, the specific findings from this study are as follows:

- The commercial catalysts of Ga_2O_3, TiO_2, CeO_2 and In_2O_3 were able to degrade PFOA at various contents within 10 h while. Among them, Ga_2O_3 had best performance with 100% PFOA removal. Nevertheless, CdS showed no ability for PFOA removal under same condition.
- The quantum yield during the UV irradiation was 0.0032, 0.0075, 0.0041 and 0.0005 mol $Einstein^{-1}$, respectively by the catalysts of Ga_2O_3, TiO_2, CeO_2 and In_2O_3. In addition, their band gap energy followed the order of $Ga_2O_3 = 7.3 \times 10^{-19}$ J > $TiO_2 = 5.0 \times 10^{-19}$ J > $CeO_2 = 4.7 \times 10^{-19}$ J > $In_2O_3 = 4.5 \times 10^{-19}$ J > CdS = 3.9×10^{-19} J.
- During the photocatalysis, photogenerated electrons played the main role in the system of Ga_2O_3/UV, while photogenerated holes were more important in the system of TiO_2, CeO_2 and In_2O_3 under UV light.
- PFOA was degraded into shorter carbon chain stepwise (PFHpA, PFHxA, PFPeA, PFBA, PFPA and TFA) and finally turned to CO_2 and H_2O.

- 1.23 g L^{-1} of PMS and 0.25 g L^{-1} of Ga_2O_3 was able to degrade 100% PFOA in aqueous solution within 90 min under 254 nm UV and 60 min under 185 nm UV, respectively.
- Acidic condition at pH 3 was favourable for PFOA degradation in PMS/Ga_2O_3/UV system. Such degradation was not affected by the initial concentration of PFOA ranged from 50 ng L^{-1} to 50 mg L^{-1}.
- The quantum yield during photocatalysis by PMS/Ga_2O_3 under UV light (254 nm) was 0.009 mol $Einstein^{-1}$. Through the analysis of intermediates, PFOA was gradually degraded from long chian species into short chain intermediates. Scavenger experiments proved that $SO_4^{\bullet-}$ radicals, $O_2^{\bullet-}$ radicals and photogenerated electrons were the most important active species contributing to the PFOA photodegradation.
- TiO_2 with PMS addition could degrade 100% of PFOA (50 mg L^{-1}) within 8 h under 300 W visible light, which was better than sole PMS or TiO_2 under the same conditions.
- 0.25 g L^{-1} TiO_2 and 0.75 g L^{-1} PMS added in the reaction solution with the initial pH 3 showed better performance than on the other conditions studied in this study.
- TiO_2/PMS both achieved excellent degradation efficacy of PFOA (almost 100%) within 1.5 h under UV light irradiation at 254 and 185 nm wavelengths,
- PFOA was gradually from the long chain into shorter chain species during the photocatalytic process in the system of 300 Vis/TiO_2/PMS.
- Scavenger experiments proved that $SO_4^{\bullet-}$ radicals and photogenerated holes were the most important active species contributing to the PFOA photodegradation during the photocatalysis by TiO_2/PMS under 300 W visible light.

- For PFOA in real wastewater treatment, Ga_2O_3/PMS was able to degrade almost PFOA in wastewater within 60 min under 185 nm Visible and 90 min under 254 nm UV light, respectively. TiO_2/PMS also had the similar photocatalytic ability for PFOA removal in wastewater.
- Ga_2O_3/PMS and TiO_2/PMS both could remove 75% and 65% TOC in wastewater under 254 nm UV light irradiation, respectively. Comparatively, under 185 nm and 300 W visible, the removal rate was lower by Ga_2O_3/PMS and TiO_2/PMS.
- For PFOA removal in both pure and wastewater, the degradation efficiency was similar by Ga_2O_3/PMS and TiO_2/PMS under UV light. The different presented on the performance under 300 W visible light that TiO_2/PMS was able to degrade PFOA in both pure water and wastewater while Ga_2O_3/PMS could not.

8.2. Recommendation

Although this research has found that TiO_2 or Ga_2O_3 with PMS performed well for PFOA removal, the immobilization and reusability of these technology were also important and necessary to be further studied. Photocatalytic reactor is designed for the photodegradation of the pollutants from water and wastewater. Many reactors have been designed for TiO_2 immobilization as shown in **Fig. 8-1A**. The photocatalytic experiments conducted in the laboratory use a suspension photocatalytic reactor, which possesses the advantages of simple structure, convenient operation, efficient compound transmission, and high rate of reaction. Nevertheless, it also has several disadvantages: firstly, the particle size has strong influence on the suspended state of the catalyst, namely, too small size would lead to a difficult separation while too large size would result in particle deposition. In addition, the particle size also affects the light transmission as large size or high concentration would lead to a turbid solution so that the light transmission will be

disturbed and light absorption reduced. More importantly, the catalysts suspended in the solution are hard to be separated and re-used. Thus, the loaded photocatalytic reactor is preferable to be used for the catalyst application. As shown in **Fig. 8-1B**, g-C_3N_4 on structured Al_2O_3 ceramic foam synthesized could be fixed at one side of the reaction pool and the contaminated water flows from intake to outlet passing though the loaded g-C_3N_4 materials (Dong et al., 2014). However, such a reactor structure would easily produce two problems: one is the limited reaction area, which is just the cross-sectional area of g-C_3N_4 on the Al_2O_3 foam; the other one is comparatively short residence time of contacting the catalysts, which will lead to the incomplete photodegradation. Accordingly, tubes, fibres, and floated glass balls have been designed for the substitution of the single tiled catalysts. Notably, among them, fibres have the advantages of large reaction area, low catalyst loss during the transmission, and high efficacy of optical transmission. For instance, the doped TiO_2 coated quartz fibre membranes was used in a photocatalytic reactor as shown in **Fig. 8-1C,** which turned out to have durable degradation ability with high efficacy (Hatat-Fraile et al., 2017). It is reasonable to predict that this reactor could be applied for TiO_2/PMS or Ga_2O_3/PMS, which could also achieve similarly stable and high degradation performance for the contaminant removal. However, the fibre reactor also has its drawbacks such as being easily broken, expensive, and difficult to load the catalysts on the fibre. Therefore, different types of photocatalytic reactors should be fully evaluated when treating real wastewater.

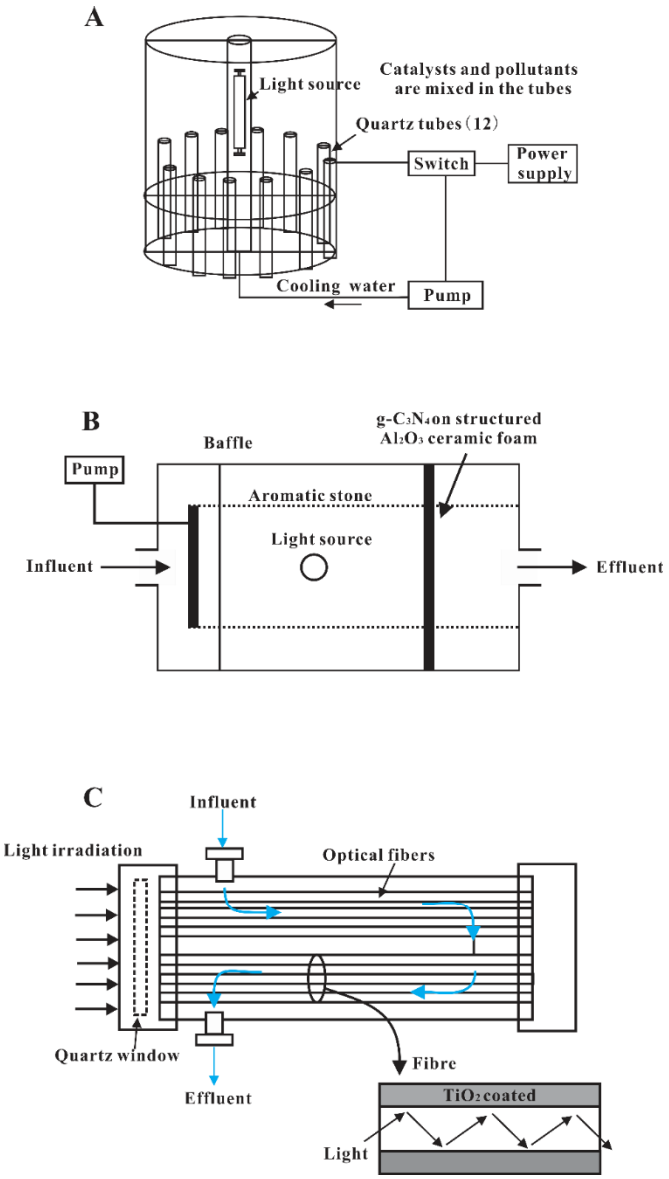

Fig. 8-1. Different types of photocatalytic reactors for practical applications: (A) suspension photocatalytic reactor; (B) photocatalytic pool with g-C_3N_4 on structured Al_2O_3 ceramic foam; (C) catalyst coated optical fibre reactor. The figures are referred from the ref. (Dong et al., 2014; Hatat-Fraile et al., 2017; Xu et al., 2017b).

Furthermore, future research challenges and opportunities with the critical thinking and knowledge base acquired from this project were listed as follows:

- ❖ The redox potentials of the reactions during the photocatalytic process and their alignment with the bands in the catalysts should be clarified;

- Commercial TiO_2/Ga_2O_3 could be doped with other materials to have better visible light absorption and stronger photocatalytic capability;
- The phototcatalysis treatment should be tried to conducted under solar irradiation to further reduce the cost of this technology;
- Other materials could be tried to degrade aqueous PFAS and their photocatalytic capability evaluated;
- The photocatalysis of PFOA intermediates should be conducted to explore the influence by the chain length of the target pollutants;
- Different kinds of PFAS such as PFOS or PFHxS should be photodegraded to discuss the influence by the functional group of the target pollutants;
- More investigation should be done in the highly contaminated area where this technology should be tested for the PFAS control;
- The immobilization and recycle of catalysts should be discussed, especially the PMS use in water which was not easily reused;
- The TiO_2/Ga_2O_3 doped on fibers could be applied on the water supply process;
- For easy separation of the catalyst from the aqueous solution, fiber based composite structure can be produced by using different combinations of mentioned photo catalyst in the fiber structure;
- New alternative photocatalyst need to develop based on low cost and high performance;
- Electrochemical degradation is another green and clean technology for pollutants controlling and it could be applied for PFOA degradation.

References

Anderson, R.H., Adamson, D.T. & Stroo, H.F. 2019, 'Partitioning of poly-and perfluoroalkyl substances from soil to groundwater within aqueous film-forming foam source zones', *Journal of Contaminant Hydrology*, vol. 220, pp. 59-65.

Ansari, S.A., Khan, M.M., Ansari, M.O. & Cho, M.H. 2016, 'Nitrogen-doped titanium dioxide (N-doped TiO_2) for visible light photocatalysis', *New Journal of Chemistry*, vol. 40, no. 4, pp. 3000-3009.

Aoudjit, F., Cherifi, O. & Halliche, D. 2019, 'Simultaneously efficient adsorption and photocatalytic degradation of sodium dodecyl sulfate surfactant by one-pot synthesized TiO2/layered double hydroxide materials', *Separation Science and Technology*, vol. 54, no. 7, pp. 1095-1105.

Apelberg, B.J., Witter, F.R., Herbstman, J.B., Calafat, A.M., Halden, R.U., Needham, L.L. & Goldman, L.R. 2007, 'Cord serum concentrations of perfluorooctane sulfonate (PFOS) and perfluorooctanoate (PFOA) in relation to weight and size at birth', *Environmental Health Perspectives*, vol. 115, no. 11, pp. 1670-1676.

Appleman, T.D., Higgins, C.P., Quiñones, O., Vanderford, B.J., Kolstad, C., Zeigler-Holady, J.C. & Dickenson, E.R. 2014, 'Treatment of poly-and perfluoroalkyl substances in US full-scale water treatment systems', *Water Research*, vol. 51, pp. 246-255.

Armitage, J., Cousins, I.T., Buck, R.C., Prevedouros, K., Russell, M.H., MacLeod, M. & Korzeniowski, S.H. 2006, 'Modeling global-scale fate and transport of perfluorooctanoate emitted from direct sources', *Environmental Science & Technology*, vol. 40, no. 22, pp. 6969-6975.

Armitage, J.M., MacLeod, M. & Cousins, I.T. 2009, 'Comparative assessment of the global fate and transport pathways of long-chain perfluorocarboxylic acids

(PFCAs) and perfluorocarboxylates (PFCs) emitted from direct sources', *Environmental Science & Technology*, vol. 43, no. 15, pp. 5830-5836.

Arvaniti, O.S. & Stasinakis, A.S. 2015, 'Review on the occurrence, fate and removal of perfluorinated compounds during wastewater treatment', *Science of the Total Environment*, vol. 524, pp. 81-92.

Bahnemann, D. 2004, 'Photocatalytic water treatment: solar energy applications', *Solar Energy*, vol. 77, no. 5, pp. 445-459.

Bai, J., Xu, Z., Zheng, Y. & Yin, H. 2006, 'Shape control of CeO_2 nanostructure materials in microemulsion systems', *Materials Letters*, vol. 60, no. 9-10, pp. 1287-1290.

Bassler, J., Ducatman, A., Elliott, M., Wen, S., Wahlang, B., Barnett, J. & Cave, M.C. 2019, 'Environmental perfluoroalkyl acid exposures are associated with liver disease characterized by apoptosis and altered serum adipocytokines', *Environmental Pollution*, vol. 247, pp. 1055-1063.

Behafarid, F. & Cuenya, B.R. 2012, 'Coarsening phenomena of metal nanoparticles and the influence of the support pre-treatment: Pt/TiO_2 (110)', *Surface Science*, vol. 606, no. 11, pp. 908-918.

Behr, A.-C., Lichtenstein, D., Braeuning, A., Lampen, A. & Buhrke, T. 2018, 'Perfluoroalkylated substances (PFAS) affect neither estrogen and androgen receptor activity nor steroidogenesis in human cells in vitro', *Toxicology Letters*, vol. 291, pp. 51-60.

Blake, B.E., Pinney, S.M., Hines, E.P., Fenton, S.E. & Ferguson, K.K. 2018, 'Associations between longitudinal serum perfluoroalkyl substance (PFAS) levels and measures of thyroid hormone, kidney function, and body mass index in the Fernald Community Cohort', *Environmental Pollution*, vol. 242, pp. 894-904.

Bräunig, J., Baduel, C., Barnes, C.M. & Mueller, J.F. 2019, 'Leaching and bioavailability of selected perfluoroalkyl acids (PFAAs) from soil contaminated by firefighting activities', *Science of the Total Environment*, vol. 646, pp. 471-479.

Burns, D.C., Ellis, D.A., Li, H., McMurdo, C.J. & Webster, E. 2008, 'Experimental pK a determination for perfluorooctanoic acid (PFOA) and the potential impact of pK a concentration dependence on laboratory-measured partitioning phenomena and environmental modeling', *Environmental Science & Technology*, vol. 42, no. 24, pp. 9283-9288.

Cao, M., Wang, B., Yu, H., Wang, L., Yuan, S. & Chen, J. 2010, 'Photochemical decomposition of perfluorooctanoic acid in aqueous periodate with VUV and UV light irradiation', *Journal of Hazardous Materials*, vol. 179, no. 1-3, pp. 1143-1146.

Cao, S., Zhou, N., Gao, F., Chen, H. & Jiang, F. 2017, 'All-solid-state Z-scheme 3, 4-dihydroxybenzaldehyde-functionalized Ga_2O_3/graphitic carbon nitride photocatalyst with aromatic rings as electron mediators for visible-light photocatalytic nitrogen fixation', *Applied Catalysis B: Environmental*, vol. 218, pp. 600-610.

Cao, Y., Li, Q., Li, C., Li, J. & Yang, J. 2016, 'Surface heterojunction between (001) and (101) facets of ultrafine anatase TiO_2 nanocrystals for highly efficient photoreduction CO_2 to CH_4', *Applied Catalysis B: Environmental*, vol. 198, pp. 378-388.

Carbajo, J., Tolosana-Moranchel, A., Casas, J., Faraldos, M. & Bahamonde, A. 2018, 'Analysis of photoefficiency in TiO_2 aqueous suspensions: Effect of titania hydrodynamic particle size and catalyst loading on their optical properties', *Applied Catalysis B: Environmental*, vol. 221, pp. 1-8.

Chai, B., Peng, T., Zeng, P. & Mao, J. 2011, 'Synthesis of floriated In_2S_3 decorated with TiO_2 nanoparticles for efficient photocatalytic hydrogen production under visible light', *Journal of Materials Chemistry*, vol. 21, no. 38, pp. 14587-14593.

Chen, H., Chen, K.-F., Lai, S.-W., Dang, Z. & Peng, Y.-P. 2015a, 'Photoelectrochemical oxidation of azo dye and generation of hydrogen via CN co-doped TiO_2 nanotube arrays', *Separation and Purification Technology*, vol. 146, pp. 143-153.

Chen, H., Han, J., Zhang, C., Cheng, J., Sun, R., Wang, X., Han, G., Yang, W. & He, X. 2017a, 'Occurrence and seasonal variations of per-and polyfluoroalkyl substances (PFASs) including fluorinated alternatives in rivers, drain outlets and the receiving Bohai Sea of China', *Environmental Pollution*, vol. 231, pp. 1223-1231.

Chen, H., Wang, X., Zhang, C., Sun, R., Han, J., Han, G., Yang, W. & He, X. 2017b, 'Occurrence and inputs of perfluoroalkyl substances (PFASs) from rivers and drain outlets to the Bohai Sea, China', *Environmental Pollution*, vol. 221, pp. 234-243.

Chen, M.-J., Lo, S.-L., Lee, Y.-C. & Huang, C.-C. 2015b, 'Photocatalytic decomposition of perfluorooctanoic acid by transition-metal modified titanium dioxide', *Journal of Hazardous Materials*, vol. 288, pp. 168-175.

Chen, M.-J., Lo, S.-L., Lee, Y.-C., Kuo, J. & Wu, C.-H. 2016, 'Decomposition of perfluorooctanoic acid by ultraviolet light irradiation with Pb-modified titanium dioxide', *Journal of Hazardous Materials*, vol. 303, pp. 111-118.

Chen, X., Li, R., Pan, X., Huang, X. & Yi, Z. 2017c, 'Fabrication of In2O3-Ag-Ag3PO4 composites with Z-scheme configuration for photocatalytic ethylene degradation under visible light irradiation', *Chemical Engineering Journal*, vol. 320, pp. 644-652.

Chen, X., Wang, W., Xiao, H., Hong, C., Zhu, F., Yao, Y. & Xue, Z. 2012, 'Accelerated TiO2 photocatalytic degradation of Acid Orange 7 under visible light mediated by peroxymonosulfate', *Chemical Engineering Journal*, vol. 193-194, pp. 290-295.

Chen, Y.-C., Lo, S.-L. & Kuo, J. 2011, 'Effects of titanate nanotubes synthesized by a microwave hydrothermal method on photocatalytic decomposition of perfluorooctanoic acid', *Water Research*, vol. 45, no. 14, pp. 4131-4140.

Chou, J.-C. & Liao, L.P. 2005, 'Study on pH at the point of zero charge of TiO_2 pH ion-sensitive field effect transistor made by the sputtering method', *Thin Solid Films*, vol. 476, no. 1, pp. 157-161.

Dai, Z.R., Pan, Z.W. & Wang, Z.L. 2003, 'Novel nanostructures of functional oxides synthesized by thermal evaporation', *Advanced Functional Materials*, vol. 13, no. 1, pp. 9-24.

Ding, G. & Peijnenburg, W.J. 2013, 'Physicochemical properties and aquatic toxicity of poly-and perfluorinated compounds', *Critical Reviews in Environmental Science and Technology*, vol. 43, no. 6, pp. 598-678.

Dong, F., Wang, Z., Li, Y., Ho, W.-K. & Lee, S. 2014, 'Immobilization of polymeric g-C3N4 on structured ceramic foam for efficient visible light photocatalytic air purification with real indoor illumination', *Environmental Science & Technology*, vol. 48, no. 17, pp. 10345-10353.

Eriksson, U., Mueller, J.F., Toms, L.-M.L., Hobson, P. & Kärrman, A. 2017, 'Temporal trends of PFSAs, PFCAs and selected precursors in Australian serum from 2002 to 2013', *Environmental Pollution*, vol. 220, pp. 168-177.

Estrellan, C.R., Salim, C. & Hinode, H. 2010, 'Photocatalytic decomposition of perfluorooctanoic acid by iron and niobium co-doped titanium dioxide', *Journal of Hazardous Materials*, vol. 179, no. 1-3, pp. 79-83.

Feng, Y., Liao, C., Kong, L., Wu, D., Liu, Y., Lee, P.-H. & Shih, K. 2018, 'Facile synthesis of highly reactive and stable Fe-doped g-C3N4 composites for peroxymonosulfate activation: A novel nonradical oxidation process', *Journal of Hazardous Materials*, vol. 354, pp. 63-71.

Flores, C., Ventura, F., Martin-Alonso, J. & Caixach, J. 2013, 'Occurrence of perfluorooctane sulfonate (PFOS) and perfluorooctanoate (PFOA) in NE Spanish surface waters and their removal in a drinking water treatment plant that combines conventional and advanced treatments in parallel lines', *Science of the Total Environment*, vol. 461, pp. 618-626.

Gallen, C., Baduel, C., Lai, F.Y., Thompson, K., Thompson, J., Warne, M. & Mueller, J.F. 2014, 'Spatio-temporal assessment of perfluorinated compounds in the Brisbane River system, Australia: Impact of a major flood event', *Marine Pollution Bulletin*, vol. 85, no. 2, pp. 597-605.

Gao, H., Chen, J., Zhang, Y. & Zhou, X. 2016, 'Sulfate radicals induced degradation of Triclosan in thermally activated persulfate system', *Chemical Engineering Journal*, vol. 306, pp. 522-30.

Gatto, S., Sansotera, M., Persico, F., Gola, M., Pirola, C., Panzeri, W., Navarrini, W. & Bianchi, C.L. 2015, 'Surface fluorination on TiO_2 catalyst induced by photodegradation of perfluorooctanoic acid', *Catalysis Today*, vol. 241, pp. 8-14.

Giri, R., Ozaki, H., Morigaki, T., Taniguchi, S. & Takanami, R. 2011, 'UV photolysis of perfluorooctanoic acid (PFOA) in dilute aqueous solution', *Water Science and Technology*, vol. 63, no. 2, pp. 276-282.

Giri, R.R., Ozaki, H., Okada, T., Taniguchi, S. & Takanami, R. 2012, 'Factors influencing UV photodecomposition of perfluorooctanoic acid in water', *Chemical Engineering Journal*, vol. 180, pp. 197-203.

Gomez-Ruiz, B., Ribao, P., Diban, N., Rivero, M.J., Ortiz, I. & Urtiaga, A. 2018, 'Photocatalytic degradation and mineralization of perfluorooctanoic acid (PFOA) using a composite TiO_2− rGO catalyst', *Journal of Hazardous Materials*, vol. 344, pp. 950-7.

Goosey, E. & Harrad, S. 2011, 'Perfluoroalkyl compounds in dust from Asian, Australian, European, and North American homes and UK cars, classrooms, and offices', *Environment International*, vol. 37, no. 1, pp. 86-92.

Gorrochategui, E., Pérez-Albaladejo, E., Casas, J., Lacorte, S. & Porte, C. 2014, 'Perfluorinated chemicals: differential toxicity, inhibition of aromatase activity and alteration of cellular lipids in human placental cells', *Toxicology and Applied Pharmacology*, vol. 277, no. 2, pp. 124-130.

Goss, K.-U. 2007, 'The pK a values of PFOA and other highly fluorinated carboxylic acids', *Environmental Science & Technology*, vol. 42, no. 2, pp. 456-458.

Gremmel, C., Frömel, T. & Knepper, T.P. 2017, 'HPLC–MS/MS methods for the determination of 52 perfluoroalkyl and polyfluoroalkyl substances in aqueous samples', *Analytical and Bioanalytical Chemistry*, vol. 409, no. 6, pp. 1643-1655.

Grilla, E., Matthaiou, V., Frontistis, Z., Oller, I., Polo, I., Malato, S. & Mantzavinos, D. 2019, 'Degradation of antibiotic trimethoprim by the combined action of sunlight, TiO_2 and persulfate: A pilot plant study', *Catalysis Today*, vol. 328, pp. 216-222.

Guan, M., Xiao, C., Zhang, J., Fan, S., An, R., Cheng, Q., Xie, J., Zhou, M., Ye, B. & Xie, Y. 2013, 'Vacancy associates promoting solar-driven photocatalytic activity

of ultrathin bismuth oxychloride nanosheets', *Journal of the American Chemical Society*, vol. 135, no. 28, pp. 10411-10417.

Hamid, H. & Li, L.Y. 2018, 'Fate of perfluorooctanoic acid (PFOA) in sewage sludge during microwave-assisted persulfate oxidation treatment', *Environmental Science and Pollution Research*, vol. 25, no. 10, pp. 10126-10134.

Hansen, K.J., Clemen, L.A., Ellefson, M.E. & Johnson, H.O. 2001, 'Compound-specific, quantitative characterization of organic: Fluorochemicals in biological matrices', *Environment Science & Technology*, vol. 35, pp. 766-770.

Hanssen, L., Dudarev, A.A., Huber, S., Odland, J.Ø., Nieboer, E. & Sandanger, T.M. 2013, 'Partition of perfluoroalkyl substances (PFASs) in whole blood and plasma, assessed in maternal and umbilical cord samples from inhabitants of arctic Russia and Uzbekistan', *Science of the Total Environment*, vol. 447, pp. 430-437.

Hao, Q., Liu, Y., Chen, T., Guo, Q., Wei, W. & Ni, B.-J. 2019, 'Bi_2O_3@Carbon Nanocomposites for Solar-Driven Photocatalytic Degradation of Chlorophenols', *ACS Applied Nano Materials*, vol. 2, pp. 2308-2316.

Hatat-Fraile, M., Liang, R., Arlos, M.J., He, R.X., Peng, P., Servos, M.R. & Zhou, Y.N. 2017, 'Concurrent photocatalytic and filtration processes using doped TiO_2 coated quartz fiber membranes in a photocatalytic membrane reactor', *Chemical Engineering Journal*, vol. 330, pp. 531-40.

He, F. 2017, 'Review in the TiO_2 Photocatalytic Degradation of Organic Matter in Radioactive Waste Water', *DEStech Transactions on Environment, Energy and Earth Science*, no. apeesd.

Hoffmann, M.R., Martin, S.T., Choi, W. & Bahnemann, D.W. 1995, 'Environmental applications of semiconductor photocatalysis', *Chemical Reviews*, vol. 95, no. 1, pp. 69-96.

Holtcamp, W. 2012, 'Pregnancy-induced hypertension “probably linked” to PFOA contamination', National Institute of Environmental Health Sciences.

Hori, H., Hayakawa, E., Einaga, H., Kutsuna, S., Koike, K., Ibusuki, T., Kiatagawa, H. & Arakawa, R. 2004, 'Decomposition of environmentally persistent perfluorooctanoic acid in water by photochemical approaches', *Environmental Science & Technology*, vol. 38, no. 22, pp. 6118-6124.

Hori, H., Nagaoka, Y., Murayama, M. & Kutsuna, S. 2008a, 'Efficient decomposition of perfluorocarboxylic acids and alternative fluorochemical surfactants in hot water', *Environmental Science & Technology*, vol. 42, no. 19, pp. 7438-7443.

Hori, H., Yamamoto, A., Koike, K., Kutsuna, S., Murayama, M., Yoshimoto, A. & Arakawa, R. 2008b, 'Photocatalytic decomposition of a perfluoroether carboxylic acid by tungstic heteropolyacids in water', *Applied Catalysis B: Environmental*, vol. 82, no. 1-2, pp. 58-66.

Houtz, E.F., Higgins, C.P., Field, J.A. & Sedlak, D.L. 2013, 'Persistence of perfluoroalkyl acid precursors in AFFF-impacted groundwater and soil', *Environmental Science & Technology*, vol. 47, no. 15, pp. 8187-8195.

Huang, B., Zhang, Z., Zhao, C., Cairang, L., Bai, J., Zhang, Y., Mu, X., Du, J., Wang, H. & Pan, X. 2018, 'Enhanced gas-sensing performance of ZnO@ In_2O_3 core@ shell nanofibers prepared by coaxial electrospinning', *Sensors and Actuators B: Chemical*, vol. 255, pp. 2248-2257.

Huang, J., Wang, X., Pan, Z., Li, X., Ling, Y. & Li, L. 2016, 'Efficient degradation of perfluorooctanoic acid (PFOA) by photocatalytic ozonation', *Chemical Engineering Journal*, vol. 296, pp. 329-334.

Hurley, S., Goldberg, D., Wang, M., Park, J.-S., Petreas, M., Bernstein, L., Anton-Culver, H., Nelson, D.O. & Reynolds, P. 2018, 'Breast cancer risk and serum levels of

per-and poly-fluoroalkyl substances: a case-control study nested in the California Teachers Study', *Environmental Health*, vol. 17, no. 1, p. 83.

Hussain, M., Ceccarelli, R., Marchisio, D.L., Fino, D., Russo, N. & Geobaldo, F. 2010, 'Synthesis, characterization, and photocatalytic application of novel TiO2 nanoparticles', *Chemical Engineering Journal*, vol. 157, no. 1, pp. 45-51.

Imoberdorf, G. & Mohseni, M. 2011, 'Degradation of natural organic matter in surface water using vacuum-UV irradiation', *Journal of Hazardous Materials*, vol. 186, no. 1, pp. 240-6.

Janda, J., Nödler, K., Brauch, H.-J., Zwiener, C. & Lange, F.T. 2019, 'Robust trace analysis of polar (C2-C8) perfluorinated carboxylic acids by liquid chromatography-tandem mass spectrometry: method development and application to surface water, groundwater and drinking water', *Environmental Science and Pollution Research*, vol. 26, no. 8, pp. 7326-7336.

Janousek, R.M., Mayer, J. & Knepper, T.P. 2019, 'Is the phase-out of long-chain PFASs measurable as fingerprint in a defined area? Comparison of global PFAS concentrations and a monitoring study performed in Hessen, Germany from 2014-2018', *TrAC Trends in Analytical Chemistry*.

Jian, J.-M., Chen, D., Han, F.-J., Guo, Y., Zeng, L., Lu, X. & Wang, F. 2018, 'A short review on human exposure to and tissue distribution of per-and polyfluoroalkyl substances (PFASs)', *Science of The Total Environment*, vol. 636, pp. 1058-1069.

Jiang, F., Zhao, H., Chen, H., Xu, C. & Chen, J. 2016, 'Enhancement of photocatalytic decomposition of perfluorooctanoic acid on CeO_2/In_2O_3', *RSC Advances*, vol. 6, no. 76, pp. 72015-72021.

Jo, Y., Kim, C., Moon, G.-H., Lee, J., An, T. & Choi, W. 2018, 'Activation of peroxymonosulfate on visible light irradiated TiO_2 via a charge transfer complex path', *Chemical Engineering Journal*, vol. 346, pp. 249-257.

Khan, S., Han, C., Khan, H.M., Boccelli, D.L., Nadagouda, M.N. & Dionysiou, D.D. 2017a, 'Efficient degradation of lindane by visible and simulated solar light-assisted S-TiO_2 /peroxymonosulfate process: Kinetics and mechanistic investigations', *Molecular Catalysis*, vol. 428, pp. 9-16.

Khan, S., He, X., Khan, J.A., Khan, H.M., Boccelli, D.L. & Dionysiou, D.D. 2017b, 'Kinetics and mechanism of sulfate radical-and hydroxyl radical-induced degradation of highly chlorinated pesticide lindane in UV/peroxymonosulfate system', *Chemical Engineering Journal*, vol. 318, pp. 135-142.

Kitsiou, V., Filippidis, N., Mantzavinos, D. & Poulios, I. 2009, 'Heterogeneous and homogeneous photocatalytic degradation of the insecticide imidacloprid in aqueous solutions', *Applied Catalysis B: Environmental*, vol. 86, no. 1-2, pp. 27-35.

Kommireddy, D.S., Patel, A.A., Shutava, T.G., Mills, D.K. & Lvov, Y.M. 2005, 'Layer-by-layer assembly of TiO_2 nanoparticles for stable hydrophilic biocompatible coatings', *Journal of Nanoscience and Nanotechnology*, vol. 5, no. 7, pp. 1081-1087.

Konyar, M., Yildiz, T., Aksoy, M., Yatmaz, H. & Öztürk, K. 2017, 'Reticulated ZnO Photocatalyst: Efficiency Enhancement in Degradation of Acid Red 88 Azo Dye by Catalyst Surface Cleaning', *Chemical Engineering Communications*, vol. 204, no. 6, pp. 705-710.

Kosmulski, M. 2001, 'Pristine points of zero charge of gallium and indium oxides', *Journal of Colloid and InterfaceScience*, vol. 238, no. 1, pp. 225-257.

Kotthoff, M., Müller, J., Jürling, H., Schlummer, M. & Fiedler, D. 2015, 'Perfluoroalkyl and polyfluoroalkyl substances in consumer products', *Environmental Science and Pollution Research*, vol. 22, no. 19, pp. 14546-14559.

Kutsuna, S., Nagaoka, Y., Takeuchi, K. & Hori, H. 2006, 'TiO2-induced heterogeneous photodegradation of a fluorotelomer alcohol in air', *Environmental Science & Technology*, vol. 40, no. 21, pp. 6824-6829.

Kwon, H.-O., Kim, H.-Y., Park, Y.-M., Seok, K.-S., Oh, J.-E. & Choi, S.-D. 2017, 'Updated national emission of perfluoroalkyl substances (PFASs) from wastewater treatment plants in South Korea', *Environmental Pollution*, vol. 220, pp. 298-306.

Lam, N.H., Cho, C.-R., Kannan, K. & Cho, H.-S. 2017, 'A nationwide survey of perfluorinated alkyl substances in waters, sediment and biota collected from aquatic environment in Vietnam: distributions and bioconcentration profiles', *Journal of Hazardous Materials*, vol. 323, pp. 116-127.

Lee, Y.-C., Lo, S.-L., Chiueh, P.-T. & Chang, D.-G. 2009, 'Efficient decomposition of perfluorocarboxylic acids in aqueous solution using microwave-induced persulfate', *Water Research*, vol. 43, no. 11, pp. 2811-2816.

Lee, Y.-C., Lo, S.-L., Chiueh, P.-T., Liou, Y.-H. & Chen, M.-L. 2010, 'Microwave-hydrothermal decomposition of perfluorooctanoic acid in water by iron-activated persulfate oxidation', *Water Research*, vol. 44, no. 3, pp. 886-892.

Lee, Y.-C., Lo, S.-L., Kuo, J. & Lin, Y.-L. 2012, 'Persulfate oxidation of perfluorooctanoic acid under the temperatures of 20–40 C', *Chemical Engineering Journal*, vol. 198, pp. 27-32.

Li, D., Yu, J.C.-C., Nguyen, V.-H., Wu, J.C. & Wang, X. 2018, 'A dual-function photocatalytic system for simultaneous separating hydrogen from water splitting

and photocatalytic degradation of phenol in a twin-reactor', *Applied Catalysis B: Environmental*, vol. 239, pp. 268-279.

Li, K., Tang, Y., Xu, Y., Wang, Y., Huo, Y., Li, H. & Jia, J. 2013a, 'A BiOCl film synthesis from Bi_2O_3 film and its UV and visible light photocatalytic activity', *Applied Catalysis B: Environmental*, vol. 140, pp. 179-188.

Li, M., Yu, Z., Liu, Q., Sun, L. & Huang, W. 2016, 'Photocatalytic decomposition of perfluorooctanoic acid by noble metallic nanoparticles modified TiO_2', *Chemical Engineering Journal*, vol. 286, pp. 232-238.

Li, Q., Guo, B., Yu, J., Ran, J., Zhang, B., Yan, H. & Gong, J.R. 2011, 'Highly efficient visible-light-driven photocatalytic hydrogen production of CdS-cluster-decorated graphene nanosheets', *Journal of the American Chemical Society*, vol. 133, no. 28, pp. 10878-10884.

Li, X., Zhang, P., Jin, L., Shao, T., Li, Z. & Cao, J. 2012a, 'Efficient photocatalytic decomposition of perfluorooctanoic acid by indium oxide and its mechanism', *Environmental Science & Technology*, vol. 46, no. 10, pp. 5528-5534.

Li, Z., Zhang, P., Li, J., Shao, T. & Jin, L. 2013b, 'Synthesis of In_2O_3-graphene composites and their photocatalytic performance towards perfluorooctanoic acid decomposition', *Journal of Photochemistry and Photobiology A: Chemistry*, vol. 271, pp. 111-116.

Li, Z., Zhang, P., Li, J., Shao, T., Wang, J. & Jin, L. 2014, 'Synthesis of In2O3 porous nanoplates for photocatalytic decomposition of perfluorooctanoic acid (PFOA)', *Catalysis Communications*, vol. 43, pp. 42-46.

Li, Z., Zhang, P., Shao, T. & Li, X. 2012b, 'In_2O_3 nanoporous nanosphere: a highly efficient photocatalyst for decomposition of perfluorooctanoic acid', *Applied Catalysis B: Environmental*, vol. 125, pp. 350-357.

Li, Z., Zhang, P., Shao, T., Wang, J., Jin, L. & Li, X. 2013c, 'Different nanostructured In_2O_3 for photocatalytic decomposition of perfluorooctanoic acid (PFOA)', *Journal of Hazardous Materials*, vol. 260, pp. 40-46.

Liang, C., Wang, Z.-S. & Bruell, C.J. 2007, 'Influence of pH on persulfate oxidation of TCE at ambient temperatures', *Chemosphere*, vol. 66, no. 1, pp. 106-113.

Lin, J.-C., Hu, C.-Y. & Lo, S.-L. 2016, 'Effect of surfactants on the degradation of perfluorooctanoic acid (PFOA) by ultrasonic (US) treatment', *Ultrasonics Sonochemistry*, vol. 28, pp. 130-135.

Liu, W., Jia, C., Jin, C., Yao, L., Cai, W. & Li, X. 2004, 'Growth mechanism and photoluminescence of CdS nanobelts on Si substrate', *Journal of Crystal Growth*, vol. 269, no. 2-4, pp. 304-309.

Liu, Y., Fan, X., Quan, X., Fan, Y., Chen, S. & Zhao, X. 2019, 'Enhanced Perfluorooctanoic Acid Degradation by Electrochemical Activation of Sulfate Solution on B/N Codoped Diamond', *Environmental Science & Technology*, vol. 53, no. 9, pp. 5191-5201.

Liu, Y., Zhang, Y., Guo, H., Cheng, X., Liu, H. & Tang, W. 2017, 'Persulfate-assisted photodegradation of diethylstilbestrol using monoclinic $BiVO_4$ under visible-light irradiation', *Environmental Science and Pollution Research*, vol. 24, no. 4, pp. 3739-3747.

Liu, Z., Lu, Y., Wang, T., Wang, P., Li, Q., Johnson, A.C., Sarvajayakesavalu, S. & Sweetman, A.J. 2016, 'Risk assessment and source identification of perfluoroalkyl acids in surface and ground water: Spatial distribution around a mega-fluorochemical industrial park, China', *Environment International*, vol. 91, pp. 69-77.

Lyu, X.-J., Li, W.-W., Lam, P.K. & Yu, H.-Q. 2015, 'Photodegradation of perfluorooctane sulfonate in environmental matrices', *Separation and Purification Technology*, vol. 151, pp. 172-176.

Magdalane, C.M., Kaviyarasu, K., Vijaya, J.J., Jayakumar, C., Maaza, M. & Jeyaraj, B. 2017, 'Photocatalytic degradation effect of malachite green and catalytic hydrogenation by UV–illuminated CeO_2/CdO multilayered nanoplatelet arrays: investigation of antifungal and antimicrobial activities', *Journal of Photochemistry and Photobiology B: Biology*, vol. 169, pp. 110-123.

Malato, S., Blanco, J., Vidal, A. & Richter, C. 2002, 'Photocatalysis with solar energy at a pilot-plant scale: an overview', *Applied Catalysis B: Environmental*, vol. 37, no. 1, pp. 1-15.

Martin, J.W., Kannan, K., Berger, U., De Voogt, P., Field, J., Franklin, J., Giesy, J.P., Harner, T., Muir, D.C.G., Scott, B., Kaiser, M., Jarnberg, U., Jones, K.C., Mabury, S.A., Schroeder, H., Simcik, M., Sottani, C., Van Bavel, B., Karrman, A., Lindstrom, G. & Van Leeuwen, S. 2004, 'Analytical challenges hamper perfluoroalky research', *Environmental Science & Technology*, vol. 38, no. 13, pp. 248A-255A.

Mastrantonio, M., Bai, E., Uccelli, R., Cordiano, V., Screpanti, A. & Crosignani, P. 2017, 'Drinking water contamination from perfluoroalkyl substances (PFAS): an ecological mortality study in the Veneto Region, Italy', *The European Journal of Public Health*, vol. 28, no. 1, pp. 180-185.

Mazzoni, M., Buffo, A., Cappelli, F., Pascariello, S., Polesello, S., Valsecchi, S., Volta, P. & Bettinetti, R. 2019, 'Perfluoroalkyl acids in fish of Italian deep lakes: Environmental and human risk assessment', *Science of the Total Environment*, vol. 653, pp. 351-358.

Meng, S. & Kaxiras, E. 2010, 'Electron and hole dynamics in dye-sensitized solar cells: influencing factors and systematic trends', *Nano letters*, vol. 10, no. 4, pp. 1238-1247.

Merino, N., Qu, Y., Deeb, R.A., Hawley, E.L., Hoffmann, M.R. & Mahendra, S. 2016, 'Degradation and removal methods for perfluoroalkyl and polyfluoroalkyl substances in water', *Environmental Engineering Science*, vol. 33, no. 9, pp. 615-649.

Moreira, N.F., Narciso-da-Rocha, C., Polo-López, M.I., Pastrana-Martínez, L.M., Faria, J.L., Manaia, C.M., Fernández-Ibáñez, P., Nunes, O.C. & Silva, A.M. 2018, 'Solar treatment (H2O2, TiO2-P25 and GO-TiO2 photocatalysis, photo-Fenton) of organic micropollutants, human pathogen indicators, antibiotic resistant bacteria and related genes in urban wastewater', *Water Research*, vol. 135, pp. 195-206.

Mulabagal, V., Liu, L., Qi, J., Wilson, C. & Hayworth, J.S. 2018, 'A rapid UHPLC-MS/MS method for simultaneous quantitation of 23 perfluoroalkyl substances (PFAS) in estuarine water', *Talanta*, vol. 190, pp. 95-102.

Murakami, M., Morita, C., Morimoto, T. & Takada, H. 2011, 'Source analysis of perfluorocarboxylates in Tokyo Bay during dry weather and wet weather using sewage markers', *Environmental Chemistry*, vol. 8, no. 4, pp. 355-362.

Naile, J.E., Khim, J.S., Wang, T., Chen, C., Luo, W., Kwon, B.-O., Park, J., Koh, C.-H., Jones, P.D. & Lu, Y. 2010, 'Perfluorinated compounds in water, sediment, soil and biota from estuarine and coastal areas of Korea', *Environmental Pollution*, vol. 158, no. 5, pp. 1237-1244.

Nohara, K., Toma, M., Kutsuna, S., Takeuchi, K. & Ibusuki, T. 2001, 'Cl atom-initiated oxidation of three homologous methyl perfluoroalkyl ethers', *Environmental Science & Technology*, vol. 35, no. 1, pp. 114-120.

Okitsu, K., Iwasaki, K., Yobiko, Y., Bandow, H., Nishimura, R. & Maeda, Y. 2005, 'Sonochemical degradation of azo dyes in aqueous solution: a new heterogeneous kinetics model taking into account the local concentration of OH radicals and azo dyes', *Ultrasonics Sonochemistry*, vol. 12, no. 4, pp. 255-262.

Ou, H.-H. & Lo, S.-L. 2007, 'Review of titania nanotubes synthesized via the hydrothermal treatment: Fabrication, modification, and application', *Separation and Purification Technology*, vol. 58, no. 1, pp. 179-191.

Pagga, U. & Brown, D. 1986, 'The degradation of dyestuffs: Part II Behaviour of dyestuffs in aerobic biodegradation tests', *Chemosphere*, vol. 15, no. 4, pp. 479-491.

Pan, M., Huang, N., Zhao, X., Fu, J. & Zhong, X. 2013, 'Enhanced efficiency of dye-sensitized solar cell by high surface area anatase-TiO_2-modified P25 paste', *Journal of Nanomaterials*, vol. 2013, p. 3.

Panchangam, S.C., Lin, A.Y.-C., Shaik, K.L. & Lin, C.-F. 2009, 'Decomposition of perfluorocarboxylic acids (PFCAs) by heterogeneous photocatalysis in acidic aqueous medium', *Chemosphere*, vol. 77, no. 2, pp. 242-248.

Panchangam, S.C., Yellatur, C.S., Yang, J.-S., Loka, S.S., Lin, A.Y.C. & Vemula, V. 2018, 'Facile fabrication of TiO_2-graphene nanocomposites (TGNCs) for the efficient photocatalytic oxidation of perfluorooctanoic acid (PFOA)', *Journal of Environmental Chemical Engineering*, vol. 6, no. 5, pp. 6359-6369.

Park, K., Ali, I. & Kim, J.O. 2018, 'Photodegradation of perfluorooctanoic acid by graphene oxide-deposited TiO_2 nanotube arrays in aqueous phase', *J Environ Manage*, vol. 218, pp. 333-339.

Pignotti, E., Casas, G., Llorca, M., Tellbüscher, A., Almeida, D., Dinelli, E., Farré, M. & Barceló, D. 2017, 'Seasonal variations in the occurrence of perfluoroalkyl

substances in water, sediment and fish samples from Ebro Delta (Catalonia, Spain)', *Science of The Total Environment*, vol. 607, pp. 933-943.

Pistocchi, A. & Loos, R. 2009, 'A map of European emissions and concentrations of PFOS and PFOA', *Environmental Science & Technology*, vol. 43, no. 24, pp. 9237-9244.

Prevedouros, K., Cousins, I.T., Buck, R.C. & Korzeniowski, S.H. 2006, 'Sources, fate and transport of perfluorocarboxylates', *Environmental Science & Technology*, vol. 40, no. 1, pp. 32-44.

Pu, S., Long, D., Liu, Z., Yang, F. & Zhu, J. 2018, 'Preparation of RGO-P25 Nanocomposites for the Photocatalytic Degradation of Ammonia in Livestock Farms', *Catalysts*, vol. 8, no. 5, p. 189.

Qi, Y., Huo, S., Xi, B., Hu, S., Zhang, J. & He, Z. 2016, 'Spatial distribution and source apportionment of PFASs in surface sediments from five lake regions, China', *Scientific Reports*, vol. 6, p. 22674.

Qu, Y., Zhang, C., Li, F., Chen, J. & Zhou, Q. 2010, 'Photo-reductive defluorination of perfluorooctanoic acid in water', *Water Research*, vol. 44, no. 9, pp. 2939-2947.

Quintana, J.B., Weiss, S. & Reemtsma, T. 2005, 'Pathways and metabolites of microbial degradation of selected acidic pharmaceutical and their occurrence in municipal wastewater treated by a membrane bioreactor', *Water Research*, vol. 39, no. 12, pp. 2654-2664.

Rappazzo, K., Coffman, E. & Hines, E. 2017, 'Exposure to perfluorinated alkyl substances and health outcomes in children: a systematic review of the epidemiologic literature', *International Journal of Environmental Research and Public Health*, vol. 14, no. 7, p. 691.

Rogatsky, E., O'Hehir, C., Daly, J., Tedesco, A., Jenny, R. & Aldous, K. 2017, 'Development of high throughput LC/MS/MS method for analysis of perfluorooctanoic acid from serum, suitable for large-scale human biomonitoring', *J Chromatogr B Analyt Technol Biomed Life Sci*, vol. 1049-1050, pp. 24-29.

Sacca, A., Carbone, A., Passalacqua, E., D'epifanio, A., Licoccia, S., Traversa, E., Sala, E., Traini, F. & Ornelas, R. 2005, 'Nafion–TiO_2 hybrid membranes for medium temperature polymer electrolyte fuel cells (PEFCs)', *Journal of Power Sources*, vol. 152, pp. 16-21.

Saleh, N.B., Khalid, A., Tian, Y., Ayres, C., Sabaraya, I.V., Pietari, J., Hanigan, D., Chowdhury, I. & Apul, O.G. 2019, 'Removal of poly-and per-fluoroalkyl substances from aqueous systems by nano-enabled water treatment strategies', *Environmental Science: Water Research & Technology*, vol. 5, no. 2, pp. 198-208.

Sansotera, M., Persico, F., Pirola, C., Navarrini, W., Di Michele, A. & Bianchi, C.L. 2014, 'Decomposition of perfluorooctanoic acid photocatalyzed by titanium dioxide: Chemical modification of the catalyst surface induced by fluoride ions', *Applied Catalysis B: Environmental*, vol. 148-149, pp. 29-35.

Schröder, H.F. & Meesters, R.J. 2005, 'Stability of fluorinated surfactants in advanced oxidation processes—a follow up of degradation products using flow injection–mass spectrometry, liquid chromatography–mass spectrometry and liquid chromatography–multiple stage mass spectrometry', *Journal of Chromatography A*, vol. 1082, no. 1, pp. 110-119.

Schwarzenbach, R.P., Gschwend, P.M. & Imboden, D.M. 2016, *Environmental organic chemistry*, John Wiley & Sons.

Shang, E., Li, Y., Niu, J., Li, S., Zhang, G. & Wang, X. 2018, 'Photocatalytic degradation of perfluorooctanoic acid over Pb-$BiFeO_3$/rGO catalyst: Kinetics and mechanism', *Chemosphere*, vol. 211, pp. 34-43.

Shao, H., Zhao, X., Wang, Y., Mao, R., Wang, Y., Qiao, M., Zhao, S. & Zhu, Y. 2017, 'Synergetic activation of peroxymonosulfate by Co_3O_4 modified g-C_3N_4 for enhanced degradation of diclofenac sodium under visible light irradiation', *Applied Catalysis B: Environmental*, vol. 218, pp. 810-818.

Shao, M., Li, Q., Xie, B., Wu, J. & Qian, Y. 2003, 'The synthesis of CdS/ZnO and CdS/Pb_3O_4 composite materials via microwave irradiation', *Materials Chemistry and Physics*, vol. 78, no. 1, pp. 288-291.

Shao, T., Zhang, P., Jin, L. & Li, Z. 2013a, 'Photocatalytic decomposition of perfluorooctanoic acid in pure water and sewage water by nanostructured gallium oxide', *Applied Catalysis B: Environmental*, vol. 142, pp. 654-661.

Shao, T., Zhang, P., Li, Z. & Jin, L. 2013b, 'Photocatalytic decomposition of perfluorooctanoic acid in pure water and wastewater by needle-like nanostructured gallium oxide', *Chinese Journal of Catalysis*, vol. 34, no. 8, pp. 1551-1559.

Simon, A., Nghiem, L.D., Le-Clech, P., Khan, S.J. & Drewes, J.E. 2009, 'Effects of membrane degradation on the removal of pharmaceutically active compounds (PhACs) by NF/RO filtration processes', *Journal of Membrane Science*, vol. 340, no. 1, pp. 16-25.

Sinclair, E. & Kannan, K. 2006, 'Mass loading and fate of perfluoroalkyl surfactants in wastewater treatment plants', *Environmental Science & Technology*, vol. 40, no. 5, pp. 1408-1414.

Song, C., Chen, P., Wang, C. & Zhu, L. 2012, 'Photodegradation of perfluorooctanoic acid by synthesized TiO_2-MWCNT composites under 365nm UV irradiation', *Chemosphere*, vol. 86, no. 8, pp. 853-859.

Song, Z., Dong, X., Wang, N., Zhu, L., Luo, Z., Fang, J. & Xiong, C. 2017, 'Efficient photocatalytic defluorination of perfluorooctanoic acid over BiOCl nanosheets via a hole direct oxidation mechanism', *Chemical Engineering Journal*, vol. 317, pp. 925-934.

Song, Z., Tang, H., Wang, N. & Zhu, L. 2013, 'Reductive defluorination of perfluorooctanoic acid by hydrated electrons in a sulfite-mediated UV photochemical system', *Journal of hazardous materials*, vol. 262, pp. 332-338.

Sornalingam, K., McDonagh, A. & Zhou, J.L. 2016, 'Photodegradation of estrogenic endocrine disrupting steroidal hormones in aqueous systems: Progress and future challenges', *Science of the Total Environment*, vol. 550, pp. 209-224.

Sornalingam, K., McDonagh, A., Zhou, J.L., Johir, M.A.H. & Ahmed, M.B. 2018, 'Photocatalysis of estrone in water and wastewater: Comparison between Au-TiO_2 nanocomposite and TiO_2, and degradation by-products', *Science of The Total Environment*, vol. 610, pp. 521-530.

Stilwell, D.E. & Park, S.M. 1988, 'Electrochemistry of conductive polymers IV electrochemical studies on polyaniline degradation—Product identification and coulometric studies', *Journal of the Electrochemical Society*, vol. 135, no. 10, pp. 2497-2502.

Svihlikova, V., Lankova, D., Poustka, J., Tomaniova, M., Hajslova, J. & Pulkrabova, J. 2015, 'Perfluoroalkyl substances (PFASs) and other halogenated compounds in fish from the upper Labe River basin', *Chemosphere*, vol. 129, pp. 170-178.

Tian, H. & Gu, C. 2018, 'Effects of different factors on photodefluorination of perfluorinated compounds by hydrated electrons in organo-montmorillonite system', *Chemosphere*, vol. 191, pp. 280-287.

Trojanowicz, M., Bojanowska-Czajka, A., Bartosiewicz, I. & Kulisa, K. 2018, 'Advanced Oxidation/Reduction Processes treatment for aqueous perfluorooctanoate (PFOA) and perfluorooctanesulfonate (PFOS)–A review of recent advances', *Chemical Engineering Journal*, vol. 336, pp. 170-199.

Urtiaga, A., Fernández-González, C., Gómez-Lavín, S. & Ortiz, I. 2015, 'Kinetics of the electrochemical mineralization of perfluorooctanoic acid on ultrananocrystalline boron doped conductive diamond electrodes', *Chemosphere*, vol. 129, pp. 20-26.

Valsecchi, S., Rusconi, M., Mazzoni, M., Viviano, G., Pagnotta, R., Zaghi, C., Serrini, G. & Polesello, S. 2015, 'Occurrence and sources of perfluoroalkyl acids in Italian river basins', *Chemosphere*, vol. 129, pp. 126-134.

Vassiliadou, I., Costopoulou, D., Ferderigou, A. & Leondiadis, L. 2010, 'Levels of perfluorooctanesulfonate (PFOS) and perfluorooctanoate (PFOA) in blood samples from different groups of adults living in Greece', *Chemosphere*, vol. 80, no. 10, pp. 1199-1206.

Wang, W.-S., Wang, D.-H., Qu, W.-G., Lu, L.-Q. & Xu, A.-W. 2012, 'Large ultrathin anatase TiO2 nanosheets with exposed {001} facets on graphene for enhanced visible light photocatalytic activity', *The Journal of Physical Chemistry C*, vol. 116, no. 37, pp. 19893-19901.

Wang, X., Wu, P., Lu, Y., Huang, Z., Zhu, N., Lin, C. & Dang, Z. 2014, 'NiZnAl layered double hydroxides as photocatalyst under solar radiation for photocatalytic degradation of orange G', *Separation and Purification Technology*, vol. 132, pp. 195-205.

Wang, Y., Li, N., Duan, P., Sun, X., Chu, B. & He, Q. 2015a, 'Properties and photocatalytic activity of β-Ga_2O_3 nanorods under simulated solar irradiation', *Journal of Nanomaterials*, vol. 16, no. 1, p. 126.

Wang, Y. & Zhang, P. 2011, 'Photocatalytic decomposition of perfluorooctanoic acid (PFOA) by TiO_2 in the presence of oxalic acid', *Journal of hazardous materials*, vol. 192, no. 3, pp. 1869-1875.

Wang, Y., Zhang, P., Pan, G. & Chen, H. 2008, 'Ferric ion mediated photochemical decomposition of perfluorooctanoic acid (PFOA) by 254nm UV light', *Journal Hazard Materials*, vol. 160, no. 1, pp. 181-186.

Wang, Y., Zhou, L., Duan, X., Sun, H., Tin, E.L., Jin, W. & Wang, S. 2015b, 'Photochemical degradation of phenol solutions on Co_3O_4 nanorods with sulfate radicals', *Catalysis Today*, vol. 258, pp. 576-584.

Williams, P.T. & Brindle, A.J. 2002, 'Catalytic pyrolysis of tyres: influence of catalyst temperature', *Fuel*, vol. 81, no. 18, pp. 2425-2434.

Wohlfahrt-Veje, C., Audouze, K., Brunak, S., Antignac, J.P., le Bizec, B., Juul, A., Skakkebæk, N. & Main, K. 2014, 'Polychlorinated dibenzo-p-dioxins, furans, and biphenyls (PCDDs/PCDFs and PCBs) in breast milk and early childhood growth and IGF1', *Reproduction*, vol. 147, no. 4, pp. 391-399.

Wu, D., Li, X., Zhang, J., Chen, W., Lu, P., Tang, Y. & Li, L. 2018, 'Efficient PFOA degradation by persulfate-assisted photocatalytic ozonation', *Separation and Purification Technology*, vol. 207, pp. 255-261.

Wu, Y., Li, Y., Tian, A., Mao, K. & Liu, J. 2016, 'Selective Removal of Perfluorooctanoic Acid Using Molecularly Imprinted Polymer-Modified TiO_2 Nanotube Arrays', *International Journal of Photoenergy*, vol. 2016, pp. 1-10.

Xiao, X., Liu, C., Hu, R., Zuo, X., Nan, J., Li, L. & Wang, L. 2012, 'Oxygen-rich bismuth oxyhalides: generalized one-pot synthesis, band structures and visible-light photocatalytic properties', *Journal of Materials Chemistry*, vol. 22, no. 43, pp. 22840-22843.

Xu, B., Ahmed, M.B., Zhou, J.L. & Altaee, A. 2020, 'Visible and UV photocatalysis of aqueous perfluorooctanoic acid by TiO_2 and peroxymonosulfate: Process kinetics and mechanistic insights', *Chemosphere*, vol. 243, p. 125366.

Xu, B., Ahmed, M.B., Zhou, J.L., Altaee, A., Wu, M. & Xu, G. 2017a, 'Photocatalytic removal of perfluoroalkyl substances from water and wastewater: Mechanism, kinetics and controlling factors', *Chemosphere*, vol. 189, pp. 717-29.

Xu, B., Ahmed, M.B., Zhou, J.L., Altaee, A., Xu, G. & Wu, M. 2018, 'Graphitic carbon nitride based nanocomposites for the photocatalysis of organic contaminants under visible irradiation: progress, limitations and future directions', *Science of the Total Environment*, vol. 633, pp. 546-559.

Xu, B., Wu, M., Pan, C., Sun, Y., Yuan, D., Tang, L. & Xu, G. 2017b, 'Aquatic photolysis of hydroxylated polybromodiphenyl ethers under direct UV irradiation: a case study of 2′-HO-BDE-68', *Environmental Science and Pollution Research*, vol. 24, no. 16, pp. 14409-14416.

Xu, B., Zhou, J.L., Altaee, A., Ahmed, M.B., Johir, M.A.H., Ren, J. & Li, X. 2019, 'Improved photocatalysis of perfluorooctanoic acid in water and wastewater by Ga_2O_3/UV system assisted by peroxymonosulfate', *Chemosphere*, vol. 239, p. 124722.

Xu, G., Zhang, J., Li, G. & Song, G. 2003, 'Effect of complexation on the zeta potential of titanium dioxide dispersions', *Journal of Dispersion Science and Technology*, vol. 24, no. 3-4, pp. 527-535.

Xu, H., Li, G., Zhu, G., Zhu, K. & Jin, S. 2015, 'Enhanced photocatalytic degradation of rutile/anatase TiO_2 heterojunction nanoflowers', *Catalysis Communications*, vol. 62, pp. 52-56.

Xu, Y. & Schoonen, M.A. 2000, 'The absolute energy positions of conduction and valence bands of selected semiconducting minerals', *American Mineralogist*, vol. 85, no. 3-4, pp. 543-556.

Yasuda, M., Matsumoto, T. & Yamashita, T. 2017, 'Sacrificial hydrogen production over TiO_2-based photocatalysts: Polyols, carboxylic acids, and saccharides', *Renewable and Sustainable Energy Reviews*, vol. 87, pp. 1621-1635.

Yates, B.J., Darlington, R., Zboril, R. & Sharma, V.K. 2014, 'High-valent iron-based oxidants to treat perfluorooctanesulfonate and perfluorooctanoic acid in water', *Environmental Chemistry Letters*, vol. 12, no. 3, pp. 413-417.

Yeung, L.W., Guruge, K.S., Taniyasu, S., Yamashita, N., Angus, P.W. & Herath, C.B. 2013, 'Profiles of perfluoroalkyl substances in the liver and serum of patients with liver cancer and cirrhosis in Australia', *Ecotoxicology and Environmental Safety*, vol. 96, pp. 139-146.

Yoo, J., Zazpe, R., Cha, G., Prikryl, J., Hwang, I., Macak, J.M. & Schmuki, P. 2018, 'Uniform ALD deposition of Pt nanoparticles within 1D anodic TiO_2 nanotubes for photocatalytic H_2 generation', *Electrochemistry Communications*, vol. 86, pp. 6-11.

Yu, J., He, C., Liu, X., Wu, J., Hu, Y. & Zhang, Y. 2014, 'Removal of perfluorinated compounds by membrane bioreactor with powdered activated carbon (PAC): adsorption onto sludge and PAC', *Desalination*, vol. 334, no. 1, pp. 23-28.

Zang, C., Yu, K., Hu, S. & Chen, F. 2018, 'Adsorption-depended Fenton-like reaction kinetics in CeO_2-H_2O_2 system for salicylic acid degradation', *Colloids and Surfaces A: Physicochemical and Engineering Aspects*, vol. 553, pp. 456-463.

Zhang, H., Lv, X., Li, Y., Wang, Y. & Li, J. 2009, 'P25-graphene composite as a high performance photocatalyst', *ACS nano*, vol. 4, no. 1, pp. 380-386.

Zhang, K.-L., Liu, C.-M., Huang, F.-Q., Zheng, C. & Wang, W.-D. 2006, 'Study of the electronic structure and photocatalytic activity of the BiOCl photocatalyst', *Applied Catalysis B: Environmental*, vol. 68, no. 3, pp. 125-129.

Zhang, T., Pan, G. & Zhou, Q. 2016, 'Temperature effect on photolysis decomposing of perfluorooctanoic acid', *Journal of Environmental Sciences*, vol. 42, pp. 126-133.

Zhang, W., Zhang, Y., Taniyasu, S., Yeung, L.W., Lam, P.K., Wang, J., Li, X., Yamashita, N. & Dai, J. 2013, 'Distribution and fate of perfluoroalkyl substances in municipal wastewater treatment plants in economically developed areas of China', *Environmental Pollution*, vol. 176, pp. 10-17.

Zhang, Y., Liu, X., Li, P., Duan, Y., Hu, X., Li, F. & Song, Y. 2019, 'Dopamine-crosslinked TiO2/perovskite layer for efficient and photostable perovskite solar cells under full spectral continuous illumination', *Nano Energy*, vol. 56, pp. 733-740.

Zhang, Y., Zhang, J., Xiao, Y., Chang, V.W. & Lim, T.-T. 2017, 'Direct and indirect photodegradation pathways of cytostatic drugs under UV germicidal irradiation: Process kinetics and influences of water matrix species and oxidant dosing', *Journal of Hazardous Materials*, vol. 324, pp. 481-488.

Zhao, B., Li, X., Yang, L., Wang, F., Li, J., Xia, W., Li, W., Zhou, L. & Zhao, C. 2015a, 'ß-Ga_2O_3 Nanorod Synthesis with a One-step Microwave Irradiation Hydrothermal Method and its Efficient Photocatalytic Degradation for

Perfluorooctanoic Acid', *Photochemistry and Photobiology*, vol. 91, no. 1, pp. 42-47.

Zhao, B., Li, X., Yang, L., Wang, F., Li, J., Xia, W., Li, W., Zhou, L. & Zhao, C. 2015b, 'ss-Ga2O3 nanorod synthesis with a one-step microwave irradiation hydrothermal method and its efficient photocatalytic degradation for perfluorooctanoic acid', *Photochem Photobiol*, vol. 91, no. 1, pp. 42-47.

Zhao, B., Lv, M. & Zhou, L. 2012, 'Photocatalytic degradation of perfluorooctanoic acid with β-Ga2O3 in anoxic aqueous solution', *Journal of Environmental Sciences*, vol. 24, no. 4, pp. 774-780.

Zhao, B. & Zhang, P. 2009, 'Photocatalytic decomposition of perfluorooctanoic acid with β-Ga 2 O 3 wide bandgap photocatalyst', *Catalysis Communications*, vol. 10, no. 8, pp. 1184-1187.

Zhao, P., Xia, X., Dong, J., Xia, N., Jiang, X., Li, Y. & Zhu, Y. 2016, 'Short-and long-chain perfluoroalkyl substances in the water, suspended particulate matter, and surface sediment of a turbid river', *Science of the Total Environment*, vol. 568, pp. 57-65.

Zhou, L., Zhang, W., Chen, L., Deng, H. & Wan, J. 2017a, 'A novel ternary visible-light-driven photocatalyst $AgCl/Ag_3PO_4/g\text{-}C_3N_4$: Synthesis, characterization, photocatalytic activity for antibiotic degradation and mechanism analysis', *Catalysis Communications*, vol. 100, pp. 191-195.

Zhou, P., Le, Z., Xie, Y., Fang, J. & Xu, J. 2017b, 'Studies on facile synthesis and properties of mesoporous CdS/TiO_2 composite for photocatalysis applications', *Journal of Alloys and Compounds*, vol. 692, pp. 170-177.

Zsilák, Z., Szabó-Bárdos, E., Fónagy, O., Horváth, O., Horváth, K. & Hajós, P. 2014, 'Degradation of benzenesulfonate by heterogeneous photocatalysis combined with ozonation', *Catalysis Today*, vol. 230, pp. 55-60.